Identification of molecular mechanisms of Wnt11 non-canonical signaling in regulation of L-type calcium channel

Inaugural-Dissertation

to obtain the academic degree

Doctor rerum naturalium (Dr. rer. nat.)

submitted to the Department of Biology, Chemistry and Pharmacy

of Freie Universität Berlin

by

Kitti Dóra Csályi

from Budapest

2018

I completed my doctorate studies from January 2014 to March 2018 under the supervision of Dr. Daniela Panáková at Max Delbrück Center for Molecular Medicine, Berlin-Buch.

1st Reviewer: Dr. Daniela Panáková

2nd Reviewer: Prof. Dr. Oliver Daumke

Date of defense: 06.07.2018

Acknowledgements

First, I would like to express my sincere gratitude to my supervisor Dr. Daniela Panáková for the patient guidance, motivation and advice she has provided throughout my time as her student. I have been extremely lucky to have a supervisor who cared so much about my work and helped me at all the times of my research.

Besides my supervisor, I would like to thank the rest of my MDC committee: Prof. Dr. Oliver Daumke, Prof. Dr. Michael Gotthardt, Prof. Dr. Harald Saumweber and Dr. Francesca Spagnoli for their insightful comments and for the questions which incented me to widen my research from various perspectives. I would like to thank PD Dr. Enno Klußmann for fruitful discussions and providing the inhibitor peptides.

I am very thankful to the MDC TransCard Research School for giving me the opportunity to attend reputable conferences, courses and to connect with people in a more relaxed setting.

I thank to the microscopy, FACS and fish facility for their support.

I would like to thank my fellow labmates Laura Bartolini, Dr. Mariana Guedes-Simões, Anne Merks, Alexander Meyer, Nicola Müller, and Dr. Marie Swinarski for helping me during these years of hard work, for the stimulating discussions and for being such good friends, inside and outside of the lab. Special thanks should be given to Dr. Tareck Rharass for providing me with cell culture insight, useful advices and for the excellent preparation of the first stage of this project. I wish to thank Maike Schulz and Hoang Quynh Mai Phan for their contribution to this project.

Most importantly, I want to thank my parents and to my brother for their moral and emotional support and encouragement throughout my study. I am very grateful for the patience of Philipp P. and my friends who experienced all of the ups and downs of my research.

Contents

Summary

The L-Type calcium channel (LTCC) is a heteromultimeric protein complex with an important function in cardiac biology since it ensures the main entry path for calcium into the cardiomyocytes. Its conductance increases during membrane depolarization, whereas decreases during calcium- and voltage-dependent inactivation. In addition, G protein-coupled receptor (GPCR) signaling provides a further regulatory layer for fine-tuning the LTCC (Catterall, 2000; van der Heyden et al., 2005).

The α1C subunit is the main pore forming subunit of the LTCC, which is expressed at high levels in cardiomyocytes and is encoded by the *CACNA1C* gene (Weiss et al., 2013). It comprises of a cytosolic N- and C-terminal tails and four transmembrane domains, which harbor the ion-selective pore, voltage sensor and gating machinery (Carafoli et al., 2001). Its C-terminal tail (CT) serves as a scaffold for channel modulating molecules downstream of the GPCR signaling, including kinases and phosphatases (Catterall, 2000). Over the past few decades the LTCC regulation via β-AR/G_s protein systems was well demonstrated. However, little attention has been paid to its regulation via alternative GPCR-like systems such as Wnt11/Calcium pathway (Panáková et al., 2010).

The present study provides evidence that Wnt11 signaling regulates the LTCC, hence the electrical gradient formation in developing zebrafish heart. I showed that loss of *WNT11* induces the generation of a CT isoform in A-kinase anchoring protein (AKAP) anchored Protein kinase A (PKA) signaling dependent manner. Systematic analysis of all the AKAP candidates revealed that PKA targeting through AKAP2 to the CT plays a pivotal role in this isoform formation. In developing zebrafish heart Akap2 is indispensable for the proper heart looping and regulates the LTCC localization and abundance. In cooperation with the Wnt11 pathway it establishes the electrical gradient formation, since loss of *akap2* rescued the abnormal cell coupling in *wnt11*-deficient hearts. These findings provide evidence that Wnt11 signaling compartmentalizes LTCC conductance by targeting PKA/AKAP2 required for the proper formation of intercellular cell coupling.

Zusammenfassung

Der L-Typ-Calciumkanal (LTCC) ist ein heteromultimerer Proteinkomplex mit einer wichtigen Funktion in der kardiovaskulären Biologie, da dieser die hauptsächliche Eintrittsmöglichkeit von Calcium in Herzmuskelzellen sicherstellt. Die Leitfähigkeit des LTCC steigt während der Membrandepolarisation und sinkt während der Calcium- oder Spannungsabhängigen Inaktivierung. Darüber hinaus stellt der G Protein-gekoppelte Rezeptor (GPCR) Signalweg eine weitere regulatorische Ebene zur Feinjustierung des LTCC dar (Catterall, 2000; M. a G. van der Heyden, Wijnhoven, & Opthof, 2005).

Die α1C Untereinheit ist hauptursächlich für die Porenbildung des LTCC, wird in großen Mengen in Herzmuskelzellen exprimiert und vom *CACNA1C* Gen kodiert (Weiss et al., 2013). Die α1C Untereinheit umfasst einen zytosolischen N- und C-terminalen Schwanz und vier Transmembrandomänen, welche die ionenselektive Pore, den Spannungssensor und die Gating-Maschinerie beherbergen (Carafoli et al., 2001). Sein C-terminaler Schwanz (CT) dient als Gerüst für kanalmodulierende Moleküle stromabwärts des GPCR-Signalwegs, einschließlich Kinasen und Phosphatasen (Catterall, 2000). In den letzten Jahren wurde die Regulation des LTCC durch das β-AR/G_s Proteinsystem ausführlich bewiesen. Jedoch ist der Regulation durch das alternative GPCR-ähnliche System, wie dem Wnt11/Calcium Signalweg, dabei wenig Aufmerksamkeit zugekommen (Panáková et al., 2010).

Die vorliegende Studie erbringt Nachweise, dass der Wnt11-Signalweg den LTCC reguliert, und damit einhergehend die elektrische Gradientenbildung im sich entwickelnden Zebrafisch Herz. Ich habe gezeigt, dass der Verlust von *WNT11* zur Erzeugung einer CT Isoform führt, abhänging von der A-Kinase Ankerprotein (AKAP)-verankerte Protein Kinase A (PKA)-Signalgebung. Eine systematische Analyse aller AKAP-Kandidaten ergab, dass PKA über AKAP2 auf den CT abzielt und so eine entscheidende Rolle bei der Bildung dieser Isoform spielt. Im sich entwickelnden Zebrafischherzen ist Akap2 unentbehrlich für das Looping des Herzens und reguliert die Lokalisation sowie Häufigkeit des LTCC. Zusammen mit dem Wnt11-Signalweg wird die elektrische Gradientenbildung etabliert, da der Verlust von akap2 die abweichende Zellkopplung in *wnt11*-defizienten Herzen wiederherstellt. Diese Erkenntnisse erbringen den Beweis dafür, dass der Wnt11-Signalweg die Leitfähigkeit des LTCC kompartmentalisiert, indem er auf die AKAP2/PKA-Interaktion abzielt, welche für die korrekte Bildung der interzellulären Kopplung benötigt wird.

1 Introduction

1.1 The L-type calcium channel function and structure

The voltage-dependent calcium channels are a highly conserved family of ion channels and play a central role in regulating the electrical and biochemical properties of neurons, endocrine and muscle cells, since they ensure predominant route for calcium entry into the cells. Based on high voltage activation, slow voltage inactivation, and inhibition by calcium antagonist drugs we can distinguish between the major channel types, which are L-, N-, P-, Q-, R- and T-types (Reuter, 1983; Reuter et al., 1982). The L-type calcium channels (LTCCs) are the most typical in a wild range of cell types beside the T-type, while the other types are more common in neurons. The LTCCs are sensitive to dihydropyridines and depending on their abundance in the different cell types they are divided into four classes. The $Ca_v1.1$ is common in skeletal muscle, the $Ca_v1.2$ in cardiac muscle, endocrine cells and neurons, the $Ca_v1.3$ in endocrine cells and neurons, and the $Ca_v1.4$ in the retina.

Activation of the $Ca_v1.2$ channels, which are the most abundant in cardiomyocytes upon membrane depolarization induces a range of intracellular events. Calcium influx establishes action potential duration and triggers calcium induced calcium release from the sarcoplasmic reticulum (SR) via ryanodine receptor 2 (RyR_2) (Fabiato, 1985). The amplified calcium signal subsequently promotes excitation-contraction, excitation-secretion and excitation-transcription coupling (Carafoli et al., 2001; Clapham, 1995; Dirksen & Beam, 1999). In parallel, feedback loops ensure the channel inhibition that can result in calcium- or voltage-dependent inactivation. Eventually, the cycle is terminated by the calcium reuptake by SR via SR Ca^{2+}-ATPase (SERCA) and Phospholamban (PLN), and calcium extrusion via Na^+/Ca^{2+} exchanger (NCX) (Figure 1). In addition, G Protein-Coupled Receptor (GPCR) signaling provides a further regulatory layer for fine-tuning the channel.

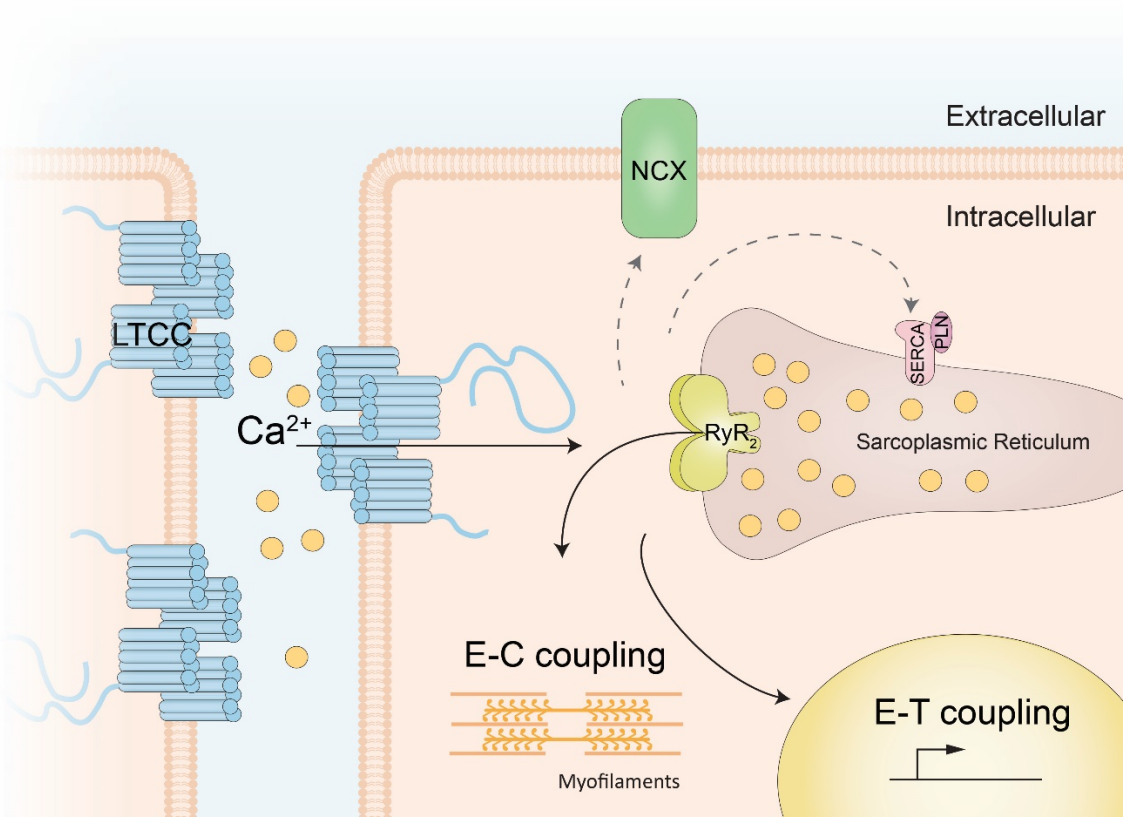

Figure 1: Schematic representation of Ca^{2+} fluxes in cardiomyocytes. Upon depolarization, the calcium influx trough the LTCC triggers the calcium release from the SR, and induces excitation-contraction (E-C) and excitation-transcription (E-T) coupling (full arrows). The baseline concentration of intracellular calcium after inactivation of the LTCC is restored via calcium re-uptake by SERCA and PLN, and extrusion by NCX (dashed arrows). LTCC- L-type calcium channel, NCX- Na^{+}/Ca^{2+} exchanger, RyR_2- Ryanodine receptor 2, SERCA- Sarcoplasmic Reticulum Ca^{2+}-ATPase, PLN- Phospholamban.

The LTCC is a heteromultimeric protein complex that in cardiomyocytes consists of a transmembrane α1C subunit, an intracellular β subunit, and $\alpha 2\delta$ subunit, which is associated with the α1C subunit via disulfide bridges. In other cell types it includes an additional transmembrane γ subunit (Ellis et al., 1988; Takahashi et al., 1987). The α1C subunit (~250 kDa) is the main pore forming subunit, comprises of a cytosolic N- and C-terminal tails and four transmembrane domains (I-IV), which contain 6 membrane spanning α-helices with a membrane associated loop between helix 5 and 6 (Takahashi et al., 1987). This subunit harbors the ion selective pore, the voltage sensor and the gating machinery, and binding sites for the channel modulating molecules. The C-terminal tail (CT) consists of the calmodulin (CaM) binding pre-IQ and IQ motif, the calcium binding EF-hand, and binding sites for kinases and

phosphatases via the A-kinase Anchoring Protein binding domain (ABD) (Takahashi et al., 1987) (Figure 2).

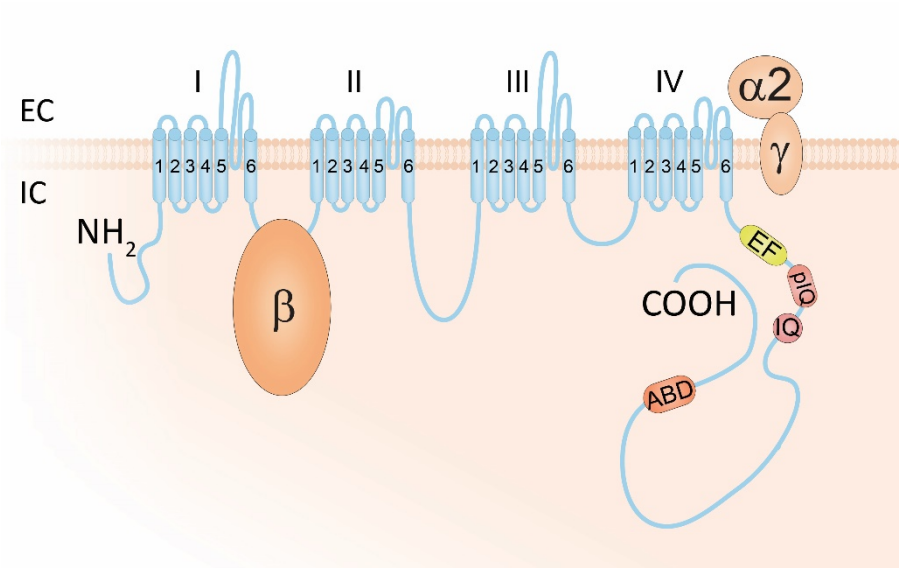

Figure 2: The LTCC complex. Schematic representation of the α1C subunit. It consists of 4 homologous transmembrane domains, each composed of six membrane spanning α -helices and intracellular N- and C-terminal tail. The C-terminal tail consists binding site for A-Kinase-Anchoring Proteins (ABD - AKAP-Binding-Domain), Calcium (EF hand) and Calmodulin (pre-IQ and IQ domains). EC- extracellular, IC- intracellular.

1.2 LTCC regulation

In cardiomyocytes the intracellular calcium level changes on a time scale of milliseconds, which requires a dynamic regulation of the LTCC. This is partially achieved via post-translational modifications of the LTCC. It has been shown that in some cases the post-translational modification can induce the cleavage of the CT generating different CT isoforms. These cleaved CT isoforms can translocate into the nucleus, where they can act as transcription factors (TF) and regulate the LTCC expression (Gomez-Ospina et al., 2006; Schroder et al., 2009), with this providing a dynamic regulatory feedback loop. This is supported with data showing that the protein turnover rate of the LTCC is quite high, as it has a half-life of about 3 h (Chien et al., 1995).

1.2.1 Regulation through transcription

The role of the different CT isoforms in the regulation of the *CACNA1C* gene expression, which encodes the α1C subunit, has been implicated across different cell types. Overexpression of the full-length CT (75 kDa) isoform together with full length *CACNA1C* promoter-reporter construct resulted in reduction in the promoter activity. Similarly, overexpression of the 40 kDa distal-CT (dCT) isoform had a greater affinity to represses the channel expression (Schroder et al., 2009). Further analysis of the serum response of the promoter activity revealed that the CT isoforms interact with serum-stimulated transcription factors to regulate LTCC expression. This observation based on the finding that overexpression of either the CT or dCT construct together with *CACNA1C* promoter deletion construct led to the repression of the promoter activity more efficiently in the presence than in the absence of the serum (Schroder et al., 2009).

Further studies revealed that the *CACNA1C* gene has a cryptic promoter in exon 46 (in murine gene). The translation of this transcript is independent from the full-length gene resulting in a 15 kDa dCT isoform. This fragment is also able to translocate into the nucleus where it acts as a TF. Its generation is regulated developmentally. It has been shown that the α1C subunit and this fragment are expressed in complementary pattern in developing brain, which is consistent with the findings that dCT suppresses the *CACNA1C* expression (Gomez-Ospina et al., 2013).

Through their transcriptional activity these different CT isoforms can also regulate the formation of adhesion complexes and junctional contacts. Their generation and nuclear accumulation is regulated developmentally as well as by intracellular calcium (Gomez-Ospina et al., 2006).

1.2.2 Regulation through post-translational modifications

In cardiomyocytes, most of the α1C subunits exist as a shorter isoform as opposed to predicted 250 kDa full-length due to proteolytic cleavage of the CT generating a truncated isoform (210 kDa) and dCT (40 kDa) (De Jongh et al., 1996). In rat α1C subunit (A0A0G2QC25) the cleavage occurs between residues aa1631-1645 (Hulme et al., 2005), and is initiated by calpain-like proteases (Hell et al., 1996). This proteolytic processing results in a non-covalently associated dCT domain, which autoinhibits the

LTCC activity (Gao et al., 2001; Hulme, Yarov-Yarovoy et al., 2006), however the autoinhibition can be relieved upon phosphorylation of the CT (Fuller et al., 2010).

1.2.2.1 Regulation via Protein Kinase A induced phosphorylation

The most thoroughly studied pathway in the LTCC regulation is the β-Adrenergic Receptor (β-AR)/G_s protein coupled signaling (Gao et al., 1997; Jurevicius & Fischmeister, 1996; Sculptoreanu et al., 1993). Upon β-AR stimulation with epinephrine or norepinephrine, guanine nucleotide exchange results in the dissociation of the $G\alpha_s$ subunit from the $G\beta\gamma$. The separated $G\alpha_s$ activates the adenylyl cyclase (AC), which leads to elevated cAMP levels. The inactive Protein kinase A (PKA) holoenzyme comprises two catalytic and dimeric regulatory (RI or RII) subunits. During PKA activation cAMP binds to the regulatory subunit, which releases the catalytic subunits (Pierce et al., 2002). The activated PKA catalytic subunit is then able to phosphorylate its substrates like the CT of the α1C subunit. The phosphorylation by PKA abolishes the autoinhibition of the dCT, since it leads to the dissociation of the non-covalently associated dCT from the proximal-CT (pCT) (Hulme, Yarov-Yarovoy, et al., 2006). As a consequence, the inactivated channels become active, in addition the opening probability of the channels increases (Yue et al., 1990). In accordance with this it has been shown that loss of the dCT greatly increases the channel activity (Wei et al., 1994; Hulme, Yarov-Yarovoy, et al., 2006). Deletion of the dCT fragment abolishes the regulation via β-AR system and leads to severe cardiac hypertrophy and perinatal death in mice (Fu et al., 2011).

Whereas both β_1-AR and β_2-AR positively couple with the stimulatory G_s, only β_2-AR can induce the inhibitory G_i protein coupled signaling (Abramson et al., 1988). Enhanced PKA activity due to β_2-AR/G_s stimulation results in the phosphorylation of the β_2-AR. This phosphorylation induces that the receptor switches its coupling specificity to G_i, hence induces the MAP kinase activation (Daaka et al., 1997). One of the most studied G_i protein-coupled receptor is the Muscarinic receptor. It has been shown that G_i suppresses channel conductance of cardiac cells by activation of phosphatases or by changing cGMP-dependent phosphodiesterase (PDE) activity (Abi-Gerges et al., 1997; Verde et al., 1999; Chen-izu et al., 2000). Consequently, G_i

stimulation inhibits the G_s coupled receptor signaling through reduction of the cAMP levels.

In the last decades, many studies investigated the relevance of the PKA phosphorylation sites on the CT in the LTCC regulation by the β-AR/G_s system, however, it is still not clear to date, which phosphorylation sites are essential for the proper channel regulation. One of the extensively studied PKA phosphorylation site is the serine 1928 (S1928) in murine model, which was initially proposed to play a role in the LTCC regulation via β-AR/G_s system (De Jongh et al., 1996; Ganesan et al., 2006; Hulme, Westenbroek et al., 2006). This was, however, ruled out using knock in mouse with targeted mutation of S1928 to alanine (S1928A), since the mutation had no impact on the channel conductance (Lemke et al., 2008). Recently, it has been shown that high fat diet induced channel activity was abolished in mice expressing the S1928A, suggesting an essential role for α1C phosphorylation at S1928 in stimulating channel conductance in the regulation of metabolism (Nystoriak et al., 2017). In addition, serine 1700 (S1700) was also proposed as an essential phosphorylation site responsible for PKA modulation of the channel (Fu et al., 2014; Fuller et al., 2010; Linghai Yang et al., 2016), but other study reported that PKA phosphorylation of S1700 is not required in the adrenergic regulation of the channel (Lin Yang et al., 2013). Furthermore, another study suggested the relevance of S1574 by PKA phosphorylation in the channel regulation (Minobe et al., 2014), while other paper implicated that none of the aforementioned PKA phosphorylation sites are required for the channel regulation in cardiomyocytes (Katchman et al., 2017). Thus, which PKA phosphorylation sites and what is their precise function in β-AR regulation of the LTCC in cardiomyocytes still remain to be established.

1.2.2.2 Regulation via Protein Kinase C induced phosphorylation

Protein kinase C (PKC) activation is a result of the agonist induced G_q protein coupled receptor stimulation, which leads to phospholipase C (PLC) catalysis. The active PLC generates inositol-1,4,5-triphosphate (IP_3) and diacylglycerol (DAG) via hydrolysis of phosphatidylinositol-4,5-bisphosphate (PIP_2), hence induces the PKC activity (Dorn & Brown, 1999). In contrast to PKA, PKC has variety of effects on the conductance of the LTCC in cardiomyocytes (Lacerda et al., 1988). Phosphorylation of the LTCC by

PKC can either decrease the channel conductance (Satoh, 1995; Zhang et al., 1997) or induce it transiently followed by decrease (Lacerda et al., 1988; Tseng & Boyden, 1991). The cardiac α1C subunit isoform is specifically sensitive to regulation by PKC compared to the brain isoform. The reason behind this phenomenon is that the brain isoform is missing the first 46 amino acids in the N-terminal tail, which contains two crucial amino acid residues, at the position T27 and T31. Mutation of these two threonine residues to alanine revealed that the channel is only sensitive to PKC modulation when both of these residues are phosphorylated (McHugh et al., 2000).

1.2.2.3 Regulation via calcium/calmodulin dependent serine/threonine kinase II induced phosphorylation

The calcium/calmodulin dependent serine/threonine kinase II (CaMKII) becomes activated upon low Ca^{2+} concentration or β-AR stimulation and induces the LTCC phosphorylation (Grimm & Brown, 2010). Two CaMKII phosphorylation sites have been identified. One of them is the S1700, which is also the phosphorylation site of the PKA. The other one is the threonine 1704 (T1704). To assess the importance of these sites in the channel regulation they were mutated to alanine. In the absence of the dCT (CaV1.2 Δ1800), neither S1700A nor A1704A had effect on the LTCC current. However, in the presence of the dCT (CaV1.2Δ1800 + dCT) both mutations decreased the channel conductance. These data indicate that basal channel activity depends on the phosphorylation of these sites (Fuller et al., 2010).

1.2.2.4 Inactivation by dephosphorylation

Dephosphorylation of the LTCC is indispensable for its dynamic regulation, since it antagonizes the protein kinase mediated phosphorylation (Davare, 2000; Ono & Fozzard, 1992; Ono & Fozzard, 1993). It has been demonstrated that Protein Phosphatase 1 (PP1), Protein Phosphatase 2A (PP2A), and Protein Phosphatase 2B (PP2B) play major role in the channel regulation. PP1 and PKA have opposing action, and often share the same substrates (William & Rogers, 2004). Inhibition of PKC signaling can be ensured by PP2A (Hansra et al., 1996). However, both PP2A and PP2B reverse the PKA mediated phosphorylation (Hall et al., 2006; Tandan et al., 2009). Two serine residues, S1928 and S1866, were shown to be dephosphorylated

by PP2A resulting in the decrease of the channel conductance (Hall et al., 2006; Shi et al., 2012).

1.2.2.5 Calcium-dependent inactivation

Many studies have demonstrated that CaM is a crucial mediator of the calcium-dependent inactivation (CDI) of the LTCC. Three domains on the CT have been identified, which play a role in this process; the calcium-binding EF hand, the calmodulin-binding isoleucine-glutamine (IQ) motif, and pre-IQ motif (Zühlke & Reuter, 1998). Upon increment in the intracellular calcium concentration the Ca^{2+} binds to the prebound CaM and accelerates the inactivation of the channel. However, the Ca^{2+}/CaM complex can also induce phosphorylation via the CaMKII, hence facilitates the channel stimulation indirectly. It has been shown that substitution of the isoleucine 1624 (I1624), which is the first amino acid in the IQ motif, to alanine (A) I1624A removed the CDI and promoted the calcium-dependent facilitation of the LTCC. Using CaM mutant (CaM3), which has in three out of four EF-hand alanines instead of aspartates, inhibited the CDI and abolished the calcium-dependent facilitation. These findings suggest that Ca^{2+}/CaM binding to the IQ motif has pivotal role in CDI, and CaM can induce both calcium-dependent inactivation and facilitation of the channel (Zülke et al., 1999).

1.3 A Kinase Anchoring Proteins

It has been shown that only increment in cAMP levels is not sufficient for the proper regulation of the PKA substrates (Bers & Ziolo, 2001). The spatiotemporal regulation of PKA activation is essential for the effective PKA signaling and is achieved by compartmentalization via AKAPs (Manni et al., 2008). At present, there are at least 17 genes annotated in human genome encoding for AKAPs with as many as 89 different isoforms. Despite the poor sequence conservation between the different AKAPs all of them share at least two similar functional properties. On one hand, AKAPs are able to bind to the docking and dimerization domain (D/D) of the regulatory subunit of PKA via a conserved amphipathic helix of 14-18 amino acids (Gold et al., 2006). On the other hand, AKAPs contain specific targeting motifs that direct the AKAPs to structural elements or membranes, which ensure the subcellular localization of the PKA. Based

on their interaction with type-I or type-II PKA regulatory subunit, they are divided into three groups. AKAPs, which only associate with either type-I or type-II, and dual specific AKAPs, which interact with both type of regulatory PKA subunit (Jarnaess et al., 2008). In addition, AKAPs form multivalent signaling complexes by anchoring simultaneously their specific-bound kinases and phosphatases.

1.3.1 AKAPs in cardiomyocytes

Over the past decades many AKAPs have been identified in cardiomyocytes. For instance the AKAP18α, AKAP18δ, AKAP79, AKAP250, Yatio, mAKAP, AKAP-Lbc, AKAP220, dual specific D-AKAP-1 and -2, AKAP95, Synemin, Ezrin, Gravin, Myosprin and Troponin T (Diviani et al., 2011). Each of these AKAPs target PKA signaling to different subcellular compartments, thereby ensuring the specificity and increasing the efficiency of the PKA substrates phosphorylation. Most of these AKAPs are also associated with proteins, which regulate calcium fluxes. mAKAP is involved in regulation of RyR_2 (Marx et al., 2000). Gravin regulates the desensitization of the β_2-AR (Fan et al., 2001). Akap18δ regulates the calcium re-uptake into the SR by forming a supramolecular complex with SERCA and PLN (Lygren et al., 2007). Furthermore, AKAP79 (AKAP150/AKAP5) and AKAP18 (AKAP15/AKAP7) were identified as crucial regulators of LTCC conductance (Gao et al., 1997; Gray et al., 1998). Hence, AKAPs are indispensable in a range of cellular events; in cardiomyocytes specifically coordinating action potential duration and cardiac contraction.

1.3.2 LTCC regulation via AKAP5

In attempt to unify the nomenclature of AKAP protein family, gene name is used throughout the study instead of protein name; for example, AKAP5 is used instead of AKAP79/150 (the human AKAP79 is the homologue of mouse/rat AKAP150 that are encoded by the *AKAP5* gene). The AKAP5 is a membrane targeted scaffold protein, which binds to PKA, PKC, PP2B, N-methyl-D-aspartate receptor, α-amino-3-hyrdoxy-5-methyl-4-isoxazolepropionic receptor, Synapse-associated protein-97 (SAP97), aquaporin water channel, and LTCC (Wong & Scott, 2004). It contains at its N-terminal tail the PKC binding domain (aa 31-52) and PP2B binding domain (aa 81-102), and at its C-terminal tail the type-II regulatory PKA subunit (RII)-binding domain (aa 388-409)

(Klauck et al., 1996). AKAP5 binds to the LTCC via modified Leucine-Zipper (LZ) motif, which are heptad-spaced hydrophobic residues in the C-terminus after the RII-binding domain (Oliveria et al., 2007).

Overexpression of AKAP5 induces the channel activity by promoting the phosphorylation by PKA (Gao et al., 1997). In neurons, the targeting of PKA and PP2B simultaneously by AKAP5 enables a bidirectional regulation of the LTCC (Oliveria et al., 2007). Overexpression of AKAP5 in the presence of HT31 peptide, which disrupts the AKAP-PKA interaction, upon β-AR stimulation reduced the channel activity (Oliveria et al., 2007). However, overexpression of AKAP5 mutant that lacks the PP2B binding motif (PXIXIT) in the presence of HT31 peptide, had no effect on the channel conductance, suggesting that AKAP5 targeted dephosphorylation by PP2B is required for the channel regulation (Oliveria et al., 2007). Using LTCC inhibitor, it has been shown that LTCC activation is required for the nuclear factor of activated T cells (NFAT) nuclear translocation. The NFAT translocation into the nucleus was abolished in neurons where the AKAP5 was downregulated or AKAP5 was lacking the PXIXIT motif. These findings suggest that PP2B anchoring by AKAP5 to the LTCC regulates NFAT signaling (Oliveria et al., 2007). Furthermore, it has been shown in HEK293 cells that AKAP5 targeted PKA phosphorylation mediates the recycling and resensitization of the β_1-AR (Gardner et al., 2006). The phosphorylation of the β_1-AR by PKA is ensured by SAP97, which targets the AKAP5-PKA complex to the receptor (Gardner et al., 2007). This role of AKAP5 was also confirmed in cardiomyocytes using neonatal AKAP5 mutant mice (Li et al., 2013), indicating an indirect effect of AKAP5 in the LTCC regulation. Nevertheless, β-AR stimulation efficiently increased LTCC current in the AKAP5 knockout (KO) adult cardiomyocytes (Nichols et al., 2010), suggesting that AKAP5 is dispensable for this process.

1.3.3 LTCC regulation via AKAP7

AKAP15 and AKAP18 were named after their protein size, however they are encoded by the same gene called *AKAP7* (Gray et al., 1998). AKAP7α and AKAP7β are the short isoforms (AKAP15), while AKAP7γ and AKAP7δ are the long isoforms (AKAP18) (Trotter et al., 1999). AKAP7 forms multivalent signaling complexes with PKA, voltage--gated calcium channels, voltage-gated sodium channels (Wong & Scott, 2004), and

with PKC (Redden et al., 2012). Previous study showed that AKAP7α directly interacts with the ABD of the α1C subunit via modified LZ motif, because either mutation in the LZ motif or in the ABD abolished their interaction. Furthermore, cardiomyocytes transfected with a competing peptide, which specifically blocks the interaction between AKAP7 and the α1C subunit, had modest increment in the LTCC conductance upon β-AR stimulation (Hulme et al.,2003).

It has been shown by Fuller and his colleagues that overexpression of the α1C subunit without the dCT ($Ca_V1.2\Delta1800$) upon β-AR stimulation greatly increases the channel activity. In contrast, coexpression of the $Ca_V1.2\Delta1800$ together with a dCT construct abolishes the channel activity, which supports the autoinhibitory function of the dCT. However, coexpression of both constructs with AKAP7 relieves the inhibition of the dCT via phosphorylation of the S1700, hence induces the LTCC conductance (Fuller et al., 2010). Surprisingly, coexpression of these constructs with AKAP5 upon β-AR stimulation had no effect on the channel activity, which indicates differences between the two AKAPs in the channel regulation. However, coexpression of $Ca_V1.2\Delta1800$, dCT and AKAP5 mutant which lacks the PXIXIT motif upon β-AR stimulation enhanced the channel activity (Fuller et al., 2014). These experiments indicate that the functional differences between AKAP5 and AKAP7 in the channel regulation are based on their ability to form multivalent signaling complexes. Furthermore, both AKAPs bind to the same modified LZ motif on the CT, which indicates potential competition between them. Hence, depending on which AKAP can bind to the channel, offers an additional regulatory layer in the LTCC regulation.

Western blot and qPCR analysis using AKAP7 KO murine heart lysates revealed that the short AKAP7 isoforms (AKAP7α/β) are not present in cardiomyocytes (Jones et al., 2012). In addition, measuring the channel conductance upon β-AR stimulation in AKAP7 KO cardiomyocytes showed similar increment as in the wild-type cells. The same effect was documented in AKAP5/AKAP7 double KO cardiomyocytes (Jones et al., 2012). These results suggest that AKAP5 and AKAP7 are not indispensable in their ability to regulate channel conductance and indicate the existence of other AKAPs in this process.

1.4 Wnt signaling

The Wnt signaling is an evolutionary conserved pathway within metazoan animals and regulates crucial aspects of development. It determines cell fate and polarity and regulates proliferation, migration and organogenesis during embryonic development. At present, 19 *WNT* genes have been identified and classified into 12 subfamilies. The Wnt ligands are secreted glycoproteins, which are divided into two major groups dependent on their ability to induce β-catenin dependent signaling. Based on this we distinguish between canonical (β-catenin dependent) and non-canonical (β-catenin independent) Wnt signaling. However, which signaling pathway becomes active is not exclusively dependent on the WNT proteins, but also on their receptors Frizzled (FZD), and their co-receptors: the low-density lipoprotein receptor related protein 5/6 (LRP5/6), tyrosine kinase-like orphan receptor (Ror2) and receptor-like tyrosine kinase (Ryk) (Hendrickx & Leyns, 2008; Schulte, 2015).

The Wnt canonical signaling is activated upon binding of either WNT1, WNT3A, WNT5A, WNT6, WNT7B and WNT8A (Jiang et al., 2017; Katoh, 2002; Posokhova et al., 2015; Dawson et al., 2013) to FZD and to LRP5/6, which triggers the Dishevelled (DVL) recruitment to the membrane. These events result in Axin being targeted to LRP5/6, and subsequent disassembly of the β-catenin destruction complex that includes Axin, Adenomatosis polyposis coli (APC), Glycogen synthase kinase 3β (GSK3β) and Casein kinase 1α (CK1α). This leads to β-catenin stabilization, accumulation in the cytoplasm, and translocation into the nucleus, where it associates with the TCF/LEF transcription factor (Gordon & Nusse, 2006; Pandur et al., 2002) (Figure 3A).

The Wnt non-canonical pathway regulates cell polarity, migration and convergent-extension movements (Veeman et al., 2003). It can be further divided into two groups. The Planar Cell Polarity pathway (PCP) is activated upon binding of either WNT2, WNT4, WNT5A, WNT7A, WNT11 or WNT16 (Chen et al., 2018; Nalesso et al., 2017; Dawson et al., 2013) to the FZD, however, the downstream signaling does not require LRP5/6 (He et al., 2004). Activation of FZD recruits DVL to the membrane, which initiates two signaling events. One of the branches is activated upon DVL binding to Dishevelled associated activator of morphogenesis 1 (Daam1), which leads to the Rho-associated kinase (ROCK) activation via Rho GTPase. The other branch of the

signaling is independent from Daam1 and stimulates c-Jun N-terminal kinase (JNK) via Rac GTPase (He et al., 2004; Pandur, Maurus, et al., 2002) (Figure 3B).

The second branch of the Wnt non-canonical signaling is the Wnt/Calcium pathway, which increases the intracellular calcium. It has been shown that this increase may occur through pertussis toxin-sensitive G_i protein; upon FZD2 stimulation with WNT5A the PLC levels increased, however treatment with pertussis toxin abolished the PLC increment. This results imply that the FZD activation resulted in the $G\alpha$ dissociation from the $G\beta\gamma$ subunits, and induced the PLC activation (Slusarski et al., 1997). The catalysis of PLC induces the conversion of the PIP_2 into IP_3 and DAG, which together with the increased intracellular calcium concentration stimulate calcium sensitive proteins like CaMKII, PP2B and PKC (Dorn & Brown, 1999). In accordance, the FZD2 activation stimulated the CaMKII and the PKC signaling in a pertussis toxin-dependent manner (Kühl et al., 2000; Li et al., 1999). Furthermore, stimulation of the Wnt/Calcium pathway induced NFAT signaling, which was cancelled by using PP2B blocker suggesting that Wnt/Calcium pathway regulates NFAT signaling on PP2B dependent manner (Saneyoshi et al., 2002). In addition, the Wnt/Calcium pathway can antagonize the canonical Wnt signaling via stimulation of the NFAT signaling (Saneyoshi et al., 2002). Overexpression of G_i rescued the Wnt signaling in FZD2-deficient drosophila embryos, which strengthened the observation that FZD2 may signal through G_i protein (Katanaev et al., 2005) (Figure 3C).

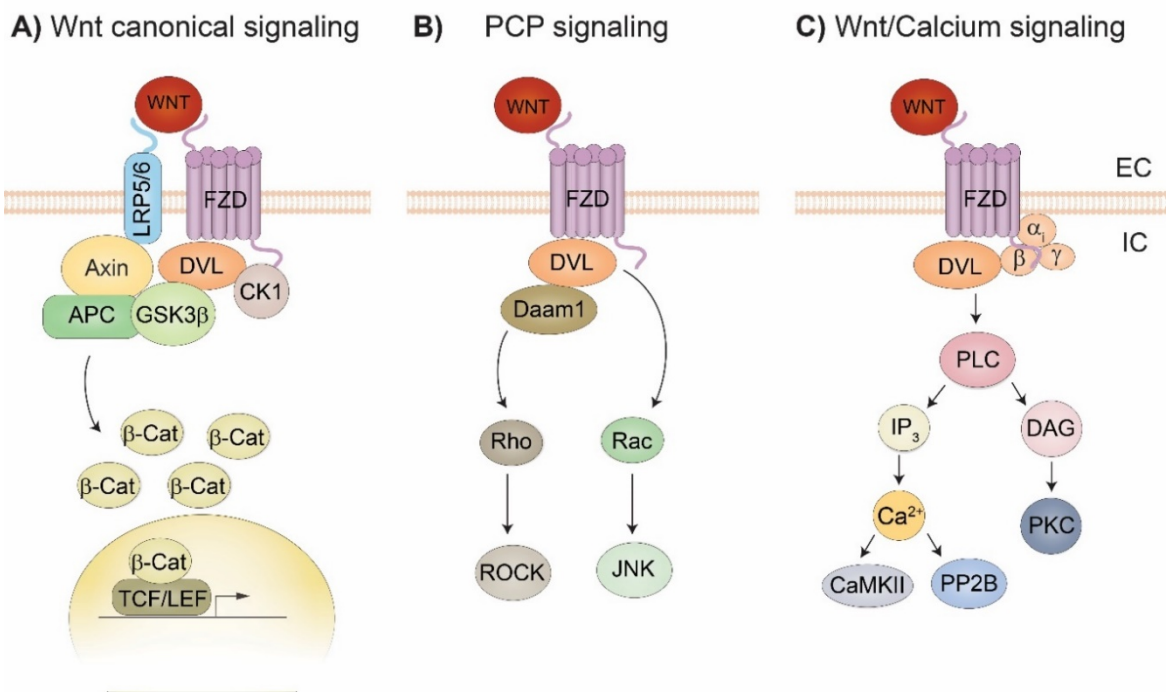

Figure 3: Three main branches of Wnt signaling. (A) Wnt canonical signaling. Wnt induces the disruption of the β-catenin (β-Cat) destruction complex, hence it activates the β-catenin dependent gene transcription. (B-C) Wnt non-canonical pathways. (B) Planar cell polarity (PCP) signaling. Stimulation of PCP leads to the activation of the Rho-associated kinase (ROCK) and c-Jun N-terminal kinase (JNK). (C) Activation of Wnt/Calcium signaling increases intracellular calcium level via Phospholipase C (PLC) catalysis, hence it induces Protein kinase C (PKC), Protein Phosphatase 2B (PP2B) and Ca^{2+}/Calmodulin-dependent kinase (CaMKII) signaling. FZD- Frizzled, DVL- Dishevelled, LRP5/6- Low-density lipoprotein related protein 5/6, APC- Adenomatosis polyposis coli, GSK3β- Glycogen synthase kinase 3β, CK1- Casein kinase 1, Daam1- Dishevelled associated activator of morphogenesis 1, $G\alpha_i$ subunit- α_i, Gβ subunit- β, Gγ subunit- γ, IP_3- inositol-1,4,5-triphosphate, DAG- Diacylglycerol, EC- extracellular, IC- intracellular.

1.4.1 Frizzled receptor couples with G proteins

The seven transmembrane (7TM) receptors belong to the largest membrane receptor family, which includes over 800 genes. These genes encode receptors for hormones, neurotransmitters, chemokines, photoreceptors and sensory receptors. The common feature of these receptors is that they are composed of seven helices of hydrophobic amino acids and couple with heterotrimeric G proteins, therefore they are also called GPCRs. Based on their sequence similarities GPCRs are divided into three groups. Photoreceptors and adrenergic receptors belong to class A, receptors like vasopressin

receptors and parathyroid hormone receptors belong to class B, while class C includes the metabotropic glutamate receptor family (Pierce et al., 2002).

Upon agonist stimulation of the GPCR, it interacts with the heterotrimeric G proteins and induces guanine diphosphate exchange to guanine triphosphate, leading to the dissociation of the $G\alpha$ subunit from the $G\beta\gamma$ (Gilman, 1987). This initiates variety of signaling events dependent on the $G\alpha$ subunit. The $G\alpha$ subunits can be divided into four main groups. The G_s protein induces AC activity, while the G_i protein has the opposite effect, since it inhibits the AC activation. The G_q protein stimulates PLC, and the $G_{12/13}$ protein induces Rho activation (Pierce et al., 2002).

At present, 10 FZD homologues have been identified, which belong to the 7TM receptor family. Despite of the similarities in their structure to other GPCRs, these proteins were separately grouped together with smoothened proteins (Foord et al., 2005). This discrimination is based on that their N-terminal tail consists of a unique cysteine rich domain, which enables them to bind the WNT ligands. Furthermore, FZD lacks DRY motif on its C-terminal tail, which is known to be important for G protein coupling (Schulte, 2010). However, there is an increasing evidence that the FZDs signal through heterotrimeric G proteins (Schulte & Bryja, 2007).

The first indications that G protein couples to FZD were obtained using pertussis toxin, where the increased PKC signaling via FZD2 stimulation was abolished by inhibition of the G_i protein (Slusarski et al., 1997). Investigation, whether other G proteins couple to FZD and influence the PKC signaling revealed that some (FZD3, FZD4, FZD6), but not all (FZD7, FZD8) regulates PKC stimulation via G_i protein dependent mechanism (Sheldahl et al., 1999). Since then only few studies investigated the interaction between FZDs and G protein system. One of the studies is provided by Nichols and her colleagues, who have demonstrated the signaling between different FZDs and G proteins using WNT8-FZD chimeras. The yeast strains that had either G_s, G_i or G_q chimeras were transformed with either WNT8-FZD1, WNT8-FZD2, WNT8-FZD6 or WNT8-FZD7 chimeras. In contrast with the expectations all WNT8-FZD chimeras did preferentially interact with G_s over G_i or G_q (Nichols et al., 2013). In accordance with this, it has been demonstrated that WNT7A induced FZD7 signaling through G_s protein. This observation was confirmed by mass spectrometry analysis using C2C12 cells, where G_s protein showed association with FZD7 (von Maltzahn et al., 2012).

1.4.2 Wnt11 non-canonical signaling

The Wnt11 non-canonical pathway promotes ventral cell fate via NFAT signaling induction (Saneyoshi et al., 2002). It controls cell contact persistence (Witzel et al., 2006), anterior-posterior axis elongation, and convergent-extension movements (Heisenberg et al., 2000; Kim et al., 2008). In addition, almost two decades ago Wnt11 has been identified as a key regulator in cardiac development (Eisenberg & Eisenberg, 1999).

Using *Xenopus* embryos, it has been shown that *wnt11* and *fzd7* have significant overlapping expression in the marginal zone of early gastrula. In addition, Wnt11 synergized with Fzd7 to inhibit gastrulation movements. Co-immunoprecipitation experiment revealed that the myc-tagged Wnt11 binds to ectopically expressed Fzd7. These data indicate that the putative receptor of WNT11 is the FZD7 (Djiane et al., 2000).

Morpholino gene knockdown (KD) of *wnt11* in *Xenopus* embryo revealed that Wnt11 induces early cardiac gene expression (like *nkx2.5*, *gata4*, *tbx5*) required for the normal cardiac differentiation. Since WNT11 acts through Wnt non-canonical pathway, it raised the question, whether the downstream components are involved in the regulation of cardiac gene expression. Treatment of the *wnt11* morphants with either CaMKII, PKC or JNK revealed that none of them could restore the gene expression. However, activation of both PKC and JNK signaling rescued the gene expression, which imply that both Wnt/Calcium and PCP pathways are important during early cardiogenesis (Pandur, Lasche et al., 2002). Furthermore, Wnt11 signaling together with the Wnt canonical signaling are required for the second heart field formation. This result was obtained from differentiating embryonic stem cells, where WNT11 induced the cardiac progenitor development by antagonizing the Wnt canonical pathway (Cohen et al., 2012).

The present study is based on the finding of Panáková and her colleagues, who have demonstrated that loss of Wnt11 signaling results in homogenous conduction velocities all over the developing zebrafish ventricle. Investigation whether the Wnt11/PCP pathway contributes to the electrical gradient patterning, revealed that neither loss of Vangl2 nor Prickle1, which are the core components of the PCP pathway, perturbed the gradient, suggesting that PCP is dispensable for this process. However, the

absence of Wnt11 increased the transient amplitude of intracellular Ca^{2+} concentration ($[Ca^{2+}]_i$) all over the ventricle. Similarly, stimulation of the LTCC activity increased the $[Ca^{2+}]_i$ transient amplitude as loss of Wnt11 did, which implied that Wnt11 might regulate the electrical gradient formation by attenuating the Ca^{2+} influx through the LTCC. Injection of *cacna1c* mutant embryos with *wnt11* morpholino resembled the wild-type conduction phenotype, suggesting that Wnt11 indeed regulates myocardial electrical formation upstream of the LTCC. In addition, loss of Wnt11 enhanced Connexin 43 (Cx43) levels, which were restored in the absence of WNT11 and the LTCC, which strengthened the idea that WNT11 acts upstream of LTCC (Panáková et al., 2010) (Figure 4).

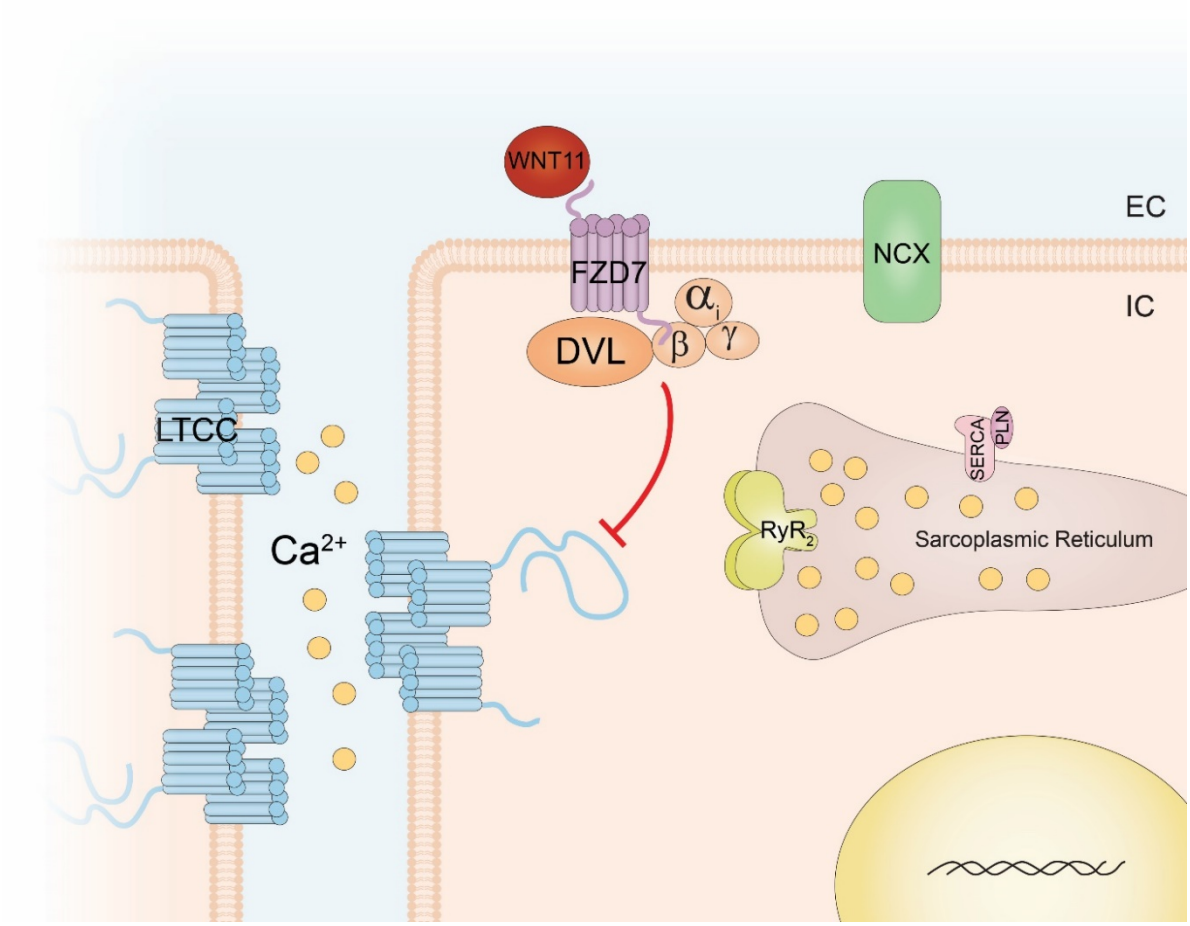

Figure 4: Schematic representation of Wnt11/Calcium signaling in cardiomyocytes. In developing zebrafish ventricle Wnt11 regulates the electrical gradient formation via attenuation of the LTCC conductance. LTCC- L-type calcium channel, NCX- Na^+/Ca^{2+} exchanger, RyR_2- Ryanodine receptor 2, SERCA- Sarcoplasmic Reticulum Ca^{2+}-ATPase, PLN- Phospholamban, DVL-Dishevelled, FZD7- Frizzled 7, $G\alpha_i$ subunit- α_i, Gβ subunit- β, Gγ subunit- γ, EC- Extracellular, IC-Intracellular.

1.5 L-type calcium channel in cardiac disease

The LTCC ensures predominant route for calcium entry into the cells, which shapes the action potential and induces E-C coupling. Furthermore, the calcium can induce many signaling transduction pathways, which have a pivotal role regulating the growth response in the heart. These hypertrophic pathways include the PP2B/NFAT (Molkentin et al., 1998) and PKC/CaMKII regulated histone deacetylase (HDAC) pathways (Vega et al., 2004). Cardiac hypertrophy leads to arrhythmia and congestive heart failure, and eventually to sudden cardiac death. Thus, abnormalities in LTCC functions have implication for cardiac output.

It has been shown that in the failing human ventricular myocytes (F-HVM) the base line phosphorylation, the open probability (P_o) and availability of a single LTCC was increased, hence the single channel current (i_{Ca}) (Schröder et al., 1998). Furthermore, many studies demonstrated the downregulation of LTCC in patients with atrial fibrillation (AF) (Brundel et al., 2001; Lai et al., 1999). Similarly, to these observations, decreased channel density (N) was documented in F-HVM concomitant with unaltered basal calcium current (I_{Ca}) density (Chen et al., 2002). In accordance with the previous finding, these data suggested that in F-HVM the basal calcium current density is maintained by increased open probability of the LTCC ($I_{Ca}=N \cdot P_o \cdot i_{Ca}$) (Chen et al., 2002). However, the studies investigating the LTCC abundance in patients with heart diseases are not always congruent. It has been also shown in human patients with chronic AF that the LTCC abundance was unaltered (Schotten et al., 2003). The linkage between LTCC and hypertrophy was strengthened when application of diltiazem (LTCC inhibitor) rescued the cardiomyopathy in mice, which carry an Arg403Gln missense mutation in one allele of the cardiac myosin heavy chain $\alpha MHC^{403/+}$ (Semsarian et al., 2002), although the underlying molecular mechanisms remained unclear. Despite of these results, clinical trials using calcium channel blockers (CCBs) for heart failure had disappointing effects. More recent study was investigating the outcome of the usage of CCBs in older patients with heart failure with preserved ejection fraction. They have documented that application of CCBs had no association with the end points of the mortality or heart failure hospitalization in these patients (Patel et al., 2014).

Besides the dysfunction of the LTCC, mutations in the *CACNA1C* gene can also lead to congenital heart disease. A novel long QT arrhythmia syndrome associated with

syndactyly was described already in the middle of the 90ties. (Marks et al., 1995). Almost 10 years later Splawksi and his colleagues have identified in patient with the aforementioned syndromes two *de novo* point mutations in the *CACNA1C* gene, which were caused by substitution of glycine with arginine at residue 406 (G406R) and glycine with serine G402S. These mutations result in multisystem disorder, called Timothy syndrome (TS), including arrhythmia disorder associated with dysfunction in multiple organ systems, congenital heart disease, syndactyly, immune deficiency and autism (Splawski et al., 2004; Splawski et al., 2005). Further studies also discussed the relevance of AKAP5/LTCC interaction in TS. AKAP5 is stabilized in the open conformation of the mutant LTCC, hence facilitated Ca^{2+} influx, which eventually resulted in sudden cardiac death. However, ablation of the AKAP5 rescued the gating in mutant LTCC and protected the heart from arrhythmias (Cheng et al., 2011; Dixon et al., 2012).

To develop more effective and specific treatments, it is crucial to improve our understanding of how the LTCC is regulated. It needs to be better defined, which signaling pathways are involved in the channel activation or inhibition, and which scaffolding molecules are able to associate with the channel, thus creating specific microenvironments.

2 Aims of the Thesis

Although the compartmentalized PKA activity via the β-AR systems and its effect in the L-type calcium channel regulation was demonstrated over the past few decades, little attention has been paid to the regulation via alternative GPCR-like systems such as the Wnt11 non-canonical pathway. The observation that Wnt11 regulates the LTCC in developing zebrafish heart (Panáková et al., 2010) brought novel insights into our understanding of the interactions between signaling pathways and ionic cues in the epithelial biology and organ development, and opened a new area of research with many questions remained to be answered. How does Wnt11 modulate the LTCC function? Is the interaction between Wnt11 and LTCC direct or indirect? Is Wnt11 affecting the expression levels of the LTCC or modulating the channel function post-translationally?

This study set out to explore the molecular mechanisms that lead to the attenuation of LTCC conductance by non-canonical Wnt11 signaling, and how this machinery affects the intercellular electrical coupling and cardiac function. The specific aims of the presented study were:

- Determine whether Wnt11 regulates the expression and/or localization of the LTCC.
- Identify the core components downstream of the Wnt11/Calcium pathway in the regulation of the LTCC.
- Analyze whether the identified downstream components contribute to the establishment of the myocardial electrical gradient in developing zebrafish heart.

This study not only improves our understanding of fundamental role of Wnt11 in regulating LTCC function, but also brings new insights into basic cardiac biology as well as pathophysiology of common cardiovascular diseases such as arrhythmias and sudden cardiac death.

3 Results

3.1 Establishment of cell based model to study Wnt11-LTCC interaction

To study Wnt11-LTCC interaction I utilized rat heart-derived myoblast cell line H9c2. Although H9c2 cells are not able to beat spontaneously, these cells have the advantage of being immortalized and animal-free alternative to study transmembrane signal transduction in cardiomyocytes. In these cells, the LTCC shows the classical characteristics of being sensitive to dihydropyridines and its open probability can be enhanced by isoproterenol (ISO) (Hescheler et al., 1991). Furthermore, *in vitro* study demonstrated that they show similar hypertrophic response as neonatal rat ventricular myocytes (NRVMs) (Watkins et al., 2011). First, I had to establish applicability of studying the molecular Wnt11-LTCC interaction in this cell model. I showed in collaboration with Dr. Tareck Rharass that the components of the Wnt11 signaling pathway including *WNT11*, its putative receptor *FZD7*, *DVL*1/2/3 and *β-CAT* are expressed in H9c2 cells. I also confirmed the expression of the *CACNA1C* gene, which encodes the α1C subunit of the channel, which is in line with published data investigating the electrophysiological properties of H9c2 cells (Hescheler et al., 1991). Furthermore, I showed that these cells are expressing *TROPONIN-T* (*TPM*), which confers calcium sensitivity, and *MYOGENIN* (*MYOG*), which is a typical muscle-specific transcription factor (Figure 5A). It has been shown by Panáková and her colleagues that the absence of *wnt11* results in increment in Connexin 43 (Cx43) levels in developing zebrafish embryos (Panáková et al., 2010). To confirm this observation in H9c2 cells, first the efficiency of the *WNT11* KD was corroborated using siRNA (Figure S1A). Next, immunoblotting of the lysates of untreated and *WNT11* siRNA transfected cells was performed (Figure 5B). Quantification of the CX43 amount in comparison to β-ACTIN amount showed that loss of *WNT11* leads to increased levels of CX43 in a similar fashion as in zebrafish embryonic hearts (Figure 5C). Taken together, the H9c2 cells express all the necessary components of the Wnt11 signaling and react similarly to the reduced levels of *WNT11* as zebrafish embryonic hearts making them a suitable model for studying the molecular interaction between Wnt11 and LTCC.

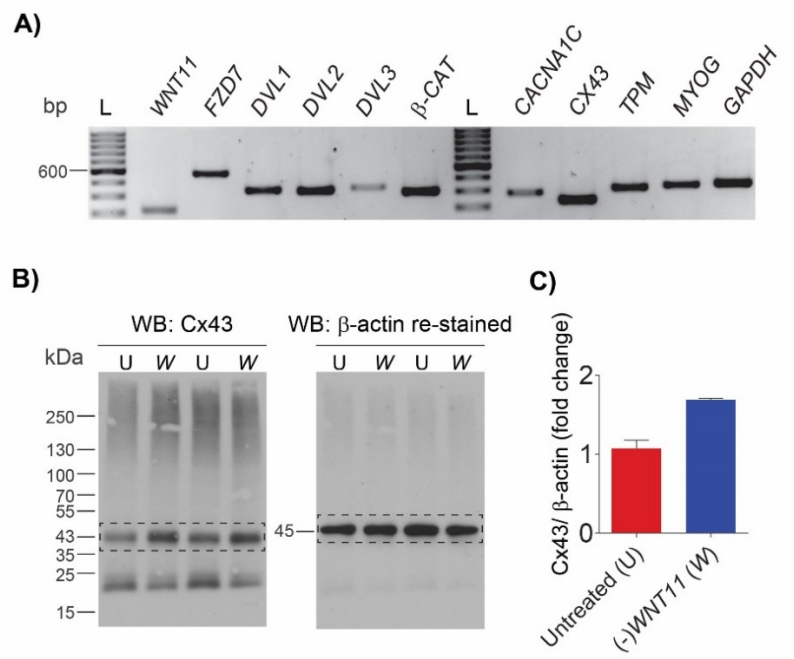

Figure 5: H9c2 cells are a suitable model to study Wnt11-LTCC interaction. (A) RT-PCR of cDNA of the indicated genes. (B) Western blot (WB) analysis of Connexin 43 (Cx43) in lysates of untreated control (U) and *WNT11* siRNA transfected (*W*) H9c2 cells. Cx43 was detected using anti-Cx43 antibody; the membrane was re-stained with anti-β-actin antibody. ROIs delimited with dashed line show relative mobility of Cx43 (left) and β-actin (right). C) Column graph displays the Cx43 protein levels that were normalized to β-actin. (Mean ± SD; N = 2). FZD-Frizzled; DVL- Dishevelled; β-CAT-β-Catenin; TPM- Troponin T, MYOG- Myogenin, GAPDH- Glyceraldehyde 3-phosphate dehydrogenase.

3.2 Wnt11 signaling prevents the CT from proteolytic processing

3.2.1 Wnt11 signaling does not alter LTCC, but dCT expression

As aforementioned, the CT isoforms (75 kDa, 40 kDa) of the α1C subunit can translocate into the nucleus, where they act as a TF or co-factors (Gomez-Ospina et al., 2006; Schroder et al., 2009). Furthermore, in brain tissue there is another dCT isoform (15 kDa), which can be translated from an independent transcript generated from a cryptic promoter (in exon 46 in murine gene) (Gomez-Ospina et al., 2013). This isoform is also able to translocate into the nucleus and act as a TF (Gomez-Ospina et al., 2013). In the light of these facts, to elucidate whether Wnt11 signaling affects the expression of the different isoforms of the α1C subunit, I used three distinct TaqMan probes targeting exon 18, 39 and 45 of the *CACNA1C* gene. These targeting sites correspond to II-III loop, proximal-CT (pCT) and distal-CT (dCT) of the α1C subunit as

it is represented in Figure 6A. Of note, the rat *CACNA1C* (ENSRNOT00000052017.6) exon 45 is identical with mouse (ENSMUST00000186889.6) exon 47. Using *CACNA1C* siRNA the specificity of the TaqMan probes were validated (Figure S1A). qPCR analysis revealed that downregulation of *WNT11* have effect neither on the LTCC nor on the CT expression levels. However, the expression of the dCT is slightly decreased (Figure 6B).

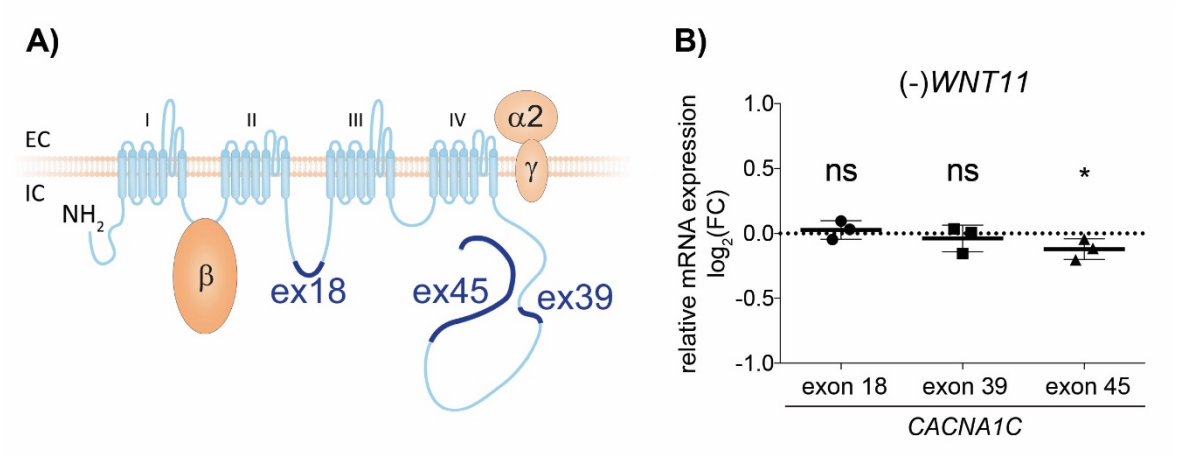

Figure 6: Wnt11 signaling does not alter LTCC, but dCT expression. (A) Schematic representation of the rat LTCC complex with the highlighted sites for the TaqMan probes on the α1C subunit (ENSRNOT00000052017.6). EC- extracellular, IC- Intracellular (B) Relative mRNA expression of *CACNA1C* gene was measured in Scramble or *WNT11* siRNA transfected H9c2 cell via quantitative RT-PCR and normalized to the relative mRNA expression of *GAPDH* in Scramble siRNA transfected cells. Data represent the fold change of $\log_2$ (2^-ΔΔCt) of the interested genes. (Mean ± SD of N = 3 experiments; ns *P*(*CACNA1C* exon 18)=0.4258; ns *P*(*CACNA1C* exon 39)=0.4258; **P*(*CACNA1C* exon 45)=0.0195; Wilcoxon test).

3.2.2 Wnt11 has no effect on the localization or abundance of LTCC

To investigate whether Wnt11 regulates the LTCC on the protein level, I performed immunostaining experiments in collaboration with Dr. Tareck Rharass. First, I used an anti-II-III-loop antibody, which recognizes the intracellular loop between transmembrane II and III domains of the α1C subunit (Figure 7).

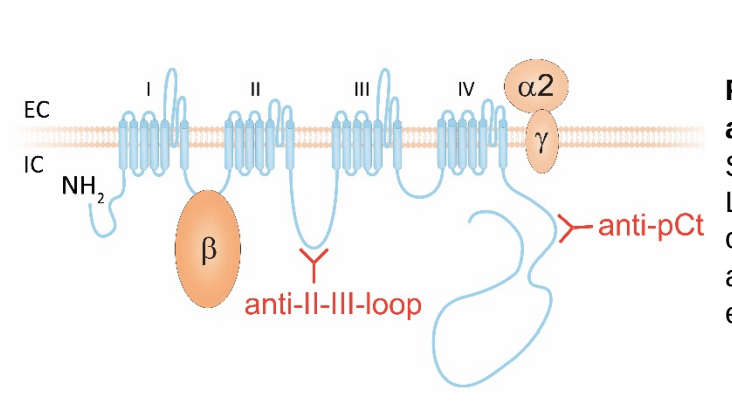

Figure 7: **Binding sites of the antibodies on the α1C subunit.** Schematic representation of the rat LTCC complex with the binding sites of the anti-II-II-loop and anti-pCt antibodies on the α1C subunit. EC- extracellular, IC- Intracellular.

The localization of the α1C subunit was unaltered in the transfected cells either with Scramble (Figure S2A) or with *WNT11* siRNA (Figure 8A) compared to the untreated cells. In these cases, the α1C subunit showed exclusively membrane and cytoplasmic localization. Transfecting the cells with *CACNA1C* siRNA reduced the protein levels of the α1C subunit compared to untreated cells (Figure S2A) corroborating the specificity of the antibody.

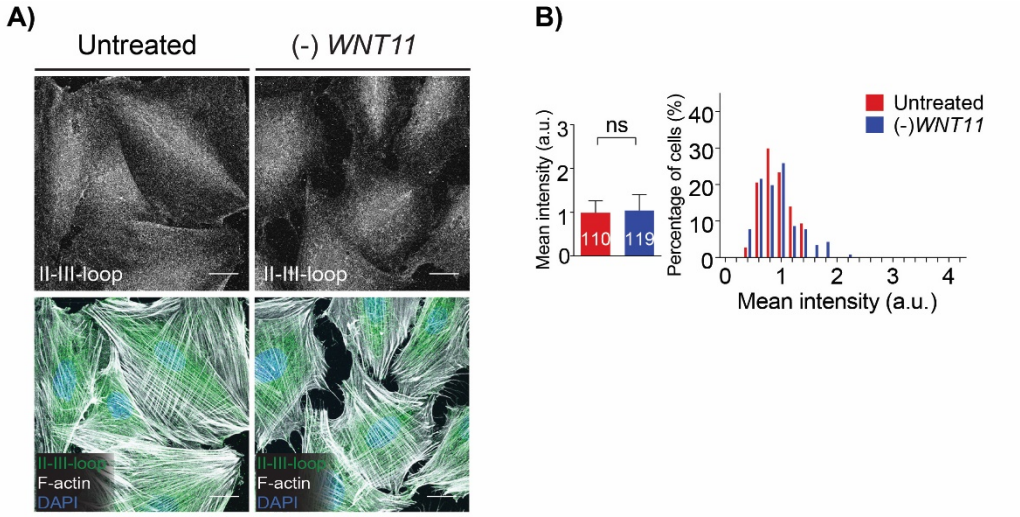

Figure 8: Wnt11 has no effect on the localization or abundance of the LTCC. (A) Maximum intensity projection of confocal images of untreated and *WNT11* siRNA transfected H9c2 cells, immunostained with anti-II-III-loop (Millipore) (gray/green), anti-F-actin (gray) antibodies, and DAPI (blue). (N ≥ 3 experiments; n ≥ 110) (B) Quantification of mean intensity of II-III-loop antibody in the whole cell. Data of column graphs expressed as mean ± SD of N ≥ 3 experiments and n ≥ 110 (ns *P* =0.2443; Welch's t test) as it is represented in the columns. Frequency distribution plot demonstrates the percentage of the cell population with the corresponding mean intensity. The scale bar represents 20 μm.

Measuring the fluorescent intensity of the II-III-loop antibody staining in the whole cell using the F-actin staining as a mask revealed that the channel abundance is similar in untreated compared to *WNT11* KD cells (Figure 8B). This result is in line with the qPCR data, since Wnt11 had no effect on the expression of transmembrane pore-forming isoform. These data suggest that in H9c2 cells the α1C subunit localization and abundance is independent of Wnt11 signaling.

3.2.3 Wnt11 signaling regulates the formation of the CT isoform

To determine the CT localization within the cells I used, in collaboration with Dr. Tareck Rharass, anti-pCt antibody, which showed specificity in recognition of the α1C subunit (Figure S2B). This antibody recognizes the pCT, therefore it detects the full-length α1C subunit as well as the cleaved CT isoform, but not the dCT fragment (Figure 7). In contrast to the II-III loop antibody in untreated cells the signal appeared also in the nucleus. Surprisingly, downregulation of Wnt11 signaling pathway achieved with *WNT11* or *FZD7* siRNA treatment led to enhanced nuclear localization of the CT fragment (Figure 9A), in which cases the intensity of the pCt staining increased by 71% in the absence of *WNT11* (Figure 9C) and by 43% in the absence of *FZD7* (Figure 9D) compared to untreated cells. Throughout the whole nucleus CT formed punctate pattern as it has been previously shown (Gomez-Ospina et al., 2006), and in addition it accumulated in 2 to 3 bigger punctae per cell. Co-staining with nucleolin antibody (anti-Nuc) revealed that the loss of Wnt11 signaling specifically induced the CT isoform localization in the nucleoli (Figure 9B). Although this phenomenon has also occurred in untreated cells, the reduction of Wnt11 signaling led to significant increase and more homogeneous cell population regarding the CT localization in the nuclei compared to untreated cells. The frequency distribution plots show clearly that higher percentage of cell population has increased accumulation of pCt in the nucleoli. Since in the absence of *WNT11* I could not detect any differences in the mRNA expression levels of the CT, but clear changes occurred in the CT localization within the cells compared to untreated cells suggesting that Wnt11 regulates the cleavage of the CT. The fact that loss of Wnt11 signaling was inducing the CT nuclear localization indicates that Wnt11 signaling may prevent the CT from proteolytic processing.

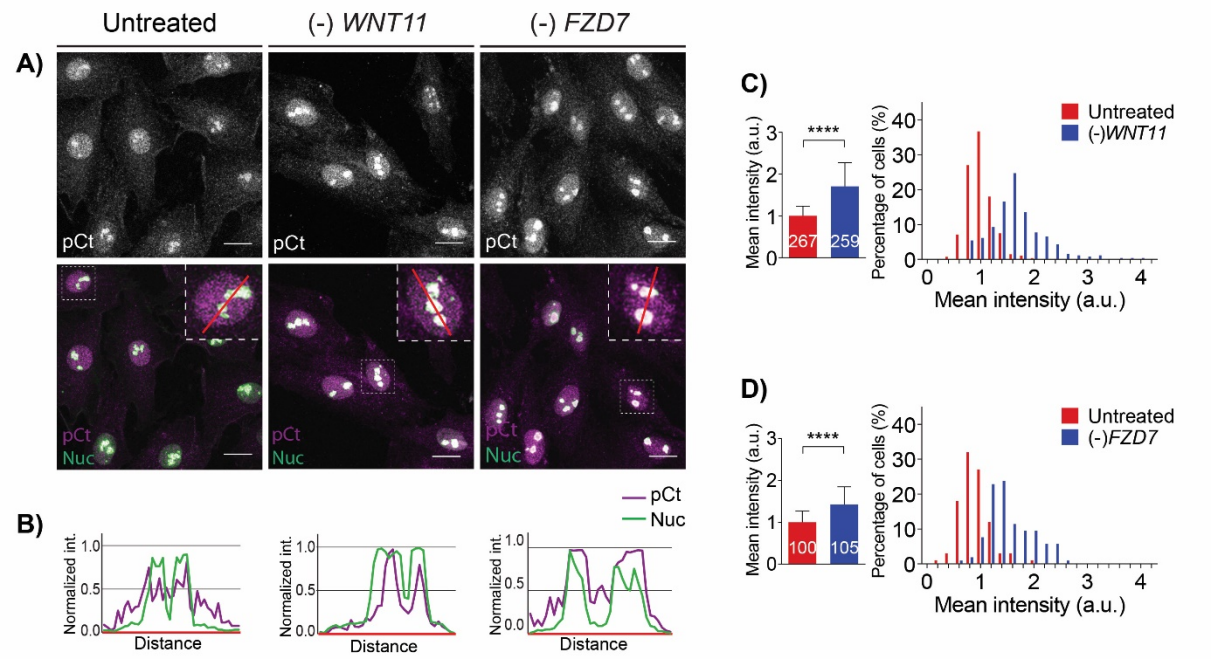

Figure 9: Wnt11 signaling regulates the formation of the CT isoform. (A) Maximum intensity projection of confocal images of untreated, *WNT11* or *FZD7* siRNA transfected H9c2 cells immunostained with commercially available anti-pCt (Abnova) (gray/magenta) and anti-Nuc (green). (N ≥ 3 experiments; n ≥ 100). (B) Line-scan analysis of pCt and nucleolin staining intensities in the nucleus. (C-D) Quantification of mean intensity of pCt antibody in nucleoli of H9c2 cells. Data of column graphs expressed as mean ± SD of N ≥ 3 experiments and n ≥ 100 (****P<0.0001; Welch's t test). Frequency distribution plots demonstrate the percentage of the cell population with the corresponding mean intensity. The scale bar represents 20 μm.

3.3 AKAP anchored PKA signaling regulates the CT formation downstream of Wnt11 pathway

3.3.1 PKA signaling stimulation leads to the CT isoform generation

Over the past few decades many studies have demonstrated that β-AR/G_s protein signaling regulates the LTCC activity through the post-translational modification of the dCT of the α1C (Fu et al., 2011; Ganesan et al., 2006), but our understanding of the regulation of the CT isoform via this pathway remains incomplete. To examine the role of the β-AR/G_s system in the CT isoform formation, the cells were exposed to β-AR pathway agonist, isoproterenol (ISO) treatment for 3 minutes prior to fixation. Induction of this pathway enhanced the CT isoform generation (pCt intensity increased in the nucleoli by 48%) in a similar fashion as the loss of Wnt11 pathway did (Figure 10A and

10B). The stimulation of β-AR pathway subsequently induces the phosphorylation of the LTCC by increasing local PKA activity, and leads to the dCT isoform generation (Hulme, Yarov-Yarovoy, et al., 2006).

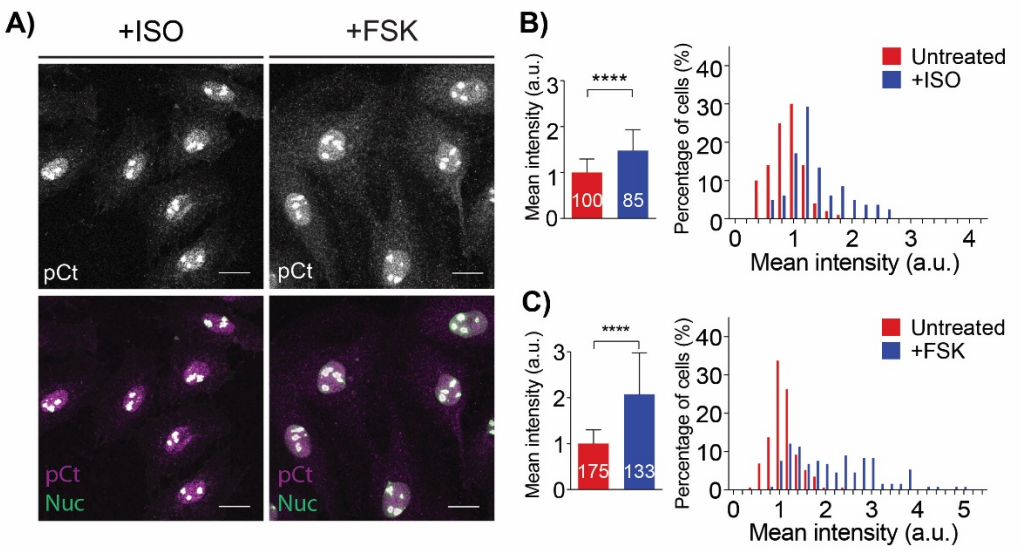

Figure 10: PKA signaling stimulation leads to the CT isoform generation. (A) Maximum intensity projection of confocal images of H9c2 cells immunostained with anti-pCt (Abnova) (gray/magenta) and anti-Nuc (green). Cells were treated with 4 μM ISO for 3 minutes or with 10 μM FSK for 1 hour. (N ≥ 3 experiments; n ≥ 85). (B-C) Quantification of mean intensity of pCt antibody in nucleoli of H9c2 cells. Data of column graphs expressed as mean ± SD of N ≥ 3 experiments and n ≥ 85 (****P <0.0001; Welch's t test). Frequency distribution plots demonstrate the percentage of the cell population with the corresponding mean intensity. The scale bar represents 20 μm.

To explore whether PKA activity affects the CT generation, the cells were treated with PKA agonist, Forskolin (FSK) at 10 μM concentration for 1 hour. The FSK exposed cells showed increment in phosphorylated PKA substrates amount compared to untreated cells (Figure 11) as well in the pCt intensity (increased by 101%) (Figure 10A and 10C). These data indicate that β-AR induced PKA signaling regulates the cleavage of the CT.

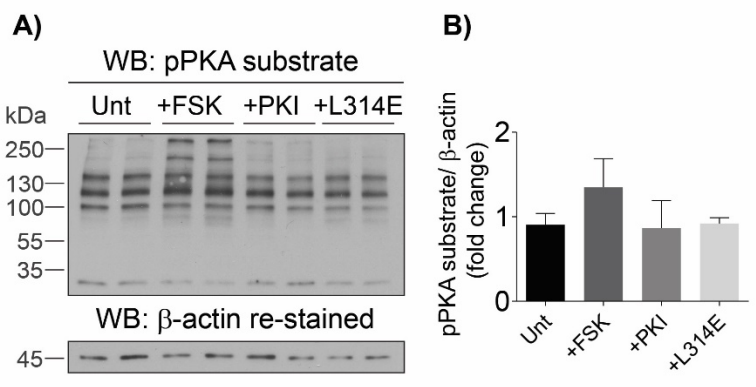

Figure 11: Phosphorylation levels of the PKA substrates upon drug treatment. (A) Western blot (WB) analysis of phosphorylated PKA substrates in lysate of untreated control (Unt) and of FSK, PKI or L314E treated H9c2 cells by using anti-pPKA substrate antibody. Below, cell lysate lanes were run on the same gel, but the membrane was cut as it is indicated by the gap and developed with β-actin. (B) Column graph represent the phosphorylated PKA substrates amount, which was normalized to β-actin amount. (N ≥ 2 experiments).

3.3.2 Wnt11 signaling regulates the CT isoform generation via AKAP anchored PKA signaling

The next question was whether there is an interaction between PKA and Wnt11 signaling in the regulation of the CT formation. To address this question, I used Protein kinase inhibitor (PKI) peptide (a gift from PD Dr. Enno Klußmann). PKI can specifically inhibit the free catalytic subunit of the PKA, hence obstructs the phosphorylation of the PKA substrates (Figure 11). Compared to cells with the reduced Wnt11 signaling, in cells treated with 10 μM PKI for 1 hour with the simultaneous *WNT11* siRNA treatment, the CT isoform formation was reduced to basal levels (pCt intensity only increased by 9%). The phenotype of these cells regarding the CT formation was very similar to the untreated cells (Figure 12A and 12B).

It has been shown that AKAP proteins play important role in the LTCC regulation, since they regulate local PKA activity by anchoring the PKA to its substrates. To investigate AKAP anchored PKA signaling in the CT formation the cells were treated with L314E peptide (a gift from PD Dr. Enno Klußmann). This membrane-permeable peptide is a general AKAP inhibitor due to its ability to abolish the interaction between the PKA regulatory subunit and any AKAP (Figure 11) (Hundsrucker et al., 2006). Cells treated with 100 μM L314E for 1 hour, in the absence of Wnt11 signaling partially rescued the loss of WNT11 phenotype. Although cells still showed slight increment in pCt intensity (pCt only increased with 13%) in comparison to untreated cell (Figure 12A and 12C),

the frequency distribution plots show a clear shift in the cell distribution that is similar to the untreated cell population. On one hand, these data suggest that Wnt11 regulates the CT isoform generation via AKAP anchored PKA signaling. On the other hand, the data also indicate that Wnt11 signaling may antagonize the β-AR/G_s system.

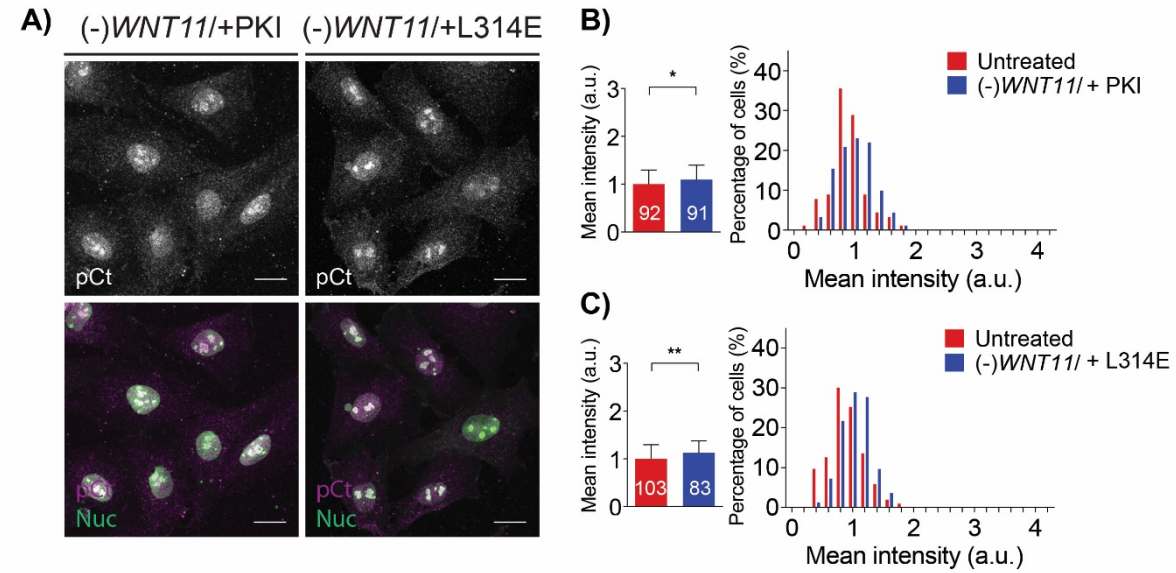

Figure 12: Wnt11 signaling regulates CT formation via AKAP anchored PKA signaling. (A) Maximum intensity projection of confocal images of H9c2 cells immunostained with anti-pCt (Abcam) (gray/magenta) and anti-Nuc (green). Cells were treated with 10 μM PKI or with 100 μM L314E for 1 hour in the presence of *WNT11* siRNA. (N ≥ 3 experiments; n ≥ 83). (B-C) Quantification of mean intensity of pCt antibody in nucleoli of H9c2 cells. Data of column graphs expressed as mean ± SD of N ≥ 3 experiments and n ≥ 83. Frequency distribution plots demonstrate the percentage of the cell population with the corresponding mean intensity. (**P*=0.0363; ***P*=0.0016; Welch's t test). The scale bar represents 20 μm.

3.4 AKAP2 anchored PKA signaling regulates the CT formation downstream of Wnt11

3.4.1 Identification of AKAP candidates which might have a role in the CT formation

The fact that some AKAP proteins function in the LTCC regulation has been already demonstrated, however, these data are not completely consistent. The underlying reason could be that several studies assume AKAP function in the LTCC regulation based on the observations using different cell lines like oocytes, skeletal muscle cells, HEK293 cells, tsA-201 cells, hippocampal neurons or cardiomyocytes from different origins. Obviously, AKAPs that may target PKA to the LTCC in neurons, are not

necessarily the same that may target PKA to the LTCC in cardiomyocytes. To identify AKAPs that are important in the CT isoform regulation in cardiomyocytes, I performed a midi-screen in collaboration with Mai Phan. In human 17 *AKAP* genes are annotated and I focused on those ones, which show heart specific expression; 10 *AKAPs* showed heart specific expression based on Human Protein Atlas expression data. Next, using Gene Ontology 6 *AKAP*s were selected, which are membrane localized and have PKA and ion-channel binding domain. The last criterion was that the selected *AKAP* must have zebrafish orthologue. Based on these requirements the following *AKAP*s were selected: *AKAP2, AKAP6, AKAP10, AKAP11, AKAP12* and *AKAP13.* TBLAST of these genes against the zebrafish genome using Ensembl Genome Browser revealed that the *AKAP2* zebrafish orthologue is called *palm2-201/202.* The zebrafish *palm2-203* transcripts from the same locus encodes Paralemmin 2, or Palm2 (ENSDARG00000099005), a completely different protein from Akap2; the transcripts can also exist in a readthrough form as Palm2-Akap2. To avoid confusion, I am going to refer to zebrafish *palm2*-201/202 as *akap2* for the rest of the study.

The literature search revealed that most of the selected AKAPs are required for the maintenance of homeostasis in the heart, and that none of them were studied in the context of LTCC regulation (Diviani et al., 2011). I extended this list with *AKAP5* and *AKAP7*, since many studies indicated their role in the LTCC regulation (Fuller et al., 2014; Jones et al., 2012; Oliveria et al., 2007), although *akap5* is not encoded in the zebrafish genome.

The next aim was to determine the relative mRNA amount of the different *akap*s in cardiomyocytes (CM) in comparison with each other. To separate the CMs from the non-CMs, *myl7:EGFP* transgenic zebrafish line was utilized (Huang et al., 2003), where the *myl7* promoter drives the heart specific expression of the *EGFP*. Fluorescence-activated cell sorting (FACS) of the EGFP positive cells followed by qPCR analysis revealed that in zebrafish embryos *akap6* is not expressed in the heart, while *akap11* is only expressed in CM cells. Furthermore, *akap2*, *akap7*, and *akap12* showed significantly higher expression levels in CMs compared to non-CMs (Figure 13A). Comparison of the relative mRNA amount of the *akap*s in the CM revealed that *akap12* is the most abundant with 41.8 %, and followed by *akap2* with 27.1%, *akap11* with 15.8%, *akap10* with 11.2%, *akap7* with 3.0%, and *akap13* with 1.1% (Figure 13B). These results are consistent with the expression data obtained by Tomo-seq (Burkhard

& Bakkers, 2018), where the highest mRNA expression levels in CMs considering *akap*s also belong to *akap12* and *akap2.* In H9c2 cells, all eight *AKAP* candidates are expressed. Although, *AKAP*s showed different expression pattern in these cells, again *AKAP12* (82.3%) and *AKAP2* (6.6%) were the most abundant from the selected *AKAP*s. The rest of the *AKAP*s were expressed in small, but not negligible quantity, *AKAP6* with 3.1%, *AKAP13* with 2.4%, *AKAP11* with 2.2%, *AKAP5* with 1.8%, *AKAP10* with 0.9%, and *AKAP7* with 0.6% (Figure 13C).

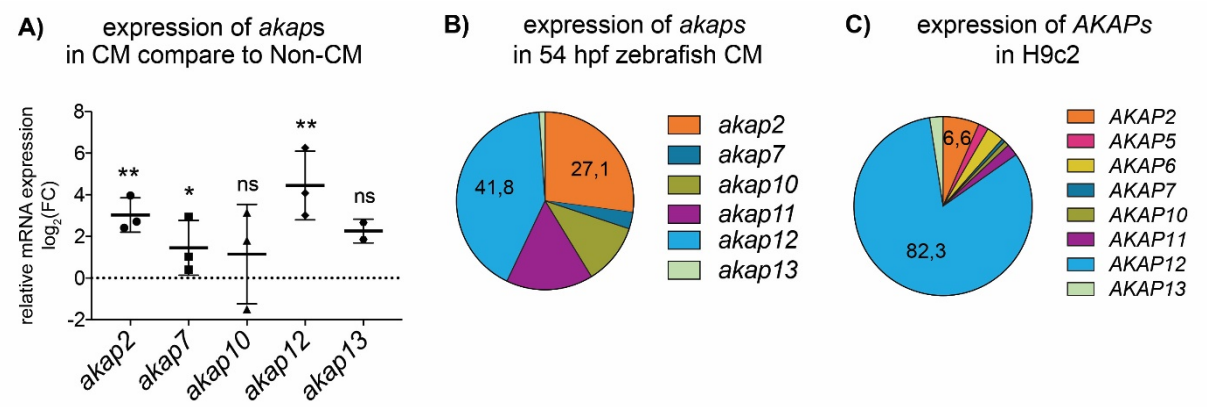

Figure 13: Identifying AKAP candidates which might have a role in the CT formation. (A) Relative mRNA expression of selected *akap* genes was measured in CM and non-CM after FACS of cell lysate from *myl7*:*EGFP* transgenic line via quantitative RT-PCR and normalized to the relative mRNA expression of *eef1a1l1*. Data represent the fold change $\log_2$ (2^-ΔΔCt) of the indicated genes in CM compared to non-CM. (Mean ± SD of N = 3 experiments; ***P*(*akap2*)=0.0039; **P*(*akap7*)=0.0391; ns *P*(*akap10*)=0.0781; ns *P*(*akap12*)=0.0079; ns *P*(*akap13*)=0.0625; Wilcoxon test). (B-C) Pie chart of the relative mRNA expression of the selected *AKAP*s. (B) Relative mRNA expression of *akaps* was measured in CM after FACS of *myl7*:*EGFP* transgenic line via quantitative RT-PCR and normalized to the relative mRNA expression of *myl7.* (C) Relative mRNA expression of *AKAPs* was measured in untreated H9c2 cell via quantitative RT-PCR and normalized to *GAPDH*. Data represent the fold change (2^-ΔΔCt) of the interested genes. (N= 3 experiments) and plotted as percentage in pie chart.

3.4.2 Downregulation of the *AKAP*s induce the CT generation except *AKAP2* and *AKAP5*

To explore AKAPs function in the CT isoform generation, I first showed in collaboration with Mai Phan that downregulation of the *AKAP*s with siRNA is efficient (Figure S3A-H). Interestingly, single knockdown of the *AKAP*s in most cases considerably increased the CT formation as this phenomenon appeared in *AKAP6*, *AKAP7*, *AKAP10*, *AKAP11*, *AKAP12,* and *AKAP13* siRNA transfected cells (Figure 14C-H). These data indicate on one hand that these AKAPs are not essential in the CT

formation, and on the other hand it showed that the disruption of the balance between the different AKAPs can trigger the AKAP anchored PKA signaling, revealed as the enhanced cleavage of the CT. Comparison of the pCt intensities in the nucleoli in untreated cells and *AKAP* siRNA transfected cells indicated that the pCt intensity increased in the absence of *AKAP11* by 65%, in the absence of *AKAP12* by 63%, in the absence of *AKAP6* by 51%, in the absence of *AKAP7* by 40%, in the absence of *AKAP10* by 40%, and in the absence of *AKAP13* by 25%. However, neither loss of *AKAP2* nor *AKAP5* enhanced significantly the pCt intensity in the nucleoli compared to untreated cell (Figure 14A-B).

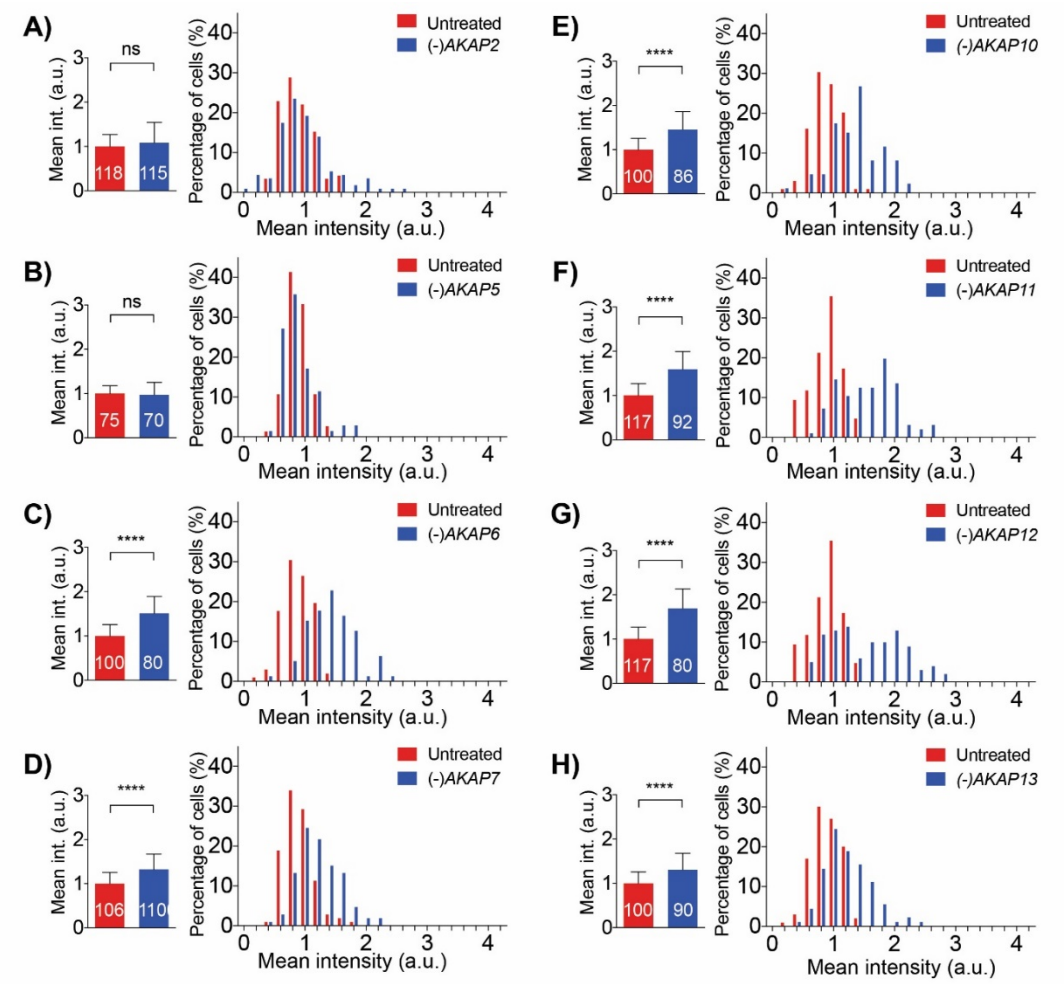

Figure 14: Downregulation of AKAPs induce the CT generation, except AKAP2 and AKAP5. (A-H) Quantification of mean intensity of pCt antibody in nucleoli of H9c2 cells transfected with selected *AKAP* siRNA. Data of column graphs expressed as mean ± SD of N = 3 experiments and n is represented in the columns. Frequency distribution plots demonstrate the percentage of the cell population with the corresponding mean intensity. (ns *P*((-)*AKAP2*)=0.0925; ns *P*((-)*AKAP5*)=0.4926; ****P<0.0001; Welch's t test).

3.4.3 Loss of AKAP2 rescues the loss of Wnt11 phenotype

To identify which AKAPs are involved in the CT regulation downstream of the Wnt11 pathway double knockdown of *AKAP* genes together with *WNT11* were performed. Downregulation of *WNT11* together with *AKAP6*, *AKAP7, AKAP10*, *AKAP11*, *AKAP12* or *AKAP13* affected the pCt intensity in a similar way, as did the single knockdown of these *AKAP* genes. pCt intensity increased by 51% in *WNT11/AKAP6*, by 73% in *WNT11/AKAP7,* by 33% in *WNT11/AKAP10*, by 60% in *WNT11/AKAP11*, by 69% in *WNT11/AKAP12*, and by 58% in *WNT11/AKAP13* siRNA transfected cells (Figure 15C-H).

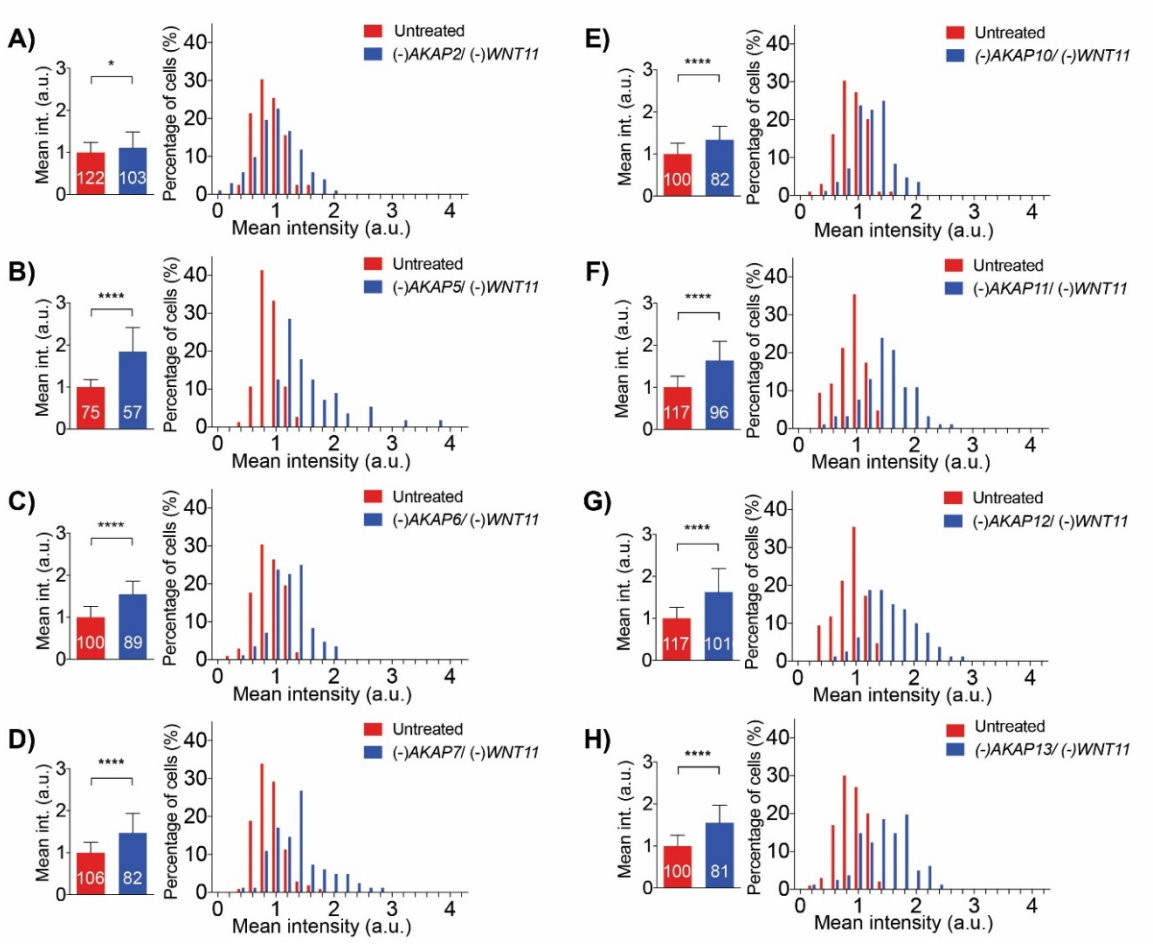

Figure 15: Loss of AKAP2 rescues the loss of Wnt11 phenotype. (A-H) Quantification of mean intensity of pCt antibody in nucleoli of H9c2 cells, transfected with selected *AKAP* and *WNT11* siRNA. Data of column graphs expressed as mean ± SD of N = 3 experiments and n is represented in the columns. Frequency distribution plots demonstrate the percentage of the cell population with the corresponding mean intensity. (**P*((-)WNT11/(-)AKAP2)=0.0109; *****P*<0.0001; Welch's t test).

However, in case of double knockdown of *AKAP5* together with *WNT11* the loss of WNT11 phenotype was more prominent, since pCt intensity increased by 85%, which suggests that AKAP5 does not play a role in the CT formation (Figure 15B). Surprisingly, loss of *AKAP2* partially rescued the loss of WNT11 effect on the CT formation, since pCt intensity only increased by 11%, which indicate that AKAP2 has a pivotal role in this process downstream of the Wnt11 pathway (Figure 15A).

3.5 Regulation feedback loop between WNT11, AKAP2, and AKAP7

As aforementioned, the cleaved CT isoform can translocate into the nucleus where it acts as a transcription factor. It has been shown by Gomez-Ospina and her colleagues that the overexpressed CT construct regulates the expression of gap junction proteins, regulators of G protein signaling, and tight junction proteins (Gomez-Ospina et al., 2006). These proteins determine the voltage propagation abilities of an excitable tissue, therefore the cleavage of the CT must be tightly regulated. Considering the previous results that disturbing the balance between the different AKAPs had huge impact on the CT formation, I hypothesized the existence of compensatory mechanisms. To identify regulatory feedback loops between the Wnt11 signaling pathway and the following AKAPs: AKAP2, AKAP5 and AKAP7, qPCR analysis was performed. Downregulation of *WNT11* had no effect on the *AKAP5* expression levels, but on *AKAP2* and *AKAP7* (Figure 16A). While loss of *WNT11* increased the expression of *AKAP2*, it had an opposite effect on *AKAP7* (Figure 16A). Measuring *WNT11* expression in *AKAP5* siRNA transfected cells revealed that there is no feedback loop between WNT11 and AKAP5. However, downregulation of *AKAP2* reduced *WNT11* amount. Although *WNT11* mRNA expression was not significantly different in the absence of *AKAP7* compared to its amount measured in scramble siRNA transfected cells, probably because of the huge standard deviation (SD), we can conclude that AKAP7 may have an impact on its expression (Figure 16B). These data strengthened the hypothesis that there is feedback loop system between WNT11 and AKAP2 as well as between WNT11 and AKAP7.

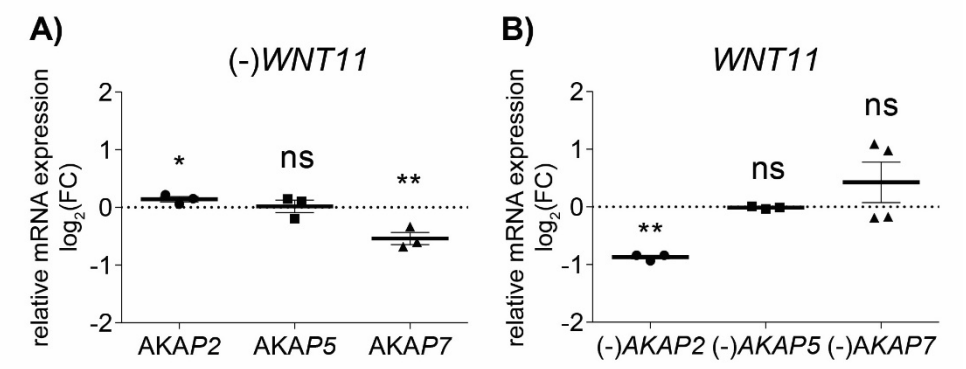

Figure 16: Regulatory feedback loop between WNT11, AKAP2, and AKAP7. (A) Relative mRNA expression of the interested *AKAP* was measured in Scramble and *WNT11* siRNA transfected H9c2 cell via quantitative RT-PCR and normalized to the relative mRNA expression of *GAPDH* in Scramble siRNA transfected cells. Data represent the fold change $\log_2$ (2^-ΔΔCt) of the indicated gene. (Mean ± SD; N = 3 experiments; **P*(*AKAP2*)=0.0195; ns *P* (*AKAP5*)=0.8203; ***P*(*AKAP7*)=0.0039; Wilcoxon test). (B) Relative mRNA expression of *WNT11* was measured in Scramble and in indicated *AKAP* siRNA transfected H9c2 cell via quantitative RT-PCR and normalized to the relative mRNA expression of *GAPDH* in Scramble siRNA transfected cells. Data represent the fold change $\log_2$ (2^-ΔΔCt) of *wnt11*. (Mean ± SD; N = 3 experiments; ***P*((-)*AKAP2*)=0.0039; ns *P*((-)*AKAP5*)=0.6406; ns *P*((-)*AKAP7*)=0.1099; Wilcoxon test).

3.6 AKAP2 forms complex with PKA and LTCC

3.6.1 AKAP2 binds the PKA Regulatory subunit I and II

AKAP2 has been shown to binds the PKA regulatory subunit II (Dong, Feldmesser, Casadevall, & Rubin, 1998; Gold et al., 2012), however other study suggested that AKAP2 similarly to AKAP10 can bind the regulatory subunit I and II as well (Aye et al., 2009). To study AKA2 binding specificity to the different PKA regulatory subunits, protein spot array was performed in collaboration with Maike Schulz. Each peptide spot includes 25 amino acids residues of a subunit type (Figure 17A) and two neighbor spots share the same 20 amino acids (see Table S4). For FLAG-IP H9c2 cell lysates were used, which beforehand were either transfected with empty FLAG/HA or with FLAG/HA-AKAP2 plasmids. Incubation of the membrane with the control protein lysates and detection with anti-FLAG antibody revealed the unspecific binding sites, labeled with red (Figure 17B). The incubation of the membrane with the lysate including the overexpressed AKAP2 (Figure 17C) resulted in three additional red spots (A3, A5 and B6), which indicate that AKAP2 can bind the PKA-RIa and –RIIa subunits. This finding suggests that AKAP2 indeed has dual specificity.

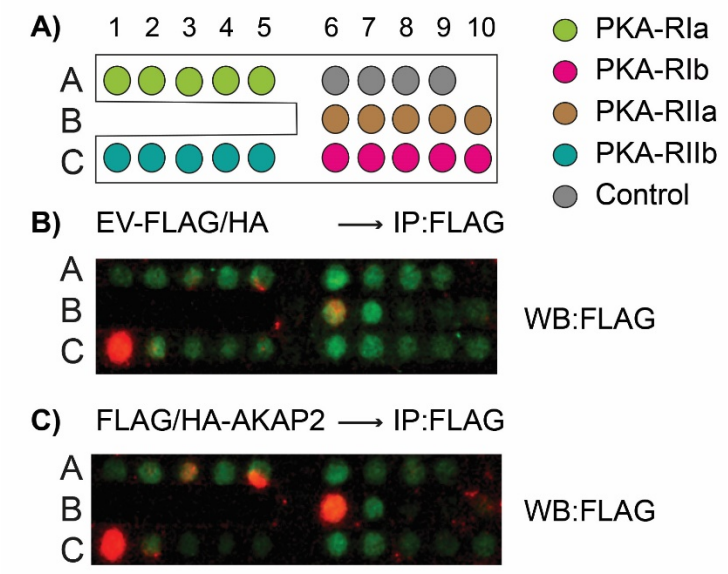

Figure 17: AKAP2 forms complex with PKA-RIa and –RIIa. (A) Schematic representation of series of immobilized 25-mer peptides (see Table S4), moving along the different PKA regulatory subunits were synthesized by spot array. (B) EV-FLAG/HA or (C) FLAG/HA-AKAP2 transfected H9c2 lysates, followed by FLAG-IP were added to the membranes. The membranes were developed with anti-FLAG antibody (Sigma 1:1000). Binding determinants are highlighted in red.

3.6.2 CT construct undergoes cleavage

The immunostaining experiments (Figure 15) suggested that AKAP2 is important for the CT isoform generation however, nothing is known about its function in the LTCC regulation. Hence the next goal of this study was to show the interaction between this novel AKAP and the α1C subunit. I designed a CT construct, which contains the rat α1C subunit (ENSRNOT00000052017.6) from amino acid (aa) 1317 to 2006, tagged with FLAG on the N-terminal part, and with mVenus on the C-terminal part as it is illustrated in Figure 18A. Immunostaining of the transfected cells with this construct showed that the CT is transported from the Golgi to the membrane (Figure 18B), suggesting its functionality. Next, I performed in collaboration with Maike Schulz immunoprecipitation (IP) experiments with FLAG and GFP antibodies (Figure 18C-D). During the detection of the FLAG-IP with FLAG antibody, a fragment around 130 kDa was detected, which corresponds to the full-length construct. A shorter fragment appeared around 80 kDa, which corresponds to the CT construct without mVenus, while an additional fragment was detected around 30 kDa, which corresponds to the pCT. During the detection of the FLAG-IP with GFP antibody only one band appeared around 130 kDa. GFP-IP of the construct and detection with FLAG antibody resulted in a band around 130 kDa. However, detection of the GFP-IP with GFP antibody resulted in two additional bands. One appeared around 90 kDa, which corresponds to dCT-mVenus. The other one was around 30 kDa, which is probably the cleaved

mVenus alone. Although the full-length construct is only 105 kDa, these data indicate that the band at 130 kDa is identical with the full-length construct. The existence of a 30 kDa fragment during the FLAG-IP FLAG antibody detection and a 90 kDa fragment during GFP-IP GFP antibody detection suggest that the CT construct is proteolytically processed possibly at the calpain cleavage site (aa 1631-1637) (Hulme et al., 2005). In addition, 7 extra bands were detected during the FLAG-IP FLAG antibody detection (Figure 18C), which either indicates the existence of other cleavage sites or other splice variants of the CT construct or the combination of these two.

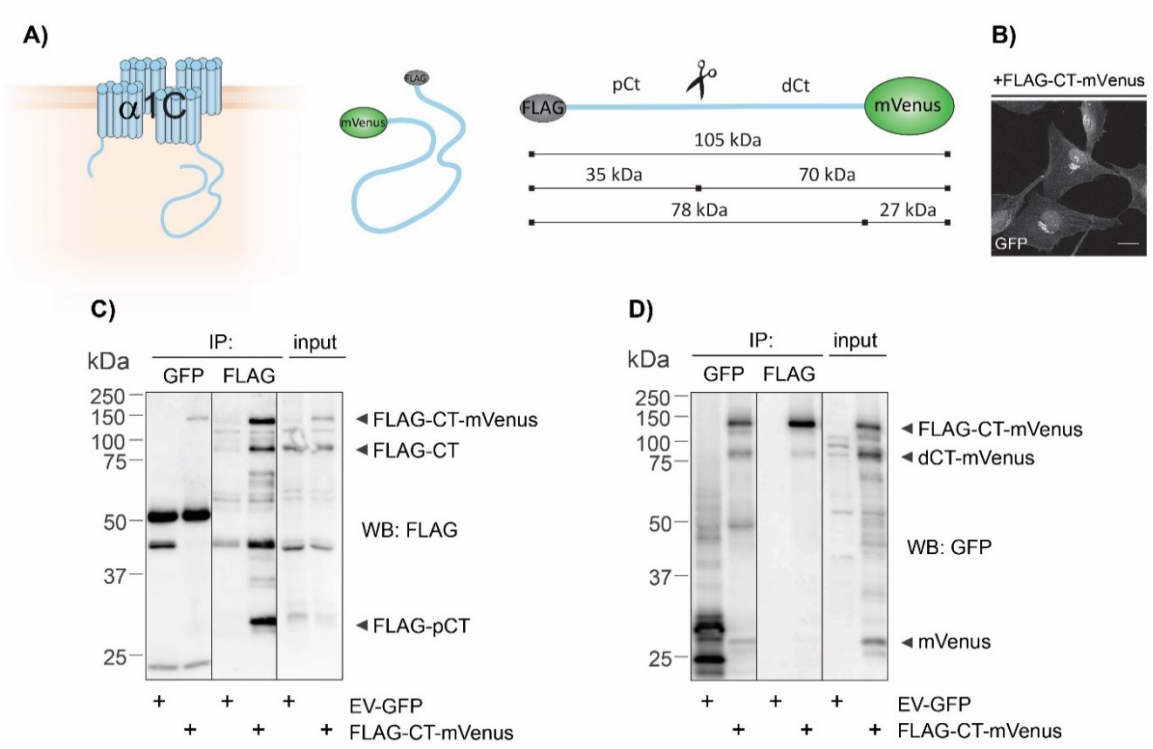

Figure 18: Overexpressed CT construct undergoes cleavage. (A) Schematic representation of the FLAG and mVenus tagged CT construct, which contains the rat α1C subunit (ENSRNOT00000052017.6) from amino acid (aa) 1317 to 1981. Scissors indicates the published calpain cleavage site (aa 1631-1638). EC- extracellular, IC- intracellular (B) Maximum intensity projection of confocal image of H9c2 cells, which were transiently transfected with the construct. The scale bar represents 20 μm. (C) FLAG or (D) GFP detection by WB of the aforementioned construct from lysate of H9c2 cells either transfected with the construct or with empty vector GFP (EV-GFP) control before and after FLAG or GFP IP. (N ≥ 10 experiments).

3.6.3 Binding between CT construct and AKAP2

To show that AKAP2 is binding to the CT construct, first the anti-AKAP2 antibody was verified. Using lysate from untreated H9c2 cells at least 5 bands appeared between

100 and 180 kDa, which showed significantly reduced signal in *AKAP2* but not in *WNT11* siRNA transfected cells (Figure 19A). In rat only two isoforms of AKAP2 (F1LPQ9 and A0A096MJ48) are annotated so far. Using Promega BioMath calculator the predicted molecular weight of these isoforms were 95.7 KDa and 13.9 KDa. These data suggest that the detected bands could be different isoforms and/or dimerized forms of the AKAP2.

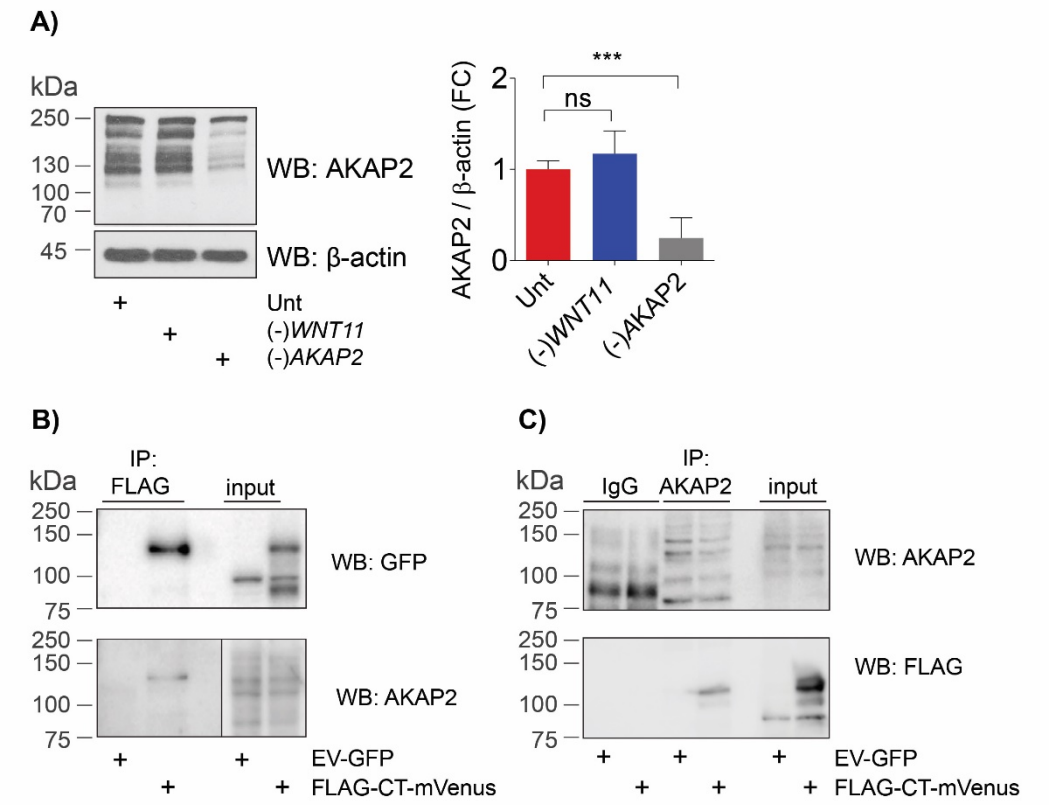

Figure 19: Binding between exogenous CT construct and AKAP2. (A) Western blot (WB) analysis of AKAP2 in lysate of untreated control (U) and *WNT11* (*W11*) and *AKAP2* (*A2*) siRNA transfected H9c2 cells detected with anti-AKAP2 antibody. Below, cell lysate lanes were run on the same gel, but the membrane was cut as it is indicated by the gap and developed with β-actin. On the right, column graph represents the AKAP2 protein amount, which was normalized to β-actin amount. (Mean ± SD; N = 4; ns *P*((-)*WNT11*)=0.5206; *** *P*((-)*AKAP2*)=0,0002); One-way ANOVA, Dunnett's multiple comparison test.) (B) CT construct or EV-GFP were transiently expressed in H9c2 cells and the cell extract was IPed with FLAG, and co-IPed proteins were probed on WB with AKAP2. (N ≥ 3 experiments). (C) Endogenous AKAP2 was IPed from CT construct or EV-GFP control transfected H9c2 cell extracts with AKAP2 antibody. The IP probed on WBs with antibodies to the indicated proteins. (N = 3 experiments).

Next, Co-IP experiments were performed in collaboration with Maike Schulz. FLAG-IP of the construct and detection with AKAP2 antibody resulted in a band around 130 kDa (Figure 19B), which could be one of the AKAP2 isoform. Reciprocal co-IP by IP the

endogenous AKAP2 and detection of the construct with FLAG antibody resulted in a band around 130 KDa, which corresponds to the full-length construct (Figure 19C). These data indicate that AKAP2 binds to the CT.

3.6.4 Binding between endogenous LTCC and AKAP2

The following aim was to study the interaction between the endogenous AKAP2 and LTCC proteins. Therefore, an anti-pCt antibody was generated, which targets the pCT at aa 1570-1589. Beforehand, I verified the specificity of this antibody, which theoretically recognizes the full-length and also the cleaved α1C subunit. On WB only one band appeared around 250 kDa, which showed decreased signal in *CACNA1C* siRNA transfected cells compared to untreated cells (Figure 20A). This result suggests that the pCt antibody only recognizes the full-length isoform. Next, in collaboration with Maike Schulz, endogenous AKAP2-IP was performed using lysates of Scramble or *AKAP2* siRNA transfected cells. With AKAP2 antibody, 3 AKAP2 isoforms were detected in the Scramble siRNA transfected cell lysate. Re-staining the same membrane with the anti-pCt resulted in an additional band around 250 kDa (labelled with asterisk) in the Scramble siRNA transfected cells, but not in *AKAP2* siRNA transfected cells (Figure 20B). This band corresponds to the full-length subunit and suggests the interaction between AKAP2 and α1C subunit. Taken together, these data provide strong evidence that AKAP2 directly interact with the LTCC.

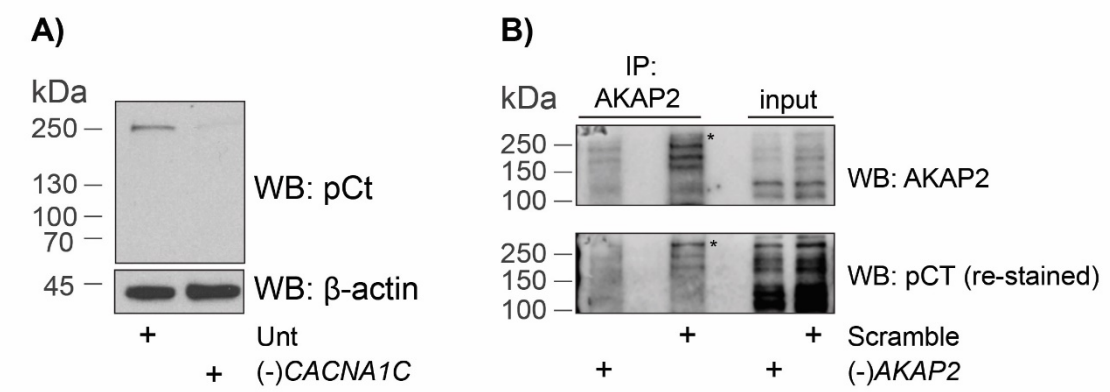

Figure 20: Binding between endogenous LTCC and AKAP2. (A) WB analysis of LTCC in lysate of untreated control and *CACNA1C* siRNA transfected H9c2 cells by using anti-pCt antibody (custom-made). Below, cell lysate lanes were run on the same gel, but the membrane was cut as it is indicated by the gap and developed with β-actin. (N = ≥ 3 experiments). (B) Endogenous AKAP2 was IPed from Scramble or *AKAP2* siRNA transfected H9c2 cell extracts with AKAP2 antibody. The IP probed on WB with antibodies to the indicated proteins. (N = 1 experiment; asterisk indicates the full-length α1C subunit.)

3.7 Akap2 regulates heart formation

3.7.1 Characteristics of loss of Akap2 phenotype

Little is known about AKAP2 function apart from its role in calcitonin-mediated cancer cell invasion (Thakkar et al., 2016) or in ocular transparency (Gold et al., 2012). We previously showed by qPCR that *akap2* (*palm2-201/202*) is highly expressed in zebrafish cardiomyocytes (Figure 13A). Furthermore, it has been shown that PKA-AKAP2 interaction is highly upregulated in human patients with dilated cardiomyopathy (DCM) (Aye et al., 2012). To further our understanding of Akap2 function during cardiac development loss of function experiments were performed using morpholino approach. The *akap2* is composed of 5 exons, from which the exon 2 consists of the PKA binding domain (LZ motif, green in Figure 21A). Keeping this in mind, the *akap2* morpholino (*akap2*^{e2i2}MO) was designed in a way to cause the exclusion of exon 2 (*akap2*∆ex2) (Figure 21A). The *akap2* morpholino-injected wild-type, 54 hours after postfertilization (hpf) embryos were shorter, developed heart edema and had small head compared to uninjected control embryos (Figure 21B). To confirm the exclusion of the exon 2, after RNA extraction from wild-type and *akap2* morphant embryos cDNA was synthetized. Next, the template cDNAs were amplified using primers, which target the beginning and the end of the *akap2.* In wild-type embryos a PCR product was detected between 2000 and 2500 bp, which is corresponds to the full-length *akap2* (2434 bp). In *akap2* morphant embryos a fragment appeared around 320 bp, which corresponds to *akap2*∆ex2 (Figure 21C). The phenotypic analysis of the injected embryos focusing on the heart revealed that a little bit less than half of the *akap2* morphants had unlooped heart compared to wild-type embryos, which I defined as abnormal looping (Figure 21D). Furthermore, in *akap2* morpholino-injected embryos the inverted heart occurred more frequently compared to wild-type embryos.

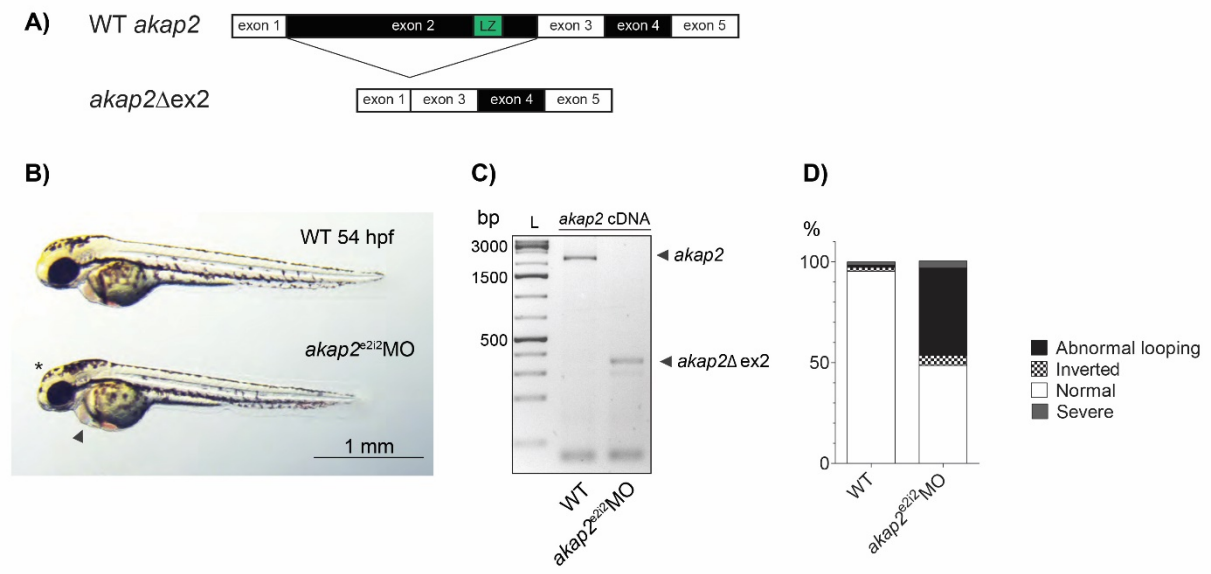

Figure 21: Loss of *akap2* phenotype. (A) Schematic representation of the zebrafish wild-type (WT) *akap2* and morpholino induced exclusion of exon 2 (*akap2*Δex2). The exons are not to scale. LZ-Leucine zipper motif (B) *In vivo* bright field image, lateral view of WT and *akap2* morpholino (*akap2*^{e2i2}MO) injected embryos at 54 hpf. (arrowhead - heart edema; asterisk-small head) (C) RT-PCR of *akap2* cDNA from WT and *akap2* morpholino-injected embryos at 54hpf. The size of the akap2 fragment is 2434 bp, while in *akap2* morphants it is only 300 bp due to exclusion of the exon 2 (2134 bp). (D) Quantification of the loss of *akap2* phenotype based on heart looping abnormalities. (N ≥ 3 experiments; n ≥ 300).

To ensure that the aforementioned phenotypic characteristics of loss of the *akap2* are not off-target effects of the morpholino, I cloned the *akap2* mRNA. To estimate the concentration of the mRNA, which has no effect on the development, but rescues the morpholino caused phenotype, titration curve of the mRNA was executed (Figure SF4A-C). Although, injection of 50 pg/ul *akap2* mRNA alone had no effect on the development, injection of the mRNA with the morpholino resulted in abnormal looping in 32.8%, and inverted heart in 6.3% of the embryos (Figure SF4A). 15.4% of the embryos injected with 100 pg/ul *akap2* mRNA had severe phenotype (Figure SF4C), and injection of the mRNA in higher concentrations caused massive death in the population (data not shown). However, 75 pg/ul *akap2* mRNA together with the morpholino efficiently rescued the loss of *akap2* phenotype, without causing any effect alone (Figure 22A and 22B).

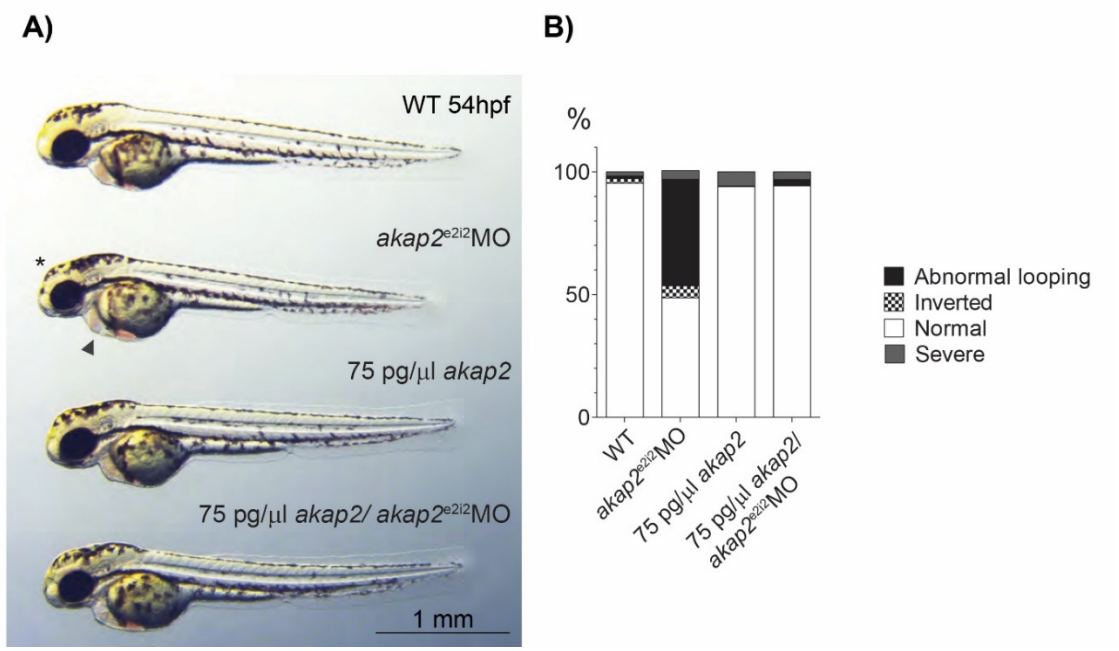

Figure 22: Rescue of *akap2* phenotype. (A) *In vivo* bright field image, lateral view of WT zebrafish embryo and WT embryo injected with *akap2* morpholino (*akap2*^{e2i2}MO), *akap2* mRNA (75 pg/µl *akap2*), and with mRNA and morpholino together. (arrowhead- heart edema; asterisk-small head) (B) Quantification of the loss of *akap2* phenotype based on heart looping abnormalities. (N ≥ 3 experiments; n ≥ 300).

3.7.2 Akap2 is required for normal heart development

In developing zebrafish embryo cardiac looping occurs from 30 to 48 hpf, when the linear heart tube morphs into two chambers, and the ventricle and atrium become morphologically distinguishable. To visualize and measure the looping defect in *akap2*-deficient heart, *myl7*:*EGFP* transgenic line was injected with *akap2* morpholino, *akap2* mRNA or in combination (Figure 23A). The heart angle was defined as the angle, which is enclosed by the midsagittal line and the atrioventricular canal, and indicates the relative position of the atrium to the ventricle (Figure 23B). In 54 hpf uninjected control embryos the averaged mean angle was 18.9° ± 7.4°, which implicates the properly looped heart, as the atrium is almost juxtaposed to the ventricle. Injection of *akap2* morpholino enhanced the angle. The *akap2* morphants had 62.4° ± 12.8° angle, in which case the atrium was diagonally below the ventricle. Injection of *akap2* mRNA alone had no effect on heart looping (17.3° ± 6.7°), however co-injection with *akap2* morpholino together successfully rescued the lopping defect (22.7° ± 7.9°) (Figure 23C). Taken together, loss of *akap2* results in heart edema, heart looping defect, smaller head and reduced body length, which can be rescued with akap2 mRNA. This indicates that the observed phenotypical characteristics are specific for loss of *akap2*

and not off-target effects of the morpholino. Hence, these data suggest that Akap2 plays pivotal role during early cardiogenesis.

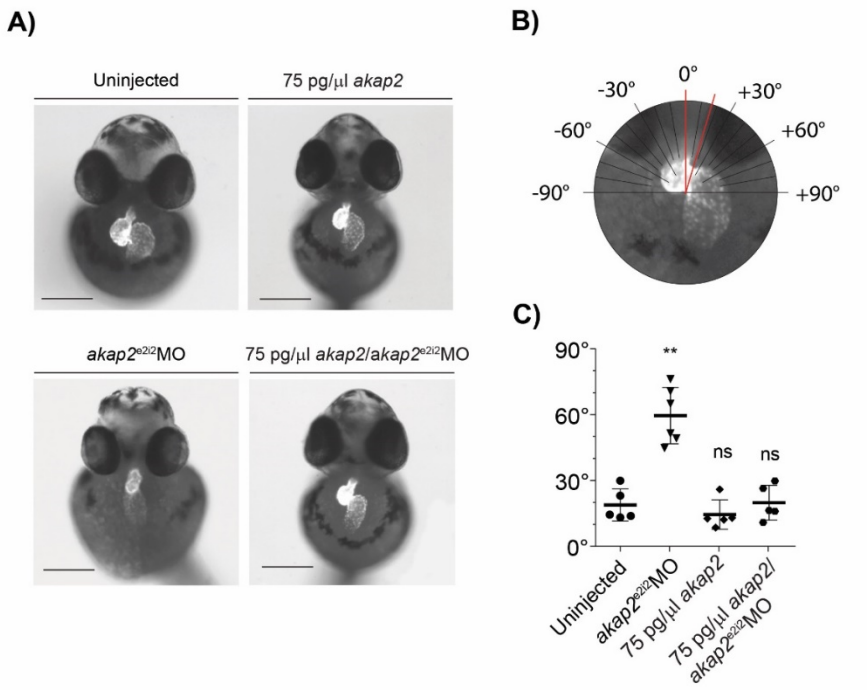

Figure 23: Akap2 is required for normal heart development. (A) Bright field image overlayed with fluorescent image, frontal view of uninjected control, *akap2* mRNA (75 pg/µl *akap2*) injected, *akap2* morpholino (*akap2*^{e2i2}MO) injected or mRNA and morpholino double injected *myl7*:*EGFP* transgenic zebrafish embryo at 54 hpf. (B) Schematic representation of the measured heart angle, which is defined by the midsagittal line and atrioventricular canal. (C) Quantification of the heart angle. Data expressed as mean ± SD of at least 5 embryos in each condition, n is represented on the columns. (***P*(*akap2*^{e2i2}MO)=0.0043; ns *P*(75 pg/µl *akap2*)=0.9444; ns *P*(75 pg/µl *akap2*/*akap2*^{e2i2}MO)=0.5317; Mann-Whitney test). The scale bar represents 200 µm.

3.8 In developing zebrafish heart the LTCC abundance and localization is regulated by Wnt11 and Akap2-PKA signaling

3.8.1 Wnt11 regulates the expression of the *cacna1c* gene

The zebrafish α1C subunit of the LTCC is encoded by the *cacna1c* gene (ENSDARG00000008398), which contains 48 exons. To study whether Wnt11 signaling pathway regulates the calcium transient amplitude via LTCC in zebrafish, first the expression level of the *cacna1c* was examined using *wnt11*^{tx226} mutant embryos (Heisenberg et al., 2000) at 54 hpf. Considering the following facts: a) in mouse the dCT isoform can be transcribed independently from the full-length *CACNA1C* (Gomez-

Ospina et al., 2013), b) in H9c2 cells I detected reduction in expression of *CACNA1C* exon 45 (dCT isoform) in the absence of WNT11, three TaqMan probes were used, which target the *cacna1c* exon 18, 40 and 45. These exons encode part of the pore-forming domain (exon 18), of the pCT (exon 40) and dCT (exon45) (Figure 24A). Surprisingly, in *wnt11* mutant embryos the expression levels of the *cacna1c* gene was decreased compared to wild-type embryos, independently from the TaqMan probes (Figure 24B). These data indicate that Wnt11 signaling may regulate the *cacna1c* expression. However, it has to be mentioned that RNA extracts were prepared from the whole embryos, therefore this effect of Wnt11 on the channel expression is general and non-exclusive for cardiomyocytes.

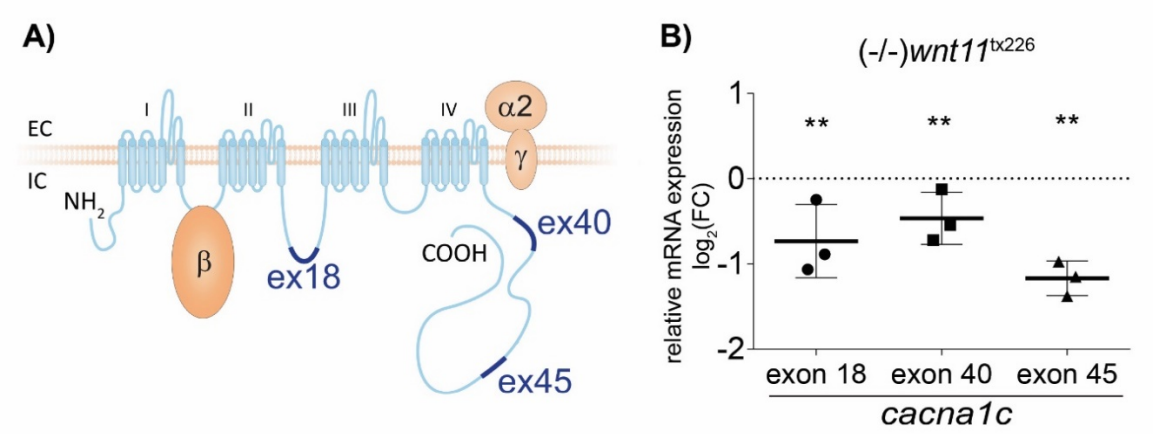

Figure 24: Wnt11 signaling alters *cacna1c* expression. (A) Schematic representation of the zebrafish LTCC complex with the highlighted sites for the TaqMan probes on the α1C subunit (ENSDARG00000008398). EC- extracellular, IC- intracellular (B) Relative mRNA expression of *cacna1c* gene was measured in WT and *wnt11* mutant ((-/-)*wnt11*^{tx226}) embryos at 54 hpf via quantitative RT-PCR and normalized to the relative mRNA expression of *eef1a1l1*. Data represent the fold change $\log_2$ (2^-ΔΔCt) of the interested genes. (Mean ± SD of N = 3 experiments; ***P*(*cacna1c* exon 18)=0.0039; ***P*(*cacna1c* exon 40)=0.0078; ***P*(*cacna1c* exon 45)=0.0039; Wilcoxon test).

3.8.2 LTCC abundance and localization in zebrafish embryonic ventricle

My next aim was to determine whether Wnt11 and Akap2-PKA signaling pathway regulate the localization and abundance of the α1C subunit in the zebrafish embryonic heart. To address this question, first the II-III-loop antibody specificity was verified in zebrafish; this part of the α1C subunit is highly conserved between the species (Figure S5). In ventricle from 54 hpf wild-type embryo the α1C subunit showed membrane localization, where the channel clusters appeared in continuous or dashed stripes along the cells' circumference (Figure 25A). Midsagittal section through the ventricle

revealed that the channel shows lateral localization within the polarized cardiac epithelial cells (Figure 25A'). The qPCR data indicated that loss of *wnt11* might reduce the *cacna1c* expression in CMs, and thus possibly its protein abundance. Although, in contrast to the expected results, injection of the embryos with *wnt11* morpholino (*wnt11*^{ATG}MO) had no effect on the α1C subunit abundance, it disturbed the localization of the channel. In *wnt11* morphant ventricle the well-defined pattern of the channel, which followed the shape of the cells was perturbed (Figure 25B). Injection of *akap2* morpholino resulted in the continuous localization of the α1C subunit along the lateral cell membranes of the epithelial myocardial cells. In comparison to the wild-type embryos, in the absence of *akap2* the channel clusters formed by dashed stripes along cells' circumference were never observed (Figure 25C). In addition, in *akap2*-deficient heart the extracellular matrix between the endocardium and myocardium showed increase, the endocardium became compact, and the myocardial monolayer was replaced by double layer (Figure 25C') indicating the role of Akap2 in tissue remodeling.

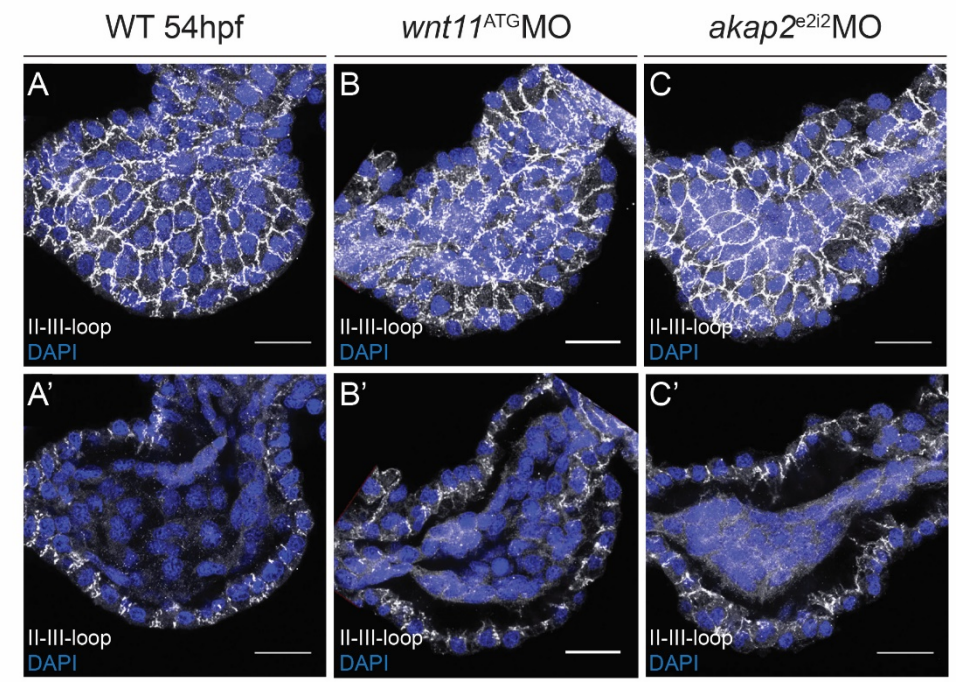

Figure 25: Localization and abundance of the α1C subunit. Maximum intensity projection of 7 μm confocal section (A,B,C) or 2,8 μm confocal section (A',B',C') of (A) WT, (B) *wnt11*^{ATG}MO and (C) *akap2*^{e2i2}MO zebrafish hearts at 54hpf. Hearts were immunostained with anti-II-III-loop antibody (Millipore) in dilution of 1:50 (gray). DAPI (blue) stains nuclei. (N ≥ 3 experiments). The scale bar represents 20 μm.

Detailed analysis of ventricles from wild-type embryos revealed that in the myocardium based on the α1C subunit distribution we can distinguish between three transversal layers. The LTCC appeared the most abundant in the apical section, where the clusters of the channels were equally scattered along the membranes (white channel in merged images show channel co-localization with ZN8 antibody) (Figure 26A-C). The channels become more clustered in patches along the membranes represented by dashed stripes along the cells' circumference in the middle sections. Here, the channel formed elongated clusters perpendicular to the membrane (Figure 26B). In the basal sections, the channel is only visible sparsely, in dispersed small clusters at the cell boundaries. The α1C subunit abundance decreased and compared to the other two section I detected less co-localization between the II-III-loop and ZN8 staining (Figure 26C).

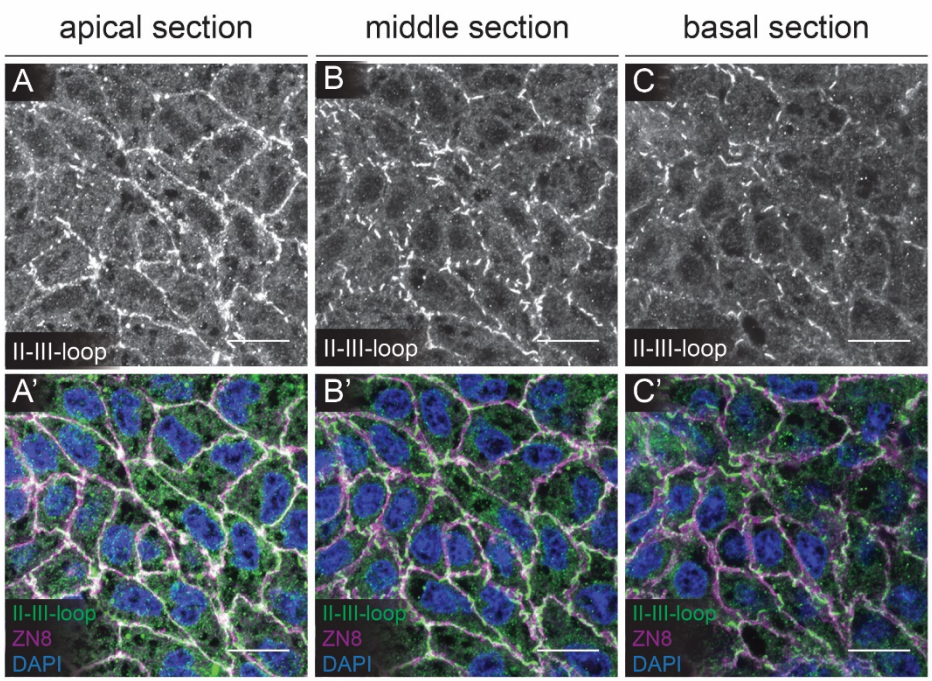

Figure 26: α1C subunit distribution within the WT myocardium. Maximum intensity projection of 2.1 μm transversal (A) apical, (B) middle or (C) basal section of WT zebrafish epithelial myocardium at 54hpf. Hearts were immunostained with anti-II-III-loop antibody (Millipore) in dilution of 1:50 (gray/green), anti-ZN8 antibody (Hybridoma Bank) in dilution of 1:50 (magenta). DAPI (blue) stains nuclei. (N ≥ 3 experiments). The scale bar represents 10 μm.

Considering the distribution of the α1C subunit in wild-type myocardium, I analyzed the distribution of the α1C subunit in ventricles dissected from *wnt11* or *akap2* morphant embryos (Figure 27). In the absence of *wnt11*, the channel localized in a very similar fashion in the apical as well as middle sections as seen in wild-type embryos. However,

in the basal sections its localization was similar to apical and middle sections, and thus was not downregulated (Figure 27B). Analyzing the maximum projections of the myocardium of several *wnt11*-deficient hearts (Figure S6) indicated that Wnt11 signaling regulates the LTCC localization in developing zebrafish heart. In the absence of *akap2*, the channel distribution was quite similar in all three sections (Figure 27C). In the apical sections, the channels were clustered in continuous lines, which defined the cell borders. This pattern of the channels was also typical in the middle sections, where it supposed to form dashed stripes. Although in the basal sections the channel abundance was reduced its pattern was similar as in the apical sections. Comparison of the different hearts isolated from *akap2* morphant embryos showed similar pattern (Figure S6). These data implicate that the LTCC localization is dependent on Akap2.

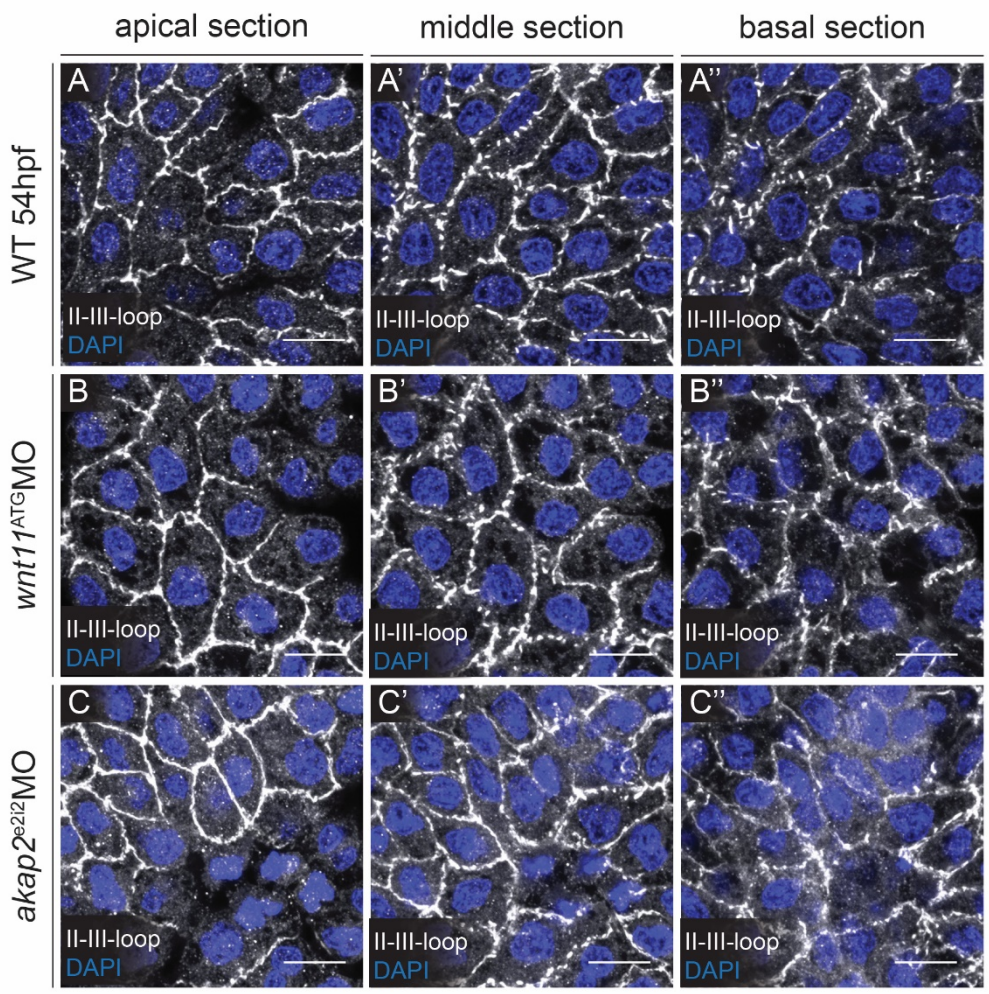

Figure 27: α1C subunit distribution in the myocardium. Maximum intensity projection of 2.1 μm transversal (A,B,C) apical, (A',B',C') middle or (A'',B'',C'') basal section of (A) WT, (B) *wnt11* (*wnt11*^{ATG}MO) or (C) *akap2* (*akap2*^{e2i2}MO) morphant myocardium at 54hpf. Hearts were immunostained with anti-II-III-loop antibody (Millipore) in dilution of 1:50 (gray). DAPI (blue) stains nuclei. (N ≥ 3 experiments). The scale bar represents 10 μm.

3.9 Loss of *akap2* rescues the electrical gradient formation in *wnt11*-deficient embryonic zebrafish heart

3.9.1 *akap2* interacts with *wnt11* genetically

To determine whether Wnt11 and Akap2 cooperate during development, phenotypic analysis of double injected embryos with *akap2* and *wnt11* morpholino was performed (Figure 28A). The *wnt11* morphants developed fused eyes, forebrain abnormalities, shorter body length and cardiac edema. The group with cyclopic eye also had cardiac edema and abnormal looping. 40% of the embryos injected with *wnt11* morpholino showed cyclopic eye and additional 10% of the population had abnormal looping. In *wnt11*; *akap2* double morphants overall 59.5% of the embryos were effected. The severe phenotype increased by 5.8% compared to the wild-type group. However, 16.5% less of these embryos developed cyclopic eye, and by 16.3% more had abnormal looping compared to the *wnt11* morphant group (Figure 28B).

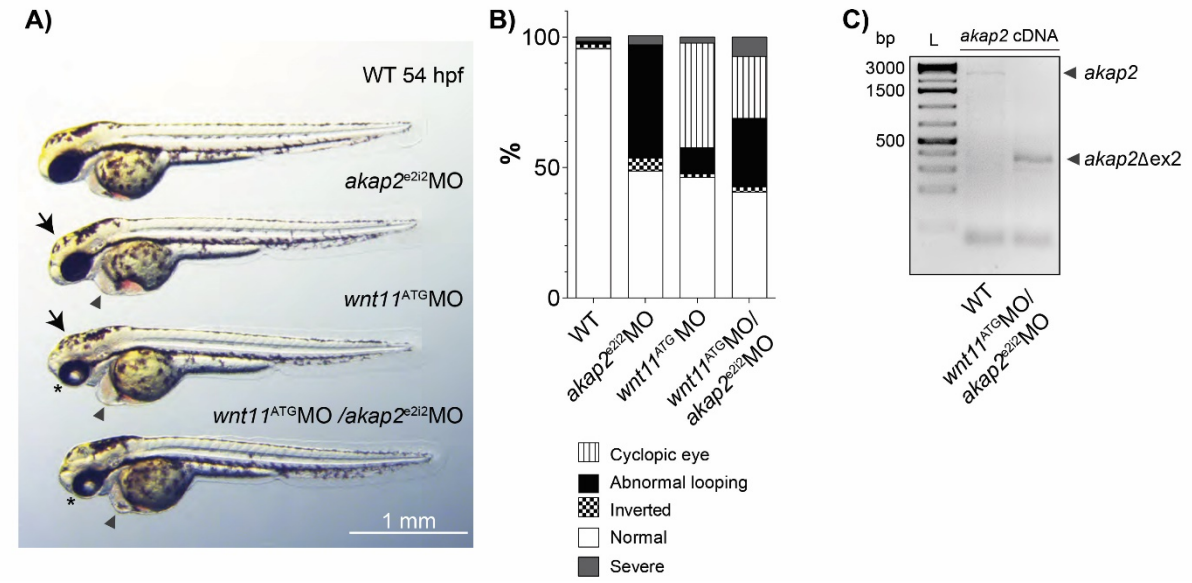

Figure 28: Loss of *akap2* and *wnt11* phenotype. (A) *In vivo* bright field image, lateral view of WT zebrafish embryo and WT embryo injected with *akap2* morpholino (*akap2*^{e2i2}MO), with *wnt11* morpholino (*wnt11*^{ATG}MO), and with both at 54 hpf. (arrowhead-heart edema; asterisk-cyclopic eyes; arrow-smaller head) (F) Quantification of the phenotypes based on heart looping abnormalities and cyclopia. (N ≥ 3 experiments; n ≥ 300). (C) RT-PCR of *akap2* cDNA from WT and double morpholino injected embryos at 54 hpf. The size of the akap2 fragment is 2434 bp, while in *akap2; wnt11* morphants it is only 300 bp due to exclusion of the exon 2 (2134 bp).

The embryos, which developed fused eyes were used for further studies as they are representative of the *wnt11* knockdown phenotype. One of these embryos is represented on the Figure 28A. Beside the cyclopia these embryos also developed heart edema, however body length and brain abnormalities seemed to be rescued by loss of *akap2*. To prove that these embryos were indeed missing the *akap2*, RNA isolation was performed followed by cDNA synthesis. RT-PCR analysis of cDNA amplified with *akap2* primer set from wild-type and double morphant embryos confirmed the exon 2 exclusion in *akap2* in double morphants (Figure 28C). These data implicate that loss of *akap2* might suppress particular aspects of the *wnt11* phenotype.

To visualize the looping defect, *myl7*:*EGFP* transgenic line was injected with *wnt11* morpholino alone and in combination with *akap2* morpholino (Figure 29A). During quantification enhanced heart angle was measured (32.5° ± 13.0°) in *wnt11* morphant embryos in comparison to control embryos (18.9° ± 7.4°).

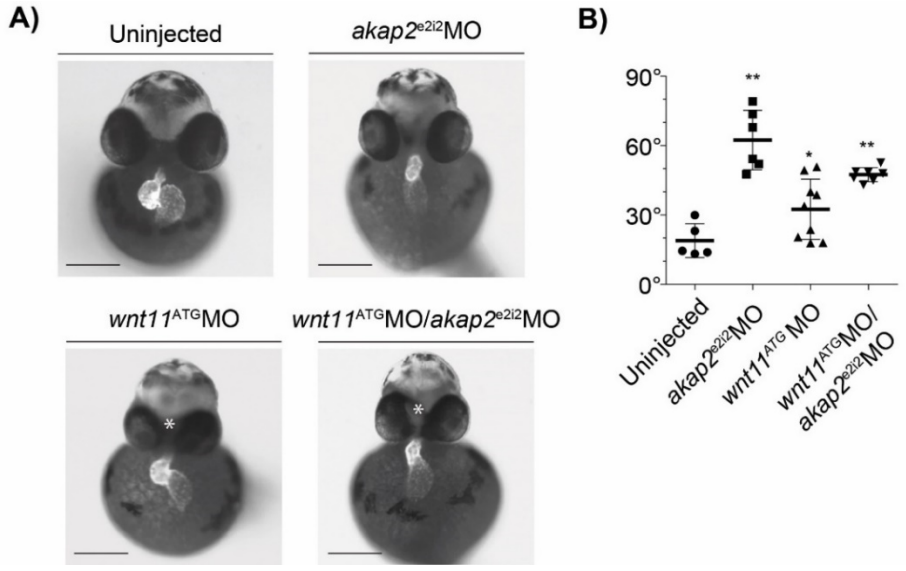

Figure 29: Loss of *akap2* is dominant over loss of *wnt11* heart phenotype. (A) Bright field image overlayed with fluorescent image, frontal view of uninjected control, *akap2* morpholino (*akap2*^{e2i2}MO) injected, *wnt11* morpholino (*wnt11*^{ATG}MO) injected, and double injected *myl7*:*EGFP* transgenic zebrafish embryo at 54 hpf. (B) Quantification of the heart angle. Data expressed the mean ± SD of at least 5 embryos in each condition, n is represented in the columns. (***P*(*akap2*^{e2i2}MO)=0.0043; **P*(*wnt11*^{ATG}MO)=0.0420; ***P*(*wnt11*^{ATG}MO/*akap2*^{e2i2}MO) = 0.0025; Mann-Whitney test). The scale bar represents 200 μm.

However, in the double morphants with cyclopic eye this angle was even larger, 47.9° ± 3.1°, which is similar to the heart angle in *akap2* morphant (62.4° ± 12.8°) (Figure 29B). This data suggest that loss of *akap2* concerning the heart phenotype is dominant over loss of *wnt11*, indicating that *akap2* might be downstream of *wnt11*.

3.9.2 Loss of *akap2* rescues the electrical gradient formation in *wnt11*-deficient embryonic heart

Cardiac pacemaker induces propagation of the action potentials from the atrium to the ventricle, where in normal condition at 54 hpf the cardiomyocytes of the outer curvature (OC) of the ventricle conduct action potentials three times faster than the inner curvature (IC) cardiomyocytes. This intercellular electrical coupling gradient is essential for the normal function of the heart and prerequisite for the generation of the sequential contraction. It has been shown that Wnt11 pathway is indispensable for the establishment and maintenance of the electrical gradient in developing zebrafish heart (Panáková et al., 2010).

To examine what is the physiological relevance of Akap2 in action potential propagation, optical mapping of zebrafish hearts at 54 hpf was performed. The conduction velocity was measured in the OC and IC regions and plotted as a ratio of the OC/IC. In uninjected control wild-type embryos this number was on average close to three (3.21 ± 0.54; n=32; data not shown) as it was previously reported. In *akap2* morphants, this ratio was 2.20 ± 0.61 (Figure 30B) meaning that the gradient formation was disturbed in these embryos. 75 pg/μl *akap2* mRNA injection had no significant effect on the action potential propagation compared to its wild-type control, since the ratio in these ventricles was 3.07 ± 0.79 (Figure 30C). In *akap2* mRNA and morpholino injected embryos the ratio was 3.06 ± 1.18 similar to the wild-type (Figure 30D). This means that mRNA injection successfully rescued the akap2 morpholino phenotype, hence the loss of *akap2* effect on the electrical gradient formation is most likely a specific effect of the morpholino.

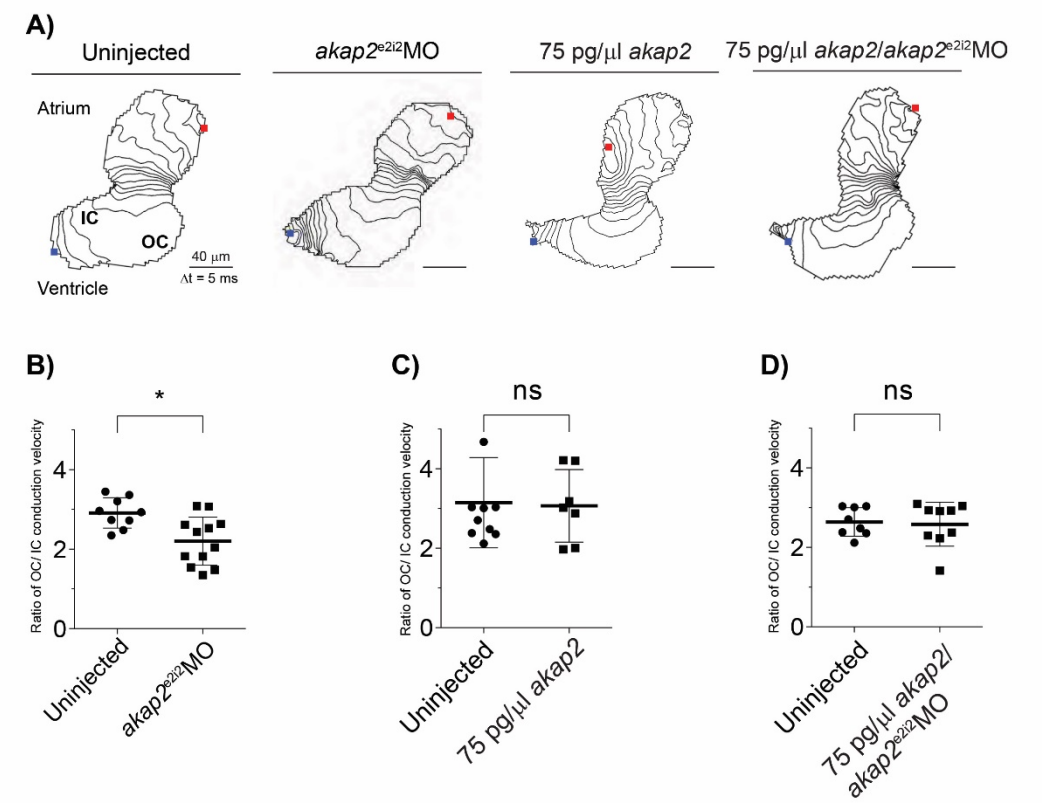

Figure 30: Akap2 regulates the electrical gradient formation. (A) Isochronal map of 54 hpf zebrafish heart from wild-type, *akap2* morphant, *akap2* mRNA injected, and *akap2* mRNA and morpholino injected embryos. Lines represent the positions of the action potential wave front at 5-ms intervals. Red dots indicate the start site of the excitation and blue dots represent the end. (IC-inner curvature, OC-outer curvature) (B-D) Quantification of the action potential propagation at 54 hpf (B) in *akap2* morpholino (*akap2*^{e2i2}MO), (C) *akap2* mRNA (75 pg/µl *akap2*), and (D) in *akap2* mRNA and morpholino (75 pg/µl *akap2*/*akap2*^{e2i2}MO) injected embryos. Data are expressed as the ratio of the OC/IC conduction velocity and are plotted as mean ± SD of N=3 experiments and n is represented on the columns. (**P* (*akap2*^{e2i2}MO)=0.0118; ns *P*(75 pg/µl *akap2*)=0.9999; ns *P*(75 pg/µl *akap2*/*akap2*^{e2i2}MO)=0.9410; Mann-Whitney test).

In addition, I confirmed that in *wnt11*-deficient heart either in *wnt11* mutant or morphant, the conduction velocity gradient formation was abolished, which is in line with published data (Panáková et al., 2010). The ratio between OC/IC in *wnt11* mutant was 1.65 ± 0.70 (Figure 31B), and in morphant was 1.47 ± 0.32 (Figure 31C).

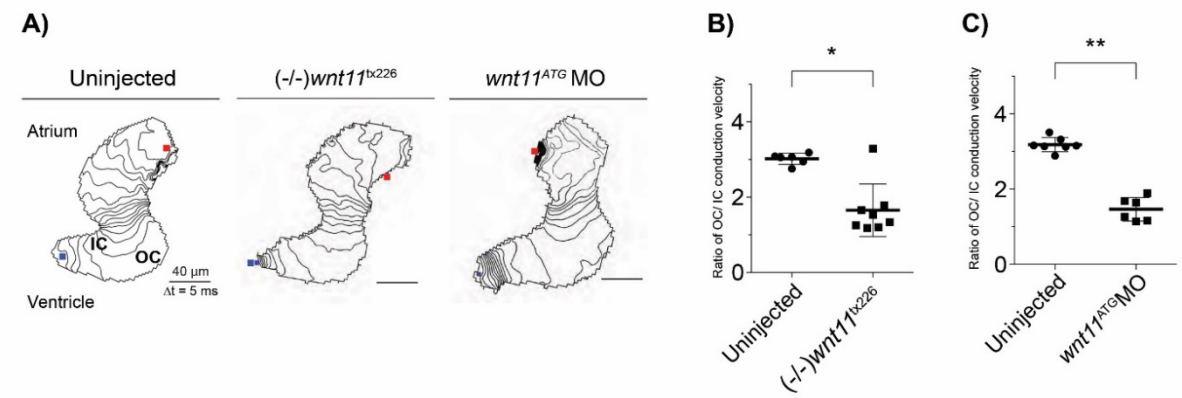

Figure 31: The action potential propagation in the hearts from *wnt11* mutants and *wnt11* morphants is similar. (A) Isochronal map of 54 hpf zebrafish heart from wild-type (uninjected), *wnt11* mutant and *wnt11* morphant embryos. (B-C) Quantification of the action potential propagation at 54 hpf (B) in *wnt11* mutant ((-/-)*wnt11*^{tx226}) and (C) in *wnt11* morphant (*wnt11*^{ATG}MO) embryos. Data are expressed as the ratio of the OC/IC conduction velocity and are plotted as mean ± SD of N=3 experiments and n is represented on the columns. (**P*((-/-)*wnt11*^{tx226})=0.0200; ***P*(*wnt11*^{ATG}MO)=0.0012; Mann-Whitney test).

Surprisingly, measuring the conduction velocity in the double *wnt11*; *akap2* morphants revealed that in these embryos the electrical gradient formation was completely rescued, since the ratio between OC/IC was at 3.22 ± 0.60 (Figure 32). This data indicates that regarding the LTCC regulation, Akap2 acts downstream of Wnt11 pathway, and that not just in H9c2 cells, but in zebrafish embryo as well. Thus, without Akap2 anchored PKA signaling Wnt11 loses its ability to regulate the LTCC.

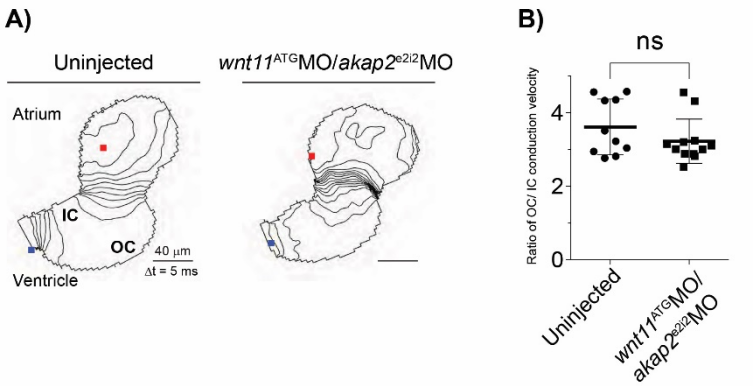

Figure 32: Loss of *akap2* rescues the electrical gradient formation in *wnt11*-deficient heart. (A) Isochronal map of 54 hpf zebrafish heart from wild-type and from double morphant (*wnt11*^{ATG}MO/*akap2*^{e2i2}MO) embryos. (B) Quantification of the action potential propagation at 54 hpf in the wild-type and in the double morphant embryos. Data are expressed as the ratio of the OC/IC conduction velocity and are plotted as mean ± SD of N=3 experiments and n is represented on the columns. (ns *P*(*wnt11*^{ATG}MO/*akap2*^{e2i2}MO) = 0.2804; Mann-Whitney test).

4 Discussion

In the current study, I describe signaling mechanisms regulating the electrical gradient formation via compartmentalized LTCC/AKAP2/PKA multivalent complex as a novel function of Wnt11 signaling in the heart. The main conclusions which could be drawn from this study are as follows: (1) Wnt11 regulates the nuclear localization of the CT of the α1C subunit via preventing it from proteolytic processing; (2) the CT isoform generation is dependent on the AKAP anchored PKA signaling downstream of the Wnt11 pathway; (3) a novel player, the AKAP2 binds to the LTCC and regulates the CT isoform generation; (4) in developing zebrafish ventricle Wnt11 and Akap2 define the distribution and cluster formation of the LTCC; (5) Wnt11 and Akap2 collaborate to maintain the electrical gradient formation.

4.1 Wnt11/CT signaling

Cardiomyocytes are coupled through intercalated discs, which not only provide mechanical connections between the cells, but also enable fast action potential propagation that is crucial for synchronous contraction. The intercalated disc is composed of desmosomes, adherens junctions and gap junctions (Rohr, 2004). The Cx43 is one of the most abundant gap junction protein in the heart and several studies suggest that its expression is under the control of Wnt signaling (van der Heyden et al., 1998). Western blot analysis of NRVMs revealed that WNT1, but not WNT4 significantly increases the Cx43 abundance (Ai et al., 2000). Furthermore, overexpression of β-catenin enhanced the promoter activity of Cx43, which indicates that Wnt canonical signaling directly regulates the Cx43 expression (Ai et al., 2000). Furthermore, the downregulation of the Wnt non-canonical pathway has the same effect. This was demonstrated in *wnt11*-deficient zebrafish heart, where the Cx43 abundance increased across the whole ventricle (Panáková et al., 2010). In accordance with this finding, western blot analysis using H9c2 cell lysates from untreated and *WNT11* siRNA transfected cells confirmed that loss of *WNT11* indeed results in elevated Cx43 abundance (Figure 5B and 5C). During cardiogenesis Wnt11 pathway was shown to antagonize the Wnt canonical pathway, hence it decreases the nuclear level of the β-catenin (Cohen et al., 2012). This finding implicates that WNT11 might regulate Cx43 expression by inhibiting the canonical pathway.

The current study showed that loss of WNT11 increased the basal levels of the CT of the α1C subunit thus resulted in more homogeneous cell population regarding the nuclear accumulation of the CT compared to untreated cells (Figure 9A and 9C). In addition, CT showed co-localization with nucleolin (Figure 9A and 9B), which indicates a potential role of CT in these structures. Nucleus gives place to ribosomal biogenesis and regulate cell cycle, stress response and telomerase activity (Pederson, 1998; Raška et al., 2006; Rubbi & Milner, 2003). However, the role of the CT in these processes needs to be elucidated. The observations that loss of WNT11 unaltered the expression level of the *CACNA1C* gene, except of the last exon, as well as the localization and abundance of pore-forming domain of the α1C subunit leads to the conclusion that the CT isoform was generated via proteolytic processing. The published cleavage site in rat α1C subunit (A0A0G2QC25) occurs between aa residues 1631-1645 (Hulme et al., 2005), and the anti-CACH2C antibody that was used for the immunostainings recognizes the pCT region between aa 1342-1568, i. e. upstream of this reported cleavage, implying the existence of an additional cleavage site upstream of aa 1568. This observation was strengthened by FLAG-IP of the overexpressed FLAG-CT-mVenus construct followed by the FLAG detection, which resulted in seven extra bands besides the expected cleaved fragments (Figure 17C). However, I could never verify the formation of the endogenous CT isoform due to negative reactivity of the antibodies on western blotting. Previously published data as well as my findings suggest the presence of several CT isoforms that can translocate into the nucleus, and potentially associate with other subcellular compartments thereby contributing to regulation of a number of physiological processes.

The nuclear localization of the CT isoform in neurons and cardiomyocytes and its function as a transcription factor has been already demonstrated (Schroder et al., 2009). Among others it can regulate the expression of several gap junction proteins like Connexin 31.1 (Gomez-Ospina et al., 2006). The behavior of the CT as a transcription factor offers an additional signaling pathway downstream of the Wnt11, which might also contribute to the regulation of Cx43 expression beside the regulation via β-catenin dependent signaling.

The nuclear localization of the CT increased upon low extracellular calcium concentration and decreased upon high intracellular calcium concentration (Gomez-Ospina et al., 2006). This suggest that the CT cleavage induces the channel

conductance, meanwhile in the nucleus it represses its own promoter activity (Schroder et al., 2009), thereby creating a negative feedback loop. The observations that in *wnt11*-deficient developing zebrafish heart the Ca^{2+} transient amplitude increased (Panáková et al., 2010), and that in H9c2 cells loss of *WNT11* increased the CT nuclear localization are in accordance with the previous findings that CT formation induces the channel conductance. Furthermore, loss of FZD7, which is the putative receptor of WNT11 (Djiane et al., 2000) also resulted in increased nuclear localization of the CT (Figure 9B and 9D). In addition, stimulation of the β-AR pathway with ISO effected the CT isoform generation in a similar fashion as loss of WNT11/FZD7 did (Figure 10B), which suggests that stimulation of the G_s protein system may induce the CT isoform generation. In the light of these observations, WNT11/FZD7 presumably induces G_i protein coupled signaling, which antagonizes the G_s system, since the absence of this signaling resulted in the increment in the CT isoform generation as the stimulation of the G_s pathway did. These findings offer a mechanism, where downregulation of the WNT11 pathway can result in similar outcome considering the intracellular calcium concentration as its stimulation. Furthermore, the findings that FZD7 can couple with G_s, G_i and G_q proteins as well (von Maltzahn et al., 2012; Nichols et al., 2013) might suggest a possible switching mechanism between FZD7 and G_i or G_s proteins in a similar way as it is in the case of β_2-AR (Daaka et al., 1997), which would offer an even more dynamic system to regulate the intracellular calcium levels.

Taken together, these findings indicate the existence of a WNT11/CT signaling system that can establish the electrochemical properties of a cardiomyocytes via the regulation the calcium influx through the LTCC as well as via the regulation of the expression of proteins involved in the action potential propagation.

4.2 AKAP2 forms multivalent complex with PKA, LTCC, and induces CT signaling

Stimulation of the β-AR/G_s signaling pathway increases the cAMP levels and subsequently induces the PKA activation, and leads to phosphorylation of proteins involved in the E-C coupling. Consequently, this signaling results in the well-characterized positive inotropic and lusitropic effects of the β-AR stimulation in cardiomyocytes (Bers, 2002). Although, it has been shown that stimulation of

glucagon-like peptide-1 receptor (GLP1R)/G_s signaling results in comparable cAMP levels as stimulation of the β-AR/G_s signaling does, it leads to a mildly negative inotropic and no lusitropic effect (Petroff et al., 2001). These findings indicate that increment in the global cAMP levels is irrelevant in regulating E-C coupling, and that the efficient phosphorylation of target proteins requires compartmentalized cAMP signaling. The compartmentalized cAMP signaling is accomplished via spatial localization in the close proximity of the key regulatory proteins in subcellular microdomains. LTCC was shown to co-assemble with β_2-AR, G_s, AC, PKA and PP2A and form macromolecular signaling complexes (Davare, 2001). In addition, AKAPs ensure correct spatial and temporal positioning of PKA near to the phosphorylation target to facilitate the specificity of signaling events (Wong & Scott, 2004). Therefore, AKAPs play an essential scaffolding role in these macromolecular complexes.

The dCT isoform generation and regulation of the α1C subunit through AKAP/PKA signaling and its role in the LTCC regulation has been well studied, however the formation of the CT isoform remained obscure. FSK treatment of the H9c2 cells showed that inducing the global PKA activity results in CT increment in the nucleus (Figure 10A and 10C), which strengthens the previous results that G_s protein signaling increases the CT isoform formation (Figure 10A and 10B). Furthermore, applying PKI in *WNT11* siRNA transfected cells resembled the untreated cells, which indicated that local cAMP increment in the presence of inactivated PKA is unable to efficiently induce the CT cleavage (Figure 12A and 12B). Inhibition of the AKAP anchored PKA signaling masked the local PKA activity and resulted in only modest increment in the CT isoform generation compared to untreated cells (Figure 12A and 12C). These data indicate that the spatiotemporal targeting of PKA by AKAP is important in the CT isoform generation downstream of the WNT11 pathway.

Over the last decades many AKAPs have been demonstrated in cardiomyocytes regulating calcium cycling, myofiber contractility, cardiac arrhythmias, hypertrophy, heart failure, and hypoxia (Diviani et al., 2016). AKAP1 is manly present in mitochondria, where it regulates the levels of reactive oxygen species and inhibits the activity of proapoptotic proteins (Perrino et al., 2010). AKAP5 is membrane associated and regulates the phosphorylation of LTCC, RyR_2, PLN (Nichols et al., 2010), the trafficking of β-AR (Li et al., 2013) and regulates NFAT signaling (Murphy et al., 2014). AKAP6 is localized to the nuclear envelope (Pare et al., 2005) and regulates cardiac

hypertrophy as well NFAT signaling by recruiting PP2B (Li et al., 2010), RyR_2 activity (Marx et al., 2000), myogenic differentiation (Vargas et al., 2012), and cardiac remodeling (Lee et al., 2015). It binds to PDE thereby induces local cAMP hydrolysis (Dodge-Kafka et al., 2005). AKAP7 is also a membrane-targeted protein as AKAP5. It directs PKA, PKC, and PP2A to the LTCC, hence it regulates the LTCC conductance (Hulme et al., 2003). AKAP9 regulates the action potential duration by targeting PKA to the potassium voltage-gated channel subfamily Q member 1 (Marx et al., 2002), and mediates cAMP hydrolysis via PDE binding (Terrenoire et al., 2009). AKAP10 regulates transferrin receptor signaling (Eggers et al., 2009), and its mutation leads to impaired cardiac rhythm (Kammerer et al., 2003). AKAP12 forms multivalent complex with PKA, PKC, and PDE, and modulates Polo-like kinase 1 (Canton et al., 2012), β_2-AR desensitization as well as resensitization (Fan et al., 2001; Lin et al., 2000). AKAP13 was shown to form complex with Protein kinase D (PKD) (Carnegie et al., 2004), PKA, and nucleates a G_{12}-mediated Rho activation pathway via its Rho-Guanine nucleotide exchange factor (GEF) activity (Diviani et al., 2001). It is cardioprotective and regulates hypertrophic signaling pathways (Carnegie et al., 2008; Edwards et al., 2012). In this study, I show that AKAP2 and AKAP11 are also expressed in embryonic zebrafish cardiomyocytes (Figure 13B) as well as in H9c2 cells (Figure 13C). However, their function in cardiomyocytes have not yet been demonstrated. AKAP2 is also membrane anchored, and forms complex with PKA and lens-specific aquaporin-0 (AQP0) (Gold et al., 2012). Furthermore, AKAP2/PKA interaction was highly upregulated in human patients diagnosed with DCM (Aye et al., 2012), which implicates its role in cardiomyocytes. AKAP11 is able to form complex with PP1, PKA, and GSK3β in COS cells (derived from monkey kidney tissue), and decreases the activity of GSK3β via its phosphorylation by the kinases (Tanji et al., 2002).

Single siRNA knockdown of the *AKAP*s in H9c2 cells revealed that loss of the following AKAPs: AKAP6, AKAP7, AKAP10, AKAP11, AKAP12, and AKAP13 induce the generation of the CT isoform (Figure 14C-H). Considering the relative abundance of the different AKAPs within the cells, and whether they affected the CT formation lead to the following conclusions: *AKAP12* was the most abundant by 82.3%, while *AKAP7* was the least present by 0.6% in the H9c2 cells (Figure 13C), which means that *AKAP12* is ~137 times more abundant than *AKAP7*. The pCt intensity increased in the

nucleoli by 63% in the absence of *AKAP12* compared to untreated cells (Figure 13F), while in the absence of the *AKAP7* it increased by 40% (Figure 13D). Taking into account the relative abundance with the measured pCt intensity would theoretically mean that loss of *AKAP7* is ~125 times more efficient in increasing pCt intensity than loss of *AKAP12*. Following this thought, it would mean that loss of AKAP7 increases the pCt intensity 3.7 times more efficiently than loss of AKAP6, 1.52 times more efficiently than loss of AKAP10, 2.6 times more efficiently than loss of AKAP11, and 4.2 times more efficiently than loss of AKAP13. Although such calculation is irrelevant, because of the limitations of the technique, it supports the notion that the relative gene expression levels do not always reflect extent of the gene function. Furthermore, AKAPs form complexes with multiple enzymes resulting in variety of signaling events, which can lead to differences in the CT isoform generation. Nevertheless, an implication of these observations could be that the loss of AKAP12 globally increased the PKA accessibility, while loss of AKAP7 locally increased it. This explanation would be in line with the findings that AKAP7 forms multivalent complex with the LTCC (Wong & Scott, 2004), while AKAP12 is not (Diviani et al., 2016). In addition, neither loss of AKAP2 (Figure 14A) nor AKAP5 (Figure 14B) had effect on the CT isoform generation. Double knockdown of *AKAP5* together with *WNT11* revealed that AKAP5 is not involved in the CT isoform generation (Figure 15B). The fact that AKAP5 forms multivalent complex with the LTCC (Wong & Scott, 2004), and is not involved in the CT isoform formation, raised the question why loss of AKAP5 did not increase the CT formation, while the other AKAPs did. One explanation could be that since AKAP5 can bind simultaneously PKA, PKC, and PP2B (Klauck et al., 1996), the loss of *AKAP5* besides PKA also induces the availability of PKC and PP2B creating an equilibrium in the channel regulation. To address whether the absence of these AKAPs effect the local PKA activity, thereby the CT formation FRET or BRET assay would be an option to perform. Surprisingly, in the absence of *AKAP2*, the loss of *WNT11* had only mild effect on the pCt intensity in the nucleoli (Figure 15A) suggesting that the increment in local PKA activity is inefficient without the AKAP2 to regulate the CT isoform generation. On the other hand, neither loss of *AKAP2* or application of the L314E peptide could completely rescue the loss of *WNT11* phenotype, which may indicate the direct binding of PKA to the channel.

The ability of AKAP2 to bind PKA-RII subunit was established many years ago (Dong et al., 1998), however later data indicated its dual specificity (Aye et al., 2009). This is in line with the protein spotting data, which suggested that AKAP2 forms complex with the PKA regulatory subunit Ia and IIa (Figure 17). AKAP2 was shown to have at least six isoforms, which are differentially expressed in various tissues (Dong et al., 1998), most of these isoforms are enriched in H9c2 cells (Figure 18A). However, FLAG-IP of the FLAG-CT-mVenus construct and detection with AKAP2 antibody only resulted in a ~130 kDa band (Figure 19B), which suggests that the CT construct only binds to one of the AKAP2 isoforms. Reciprocal co-IP strengthened the evidence of the interaction between AKAP2 and the CT construct (Figure 19C), and the binding between endogenous proteins was also confirmed (Figure 20B).

WNT11/Calcium signaling plays an important role in establishing the intracellular calcium concentration, thereby regulating a range of intracellular events. It is likely that in the absence of this signaling such compensatory mechanisms become active, which can restore the intracellular calcium concentration. The immunoprecipitation data indicate the existence of a novel LTCC multivalent complex composed by AKAP2, PKA, and LTCC. The loss of WNT11 leads to increased intracellular calcium concentration (Panáková et al., 2010), and to the AKAP2-dependent generation of the CT isoform suggesting that the loss of WNT11 induces the formation of this AKAP2/PKA/LTCC complex to regulate the intracellular calcium concentration. Furthermore, the observation that CT acts as a transcription factor, which can prevent its own promoter activity (Schroder et al., 2009) indicates a dynamic regulatory system between WNT11 and the LTCC. In addition, qPCR data might suggest the relevance of other regulatory feedback loops in this system, because downregulation of *WNT11* in H9c2 cells induced the expression of the *AKAP2* (Figure 16A), while downregulation of *AKAP2* decreased the expression of *WNT11* (Figure 16B).

In summary, these findings suggest the existence of a novel AKAP2/PKA/LTCC complex next to the known complexes, which consists either AKAP5 or AKAP7. In contrast with the other two complexes, which regulate the generation of the dCT isoform, AKAP2/PKA/LTCC complex can regulate the cleavage of the CT isoform downstream of the WNT11 and β-AR pathway, thereby might modulating the LTCC conductance.

4.3 Akap2 functions during heart development

Heart formation occurs through an evolutionary conserved program, which involves a complex series of morphogenetic events. During zebrafish cardiac development cells derived from anterior lateral plate mesoderm converge and fuse to form linear heart tube along the ventral midline (~30 hpf) (Stainier et al., 1993). The linear heart tube then under the control of genes involved in establishing the left-right asymmetry bends to the right side creating left-right polarity (Capdevila et al., 2000). During the cardiac looping, which occurs between 30-48 hpf the heart loses its tubular form as the two-chambers become morphologically distinguishable. In parallel, in the atrioventricular canal the action potential propagation becomes slow, which results in contraction delay between the atrium and the ventricle, and the peristaltic contraction is replaced by sequential contraction (Chi et al., 2008). As the chambers are ballooning, the conduction velocity within the ventricle is increasing specially in the outer curvature to enable the cardiomyocytes to contract synergistically (Chi et al., 2008). It has been shown that establishing the electrical gradient formation requires Wnt11 signaling (Panáková et al., 2010). Furthermore, the observation that the electrical gradient formation in *wnt11*-deficient heart can be rescued by inhibition of the LTCC indicates that *wnt11* can regulate the electrical gradient formation via attenuation of the LTCC conductance (Panáková et al., 2010).

Beside that the Wnt11 signaling regulating the myocardial electrical gradient formation, it has been shown to regulate cardiac looping as well (Choudhry & Trede, 2013). This is in line with the findings that the looping angle was enlarged in *wnt11* morphant heart by ~13.6° compared to uninjected control embryos (Figure 29). Furthermore, measuring the action potential propagation in either *wnt11* morphant or mutant embryos confirmed that the loss of *wnt11* abolishes the electrical gradient formation in developing zebrafish heart (Panáková et al., 2010). Since, the ratio between the conduction velocities in the OC and IC in *wnt11* mutant was at 1.65 and in *wnt11* morphant 1.47. Surprisingly, in *wnt11* mutants the mRNA expression of the *cacna1c* gene, which encodes the α1C subunit of the LTCC was significantly reduced (Figure 24) suggesting the Wnt11 role in regulation of the channel expression. Since for the qPCR analysis whole zebrafish embryo RNA extract was used, it is not clear whether Wnt11 regulates the channel expression in cardiomyocytes. Furthermore, in the absence of the Wnt11 the dCT expression was the most effected. The dCT function as

a transcription factor has been previously shown (Gomez-Ospina et al., 2013). It can be transcribed independently from the *cacna1c* gene and repress its own promoter activity (Gomez-Ospina et al., 2013). In the light of these facts the regulation of the dCT expression via Wnt11 pathway might ensure a regulatory feedback loop. LTCCs are enriched in transverse-tubules (T-tubules), which are invaginations of the plasmamembrane that form a complex network of ducts (Brette & Orchard, 2003). The local accumulation of the LTCCs is indespensible for calcium induced calcium release with nearby RyRs, hence for establishing E-C coupling. Although the adult zebrafish cardiac muscle lacks T-tubules (Iorga et al., 2011), in wild-type embryos the LTCCs form clusters at the cell-cell boundaries (Figure 26B). The formation of these custers along the cell membranes was desturbed in *wnt11*-deficient hearts (Figure S6). Altogether, these findings suggest a more dynamic and complex regulatory mechanism in zebrafish between Wnt11 signaling and LTCC than compared to H9c2 cells.

Furthermore, analysing the expression of the *akap* genes in zebrafish embryos revealed that they are differentally expressed compared to H9c2 cells. For instance, AKAP5 that regulates the LTCC conductance in mammalian cardiomyocytes (Diviani et al., 2016) has no zebrafish orthologues. The *akap6*, which establishes the intracellular calcium levels in mammalian CMs (Diviani et al., 2016) is not expressed in zebrafish CMs. In addition, measuring the relative ratio between the relative amounts of the *akap*s indicated that *akap2* is one of the most abundant *akap* in the zebrafish CMs (Figure 13B). These observations indicate that in zebrafish cardiomyocytes *akap2* might have broader function than in mammalian CMs. Analyzing the loss of *akap2* phenotype revealed that *akap2*-deficient embryos display decreased body size, perturbed brain structures, and heart edema (Figure 22A). Furthermore, loss of *akap2* effected the heart looping in little bit less than half of the embryos. Most of these embryos had unlooped hearts, in which case the looping angle occurred around 62.4° (Figure 23), while some of them (less than 10%) developed inverted hearts (Figure 22B). It has been previously proposed that in prostate cancer cells, AKAP2 induces cell invasion and proliferation downstream of the calcitonin mediated pathway via destabilizing the cell-cell junctions (Thakkar et al., 2016). Immunostaining experiments using *akap2*-deficinet embryonic zebrafish heart strengthened this observation. At 54 hpf the zebrafish heart is formed by an outer myocardial monolayer (myocardium) and

an inner endothelial monolayer (endocardium). However, in *akap2*-deficient heart the structure of the myocardium and endocardium was perturbed. The extracellular matrix between the two layers is increased, meanwhile the endocardium became compact (Figure 25C'). Furthermore, in some parts of the ventricle the monolayer of the myocardium was replaced by double layer (Figure 25C'). Since the proper looping of the heart requires cell rearrangement (Männer, 2009), it is very likely that the unlooped heart phenotype can originate from the disturbance in the cell-cell junctions. The action potential propagation was also effected in *akap2*-deficient ventricle. The ratio of the conduction velocities in these embryos between the OC and IC was significantly reduced compared to the wild-type embryos (Figure 30B). This might be the consequence of that in *akap2*-deficient heart the localization of the α1C subunit was altered. In *akap2*-deficient ventricle the longitudinal clusters of the LTCCs were less defined and instead LTCCs were localized more equally along the cell-cell boundaries (Figure 27C), which might indicate that the cluster formation of the LTCC in the subcellular microdomains is impaired in the absence of Akap2. These results combined with the previous finding that AKAP2/PKA interaction was highly increased in human patients diagnosed with DCM (Aye et al., 2012) strongly suggest that AKAP2 has a pivotal function in the regulation of the E-C coupling.

The current study suggests that *AKAP2* assembles with LTCC and PKA and regulates the formation of the CT isoform on Wnt11 signaling dependent manner. To demonstrate whether this multivalent complex is involved in the electrical gradient formation downstream of the Wnt11 pathway, double *akap2*; *wnt11* morpholino injected embryos were utilized. Phenotype analysis of the double morphant embryos revealed that some but not all of the phenotypic characteristics of the *wnt11* morphant were rescued by knockdown of *akap2*. For instance, in the double morphant the body length and brain structure resembled the wild-type phenotype. However, to ensure that loss of *akap2* indeed enable the rescue of the forebrain abnormalities in *wnt11* morphant further studies are required. Furthermore, most of the double morphant embryos developed cardiac looping defect; less than half of the cases were accompanied with fused eyes (Figure 28B). Double knockdown of *akap2* together with *wnt11* resulted in enhanced looping angle as single knockdown of the *akap2* did, however this unlooped phenotype was less strong as in *akap2*-decficient heart (Figure 29B). Considering that loss of Wnt11 signaling leads to disturbed Wnt11/PCP and

Wnt11/Calcium signaling this data may imply that loss of *akap2* abolished the effect of the loss of Wnt11/Calcium pathway, but could not rescue the loss of Wnt11/PCP effect.

Interestingly, the conduction velocities in double morphant resembled the wild-type conduction phenotype as the ratio between the conduction velocity of the OC and IC was 3.22 ± 0.60 (Figure 32) indicating that *akap2* rescued the loss of *wnt11* phenotype. It has been shown that knockdown of the core components of the Wnt11/PCP pathway has no effect on the electrical gradient formation (Panáková et al., 2010). This observation, and the findings of these experiments that loss of *akap2* could not rescue the loss of *wnt11* phenotype regarding the heart looping, but restored the action potential propagation in *wnt11*-deficient heart suggesting that Akap2 acts downstream of Wnt11/Calcium pathway.

Taken together these data suggest, that in developing zebrafish embryos the Akap2 regulates the heart development. Embryos which lack Akap2 develop unlooped heart and had disturbed action potential propagation, which implies that failure in Akap2 anchored PKA signaling might be the cause of a number of cardiomyopathies. Furthermore, the findings that the absence of the Wnt11 signaling abolished the electrical gradient formation, however knockdown of Akap2 rescued the action potential propagation lead me to the conclusion that Akap2 might be the downstream effector of the Wnt/Calcium pathway.

5 Conclusions and Outlook

The current study provides evidence that Wnt11 signaling pathway modulates the LTCC conductance, hence regulates the electrical gradient formation in developing zebrafish heart. In H9c2 cell, Wnt11 signaling prevented the CT of the α1C subunit of the LTCC from proteolytic processing. These findings are based on the observations that the loss of *WNT11* unaltered the expression of the *CACNA1C* gene, which encodes the α1C subunit. However, loss of *WNT11* and *FZD7* induced the formation of the CT isoform. Furthermore, stimulation of β-AR/G_s pathway resembled the loss of WNT11/FZD7 phenotype, which indicates that either downregulation of the FZD7/G_i system or stimulation of β-AR/G_s pathway induces the cleavage of the CT isoform. Applying PKA inhibitor on *WNT11* siRNA transfected cells revealed that the formation of the CT isoform is inefficient in the absence of the active PKA. Many studies suggested that compartmentalized cAMP activation is partially achieved via AKAPs. These scaffolding proteins enable the efficient local PKA signaling via directing the PKA to its phosphorylation targets. Applying a peptide, which disrupts the AKAP anchored PKA signaling in *WNT11* siRNA transfected cells suggested that AKAP anchored PKA signaling is important in the formation of the CT isoform downstream of the Wnt11 pathway.

Systematic analysis of the AKAPs using single knockdown of the *AKAP*s and double knockdown of the *AKAP*s together with *WNT11* by siRNA transfection in H9c2 cells revealed that AKAP2 plays pivotal role in the generation of the CT isoform downstream of the Wnt11 signaling. Furthermore, co-IP experiments suggest the existence of a novel LTCC multivalent complex composed by LTCC, AKAP2, and PKA. These findings indicate that WNT11 pathway negatively regulates the formation of the LTCC/AKAP2/PKA complex, which induces the generation of the CT isoform.

To investigate whether this complex is involved in the myocardial electrical gradient formation I performed single knockdown of *akap2* and double knockdown of *akap2* together with *wnt11* in developing zebrafish embryo using morpholino approach. *akap2*-deficient embryos developed heart edema and most of them had looping defect. Furthermore, loss of Akap2 effected the electrical gradient formation in the developing ventricle, which suggested that Akap2 is essential during cardiogenesis. In addition,

the *akap2*; *wnt11* double morphant embryos had milder looping defect, however resembled the wild-type conduction phenotype. These observations that in *wnt11*-deficient heart *akap2* could not rescue the abnormal heart looping, but restored the action potential propagation, brought me to the conclusion that Akap2 acts downstream of the Wnt11/Calcium signaling.

Taken together these results suggest, that Wnt11 signaling can modulate the channel conductance, hence the electrical gradient formation by antagonizing the β-AR/G_s signaling and preventing the CT isoform generation, which requires AKAP2 anchored PKA phosphorylation of the LTCC (Figure 33).

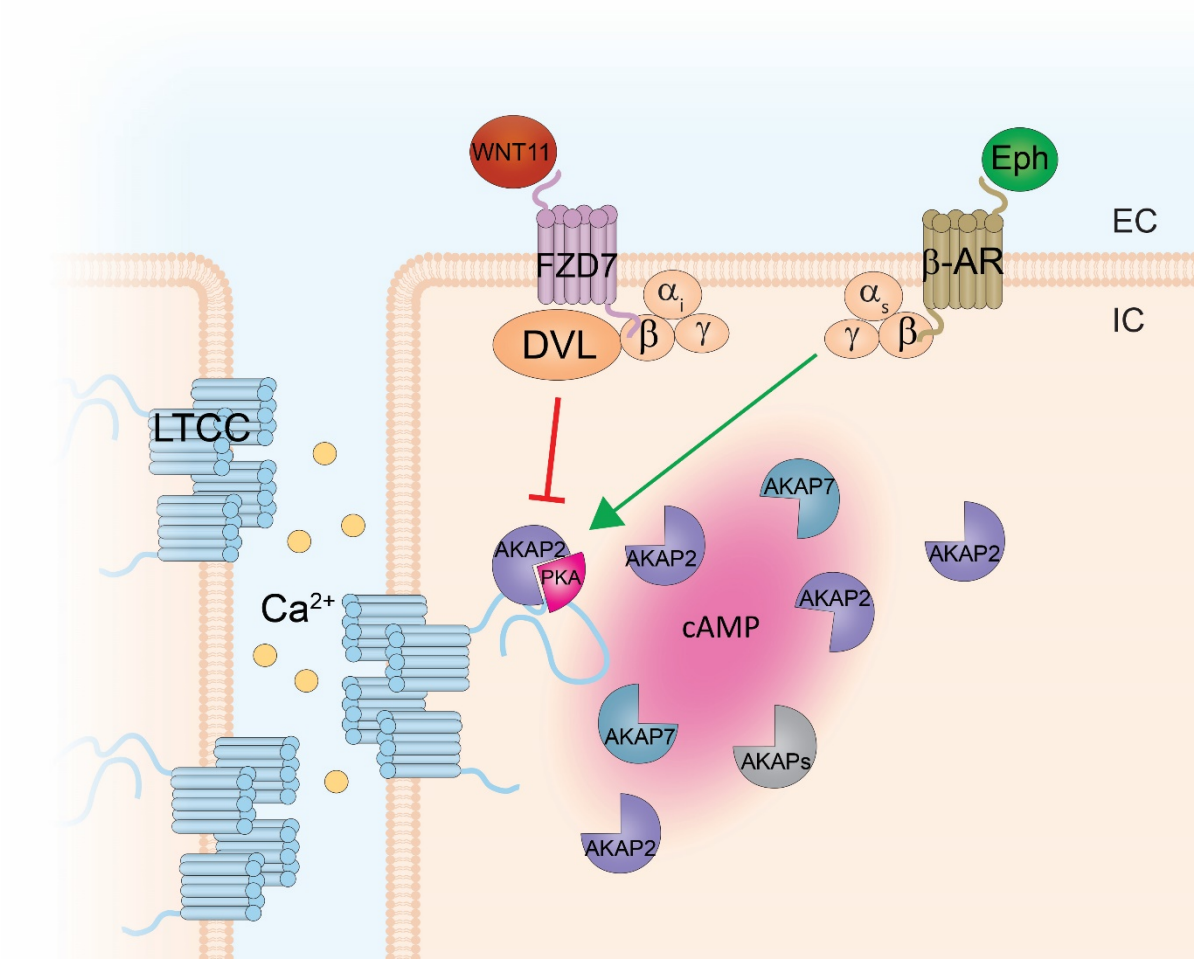

Figure 33: Model of AKAP2/LTCC/PKA complex regulated by Wnt11/Calcium signaling. Wnt11/Calcium pathway regulates the CT isoform generation via AKAP2/LTCC/PKA complex. LTCC- L-type calcium channel, AKAP- A-kinase-anchoring protein, DVL-Dishevelled, FZD7- Frizzled 7, β-AR- β-Adrenergic Receptor, Eph-Epinephrine, $G\alpha_i$ subunit- α_i, Gβ subunit- β, Gγ subunit- γ, EC- Extracellular, IC-Intracellular.

The Wnt11 signaling and its relevance during development has been extensively demonstrated, however its function in cardiac biology as an alternative GPCR like system needs to be elucidated. Future studies should aim to define the downstream components of this pathway, and whether they regulate the formation of the AKAP2 complex. Since only very limited information is available about this scaffolding protein it would be important to identify its interacting partners and build up-to-date protein interactome networks. Current study proposes that AKAP2 has pivotal role in regulating the LTCC and establishing the electrical gradient formation in developing zebrafish ventricle. Further investigation should explore, which domains are important in the AKAP2/LTCC interaction and define the cleavage site on the CT. Furthermore, it has been shown that AKAP2/PKA interaction was upregulated in patients diagnosed with DCM (Aye et al., 2012), which together with the findings of this study makes AKAP2 interesting therapeutic target for treatment of cardiac myopathies and heart failure.

6 Materials and Methods

6.1 Materials

REAGENT or RESOURCE	SOURCE	IDENTIFIER
Antibodies		
Mouse Anti-beta-Actin Monoclonal Antibody, Unconjugated, Clone AC-15	Sigma-Aldrich	Cat# A5441; RRID:AB_476744
Rabbit Anti-Nucleolin Antibody	Abcam	Cat# ab22758; RRID:AB_776878
Anti-Calcium Channel Antibody, Voltage Gated α1C	Millipore; (Dolmetsch et al., 2001)	Cat# AB5156-50UL
Alexa Fluor™ 633 Phalloidin	Thermo Fisher Scientific; (Rosado et al., 2014)	Cat# A22284
Mouse Anti-CACH2C Monoclonal Antibody, clone S57-46	Abnova Corporation	Cat# MAB6647; RRID:AB_10679701
Rabbit Anti-Human / Rat Connexin-43 Antibody, Unconjugated	Sigma-Aldrich	Cat# C6219; RRID:AB_476857
Rabbit Anti-Phospho-PKA Substrate Antibody	Cell Signaling; (Song et al., 2017)	Cat# 9624S
Mouse Anti-AKAP-KL Monoclonal Antibody, Unconjugated, Clone 41	BD Biosciences	Cat# 611134; RRID:AB_398445
Mouse Anti-FLAG M2 Monoclonal Antibody	Sigma-Aldrich	Cat# F3165; RRID:AB_259529
Rabbit Anti-GFP Polyclonal Antibody, Unconjugated	GeneTex	Cat# GTX113617; RRID:AB_1950371
Mouse Anti-ZN8	Hybridoma Bank	RRID:AB_531904
Rabbit Anti-pCt Antibody [C]-HINKTGNNQADTESPSHEKL-amide (not affinity purified)	Cambridge Research Biochemicals; (This paper)	N/A
Anti-rabbit IgG, HRP-linked Antibody	Cell Signaling	Cat# 7074, RRID:AB_2099233
Anti-mouse IgG, HRP-linked Antibody	Cell Signaling	Cat# 7076, RRID:AB_330924
Goat Anti-Rabbit IgG (H+L) Antibody, Alexa Fluor® 488 Conjugated	Thermo Fisher Scientific	Cat# A-11008, RRID:AB_143165

Donkey Anti-Mouse IgG (H+L) Antibody, Alexa Fluor® 555 Conjugated	Thermo Fisher Scientific	Cat# A-31570, RRID:AB_2536180
Bacterial Strains		
Subcloning Efficiency™ DH5α™ Competent Cells	Thermo Fisher Scientific	Cat# 18265017
One Shot™ TOP10 Chemically Competent E. coli	Thermo Fisher Scientific	Cat# C404006
Chemicals and Peptides		
Forskolin	Sigma-Aldrich	#F6886; CAS:66575-29-9
PKI (custom-made)	Leibniz-Forschungsinstitut für Molekulare Pharmakologie	N/A
L314E (custom-made)	Leibniz-Forschungsinstitut für Molekulare Pharmakologie; (Hundsrucker et al., 2006)	N/A
DharmaFECT 1 Transfection Reagent	Dharmacon	Cat# T-2001-03
Lipofectamine™ 2000 Transfection Reagent	Thermo Fisher Scientific	Cat# 11668027
cOmplete™, Mini, EDTA-free Protease Inhibitor Cocktail	Sigma-Aldrich	Cat# 04693159001
PhosSTOP™	Sigma-Aldrich	Cat# 04906845001
Anti-FLAG® M2 Magnetic Beads	Sigma-Aldrich	Cat# M8823
Dynabeads™ Protein A for Immunoprecipitation	Thermo Fisher Scientific	Cat# 10001D
Penicillin-Streptomycin (10,000 U/mL)	Thermo Fisher Scientific	Cat# 15140148
MEM Non-Essential Amino Acids Solution (100X)	Thermo Fisher Scientific	Cat# 11140050
TRIzol™ Reagent	Thermo Fisher Scientific	Cat# 15596026
Cytochalasin D	Sigma-Aldrich	Cat# C8273; CAS:22144-77-0
Tricane	Sigma-Aldrich	Cat# A5040 ; CAS: 886-86-2
Anti-Calcium Channel Antibody, Voltage Gated α1C Antigen	Millipore	Cat# AB5156-50UL
Isoproterenol hydrochloride	Sigma-Aldrich	#1351005; CAS:51-30-9
Critical Commercial Assays		
FluoVolt™ Membrane Potential Kit	Thermo Fisher Scientific	Cat# F10488
In-Fusion® HD Cloning System	Takara Bio USA Inc.	Cat# 639648
First Strand cDNA Synthesis Kit	Thermo Fisher Scientific	Cat# K1612

RNase-Free DNase Set	Qiagen	Cat# 79254
RNeasy Mini Kit	Qiagen	Cat# 74104
Phusion High-Fidelity DNA Polymerase (2 U/µL)	Thermo Fisher Scientific	Cat# F530S
mMESSAGE mMACHINE™ T3 Transcription Kit	Thermo Fisher Scientific	Cat# AM1348
Poly(A) Tailing Kit	Thermo Fisher Scientific	Cat# AM1350
Gateway™ BP Clonase™ II Enzyme mix	Thermo Fisher Scientific	Cat# 11789020
Gateway™ LR Clonase™ II Enzyme mix	Thermo Fisher Scientific	Cat# 11791020
GeneJET Gel Extraction Kit	Thermo Fisher Scientific	Cat# K0691
Experimental Models: Cell Lines		
Rat H9c2 (2-1)	ATCC	CRL-1446
Experimental Models: Organisms/Strains		
Zebrafish: Tg(myl7:EGFP)twu26: twu26Tg	(Huang et al., 2003)	ZFIN ID: ZDB-ALT-070530-1
Zebrafish: wnt11^{tx226}	(Heisenberg et al., 2000)	ZFIN ID: ZDB-ALT-980203-1302
Zebrafish: AB/TL wild-type		
Oligonucleotides		
Primers for RT-PCR Figure S1A, see Table S1	This paper	N/A
ON-TARGETplus Rat siRNA, see Table S2	Dharmacon	N/A
TaqMan™Gene Expression Assay, see Table S3	Thermo Fisher Scientific	N/A
Primers for ISH, see Table S1	This paper	N/A
Primers for Danio *akap2* mRNA, see Table S1	This paper	N/A
Primers for *akap2* cDNA, see Table S1	This paper	N/A
Primers for CRISPR-Cas9 experiment, see Table S1	This paper	N/A
Morpholino: *akap2*^{e2i2sp} MO TTGACGTAAATGTTCATACCTGGT	GeneTools This paper	N/A
Morpholino: *wnt11*^{ATG} MO GTTCCTGTATTCTGTCATGTCGCTC	GeneTools	ZFIN ID: ZDB-MRPHLNO-050318-3
Recombinant DNA		
pGEM®-T Easy Vector Systems	Promega	Cat# A1360
pBluescript KS		
MGC Rat Akap2 cDNA	Dharmacon	Cat# MRN1768-202780602; Clone ID: 7108964
Plasmid: GeneArt® cDNA Rat Cacna1c aa(1350-2090)	Thermo Fisher Scientific	N/A

Gateway™ pDONR™221 Vector	Thermo Fisher Scientific	Cat# 12536017
pFRT_TO_DESTFLAGHA	Addgene	Cat# 26361
Software and Algorithms		
ImageJ Fiji	https://imagej.net/Fiji/Downloads	
Adobe Illustrator CS5.1		
Adobe Photoshop CS5.1		
Image Studio Lite		
GraphPad Prims 6	https://www.graphpad.com/scientific-software/prism/	
MATLAB (MathWorks)	https://www.mathworks.com/products.html?s_tid=gn_ps	
Leica Application Suite (LAS)		
Omicroled LED Controller		
NeuroPlex 9.9.6 (RedShirt Imaging)	http://www.redshirtimaging.com/support/soft_ov.html	
QuantStudio™ 7		
BD FACSDiva™ software	http://www.bdbiosciences.com/in/instruments/software/facsdiva/index.jsp	

6.2 Methods

6.2.1 Zebrafish methods

6.2.1.1 Ethics Statement

All zebrafish husbandry and experiments were performed in accordance with guidelines approved by the Max-Delbrück Center for Molecular Medicine at the Helmholtz Association and the local authority for animal protection (Landesamt für Gesundheit und Soziales, Berlin, Germany) for the use of laboratory animals, and followed the “Principles of Laboratory Animal Care’ (NIH publication no. 86-23, revised 1985) as well as the current version of German Law on the Protection of Animals

6.2.1.2 Zebrafish husbandry

Zebrafish were maintained under continuous water flow and filtration with automatic control for a 14:10 hours (h) light/dark cycle at 28.5°C. Fertilized eggs were collected and raised under standard laboratory conditions (at 28.5°C in E3 solution (5 mM NaCl, 0.17 mM KCl, 0.33 mM CaCl2, 0.33 mM MgSO4, pH 7.4)). The following zebrafish lines were used: AB/TL wild-type line, Tg(*myl7*:*eGFP*) ^{twu34} transgenic line (Huang et al., 2003) and wnt11^{tx226} mutant line (Heisenberg et al., 2000).

6.2.1.3 Bright field imaging

54 hpf embryos were either anesthetized using 4 mg/ml Tricane (pH~7) or fixed in PEM solution (100 mM PIPES, 2 mM $MgSO_4$, 1mM EGTA, pH 7) with 4% Formaldehyde and 0.1% Triton X-100 for 2 h, at RT and mounted in 2% methylcellulose. For imaging Leica Fluorescence Stereo Microscope M165 equipped with Leica DFC450C camera and LAS-V4.7 software was used. Images were processed using ImageJ Fiji and Adobe Photoshop CS5.1.

6.2.1.4 Microinjection

The night before injection, male and female fish were placed in a 1l tank and separated. At morning, zebrafish embryos were obtained by removing the divider. The morpholino injection solution was prepared from RNase/DNase free water and 1mM *akap2* morpholino in a ratio 1:1 or 1mM *wnt11* morpholino in a ratio 1:6. After incubation at 65°C for 10 min 1 nl morpholino solution was injected per embryo into

the yolk of 1-4 cell stage embryos. 1 nl capped *akap2* mRNA was injected into 1-cell stage embryos (concentration is indicated on the figures).

6.2.1.5 Heart looping measurement

Heart angle was defined as the angle enclosed by the midsagittal line and the atrioventricular canal. For the images 54 hpf fixed embryos were used, embed in 2% methylcellulose. Images were analyzed using ImageJ Fiji.

6.2.1.6 Optical mapping of action potential propagation

Optical mapping and signal processing was performed as described previously (Panáková et al., 2010). Hearts were isolated from 54 hpf zebrafish embryos in normal Tyrode's solution (NST contains 136 mM NaCl, 5,4 mM KCl, 1mM $MgCl_2x6H_2O$, 5mM D-(+)-Glucose, 10mM HEPES, 0.3 mM $Na_2HPO_4x2\ H_2O$, 1. mM $CaCl_2x2\ H_2O$, pH 7.4) supplemented with 20 mg/ml BSA. To record membrane potential changes, hearts were stained for 12 minus with FluoVolt probe (Thermo Fisher Scientific), and washed with NST-BSA. Individual hearts were transferred into perfusion bath (Warner Instruments), which contained NST supplemented with 100 μM Cytochalasin D to inhibit contraction. For the imaging high-speed CCD camera (RedShirt Imaging) was used equipped with LED lamp and NeuroPlex software. Images were analyzed with MatLab (MathWork) using customized software (Panáková et al., 2010).

6.2.1.7 Zebrafish AKAP2 mRNA construction

Zebrafish *akap2* (ENSDARG00000069608) mRNA was constructed by PCR amplification of cDNA using *Danio rerio* akap2 infusion primers (see Table S1), which were designed with http://bioinfo.clontech.com/infusion/convertPcrPrimersInit.do. The cDNA fragment was cloned into pBluescript KS (-) vector with HindIII at the 5'-end and BamHI restriction enzyme site at the 3'-end using the In-Fusion® HD Cloning System. *In vitro* transcription was performed using mMessage mMachine T3 Transcription Kit and BamHI-linearized DNA template at 37°C. To increase translation initiation efficiency and transcript stability I performed polyadenylation of the mRNA using Poly(A) Tailing Kit.

6.2.1.8 Single-cell dissociation and FACS

54 hpf *myl7*.*EGFP* transgenic embryos Tg(*myl7:EGFP*) were dechorionated using Pronase and incubated in 0.25% Trypsin at 28.5 °C. Single-cell dissociation was monitored every 20 minutes and was generally achieved within 2 hours of incubation. Efficient dissociation was helped by gentle pipetting. Cell suspension was filtered through 70 μM strainer and cells were exhaustively washed three times in cold PBS supplemented with Fetal Calf Serum in reducing concentration and eventually resuspended in 1 ml of cold PBS. Single cells were filtered in a glass tube with a cell strainer cap and placed on ice until counting. Samples were analyzed using a BD FACS Aria1 flow cytometer, operating with BD LSRFortessa analyzer with BD FACSDiva software. GFP expressing cells were identified using a 488nm laser and a 530/30 BP filter.

6.2.1.9 qPCR

The total RNA was isolated from wild-type or *wnt11*^{tx226} mutant zebrafish embryos at 54 hpf using the TRIzol reagent according to the manufacturer's instruction. The RNA was digested with DNase set (Qiagen), cleaned with RNeasy Mini Kit (Qiagen) and reverse transcribed using First Strand cDNA Synthesis Kit. 100 ng of cDNA was used for real-time PCR analysis. The total RNA was isolated from EGFP positive cells of *myl7*.*EGFP* transgenic embryos Tg(*myl7:EGFP*) at 54 hpf, using the TRIzol reagent according to the manufacturer's instruction. The RNA was reverse transcribed using First Strand cDNA Synthesis Kit. 10 ng of cDNA was used for real-time PCR analysis. The relative mRNA levels were quantified using gene-specific TaqMan assays (see Table S3) ViiA 7 Real-Time PCR System and Quant Studio 7. Results were analyzed using the comparative threshold cycle (2^-ΔΔCt) method (Livak & Schmittgen, 2001), normalized to housekeeping gene. The results are expressed as fold-increase of $\log_2$ (2^-ΔΔCt) over mock. Statistical significance was assessed using ΔCt.

6.2.1.10 Confocal microscopy

Hearts were isolated from 54 hpf zebrafish embryos in normal Tyrode's solution (pH 7.4) supplemented with 20 mg/ml BSA and fixed in Glyo-Fixx for 12 minutes. Following primary antibodies were used: anti-II-III-loop (Millipore) 1:50; ZN8 (Hybridoma Bank) 1:50. For the specificity validation of the II-III loop it was pre-

incubated with its peptide in a ratio 1:1 for 2h at RT. Confocal images were obtained on Leica TCS SP5 using LAS-FX software.

6.2.2 Cell culture methods

6.2.2.1 Cell culture and transfection

H9c2(2-1) (rat [*Rattus norvegicus*] heart myoblast) cells were obtained from ATCC® (CRL-1446™), cultured in Dulbecco's Modified Eagle Medium (DMEM) supplemented with 10% of Fetal Bovine Serum (FBS), 1% of Penicillin-Streptomycin and 1% of Non-essential amino acids, and incubated at 37°C with 5% CO_2.

H9c2 cells were transfected for 24 h with a concentration of 50nM siRNA (see Table S2) using DharmaFECT 1 (Dharmacon) according to manufacturer's instructions. H9c2 cells were transfected for 24 h with a concentration of 200 ng/ml DNA using Lipofectamine™ 2000 (Thermo Fisher Scientific) according to manufacturer's instructions.

6.2.2.2 Rat AKAP2 Plasmid construction

cDNA encoding rat *AKAP2* was obtained (Dharmacon). FLAG/HA-tagged AKAP2 was cloned using Gateway technology (Invitrogen) by PCR amplification of the *AKAP2* cDNA using attB-flanked BP primers (see Table S1). attB-flanked PCR product was cloned first into a pDONR™221 vector using BP Clonase™ II Enzyme mix to generate entry clone, and subsequently transferring into a destination vector pFRT_TO_DESTFLAGHA to create expression clone using LR Clonase™ II Enzyme mix.

6.2.2.3 Immunoprecipitation

H9c2 cell were solubilized in mild lysis buffer (2mM EDTA, 2mM EGTA, Triton X-100 in PBS) containing PhosSTOP and EDTA-free Protease Inhibitor Cocktail. Lysates were passed through a syringe of 0.4mm diameter, centrifuged at 5000xg at 4°C for 5 minutes and quantified by Bradford's protein estimation method (Anal. Biochem. 72, 248-254 (1976)). Lysates were incubated over night at 4°C either with Anti-FLAG M2 Magnetic Beads or with Dynabeads Protein A, which was beforehand incubated with AKAP2 or GFP antibody. Beads were washed four times with mild lysis buffer using magnetic separator. Immunoprecipitated proteins were eluted with 0.1M glycine (pH

2.5), neutralized with 1M Tris (pH 10.6) and denatured in 1x Laemmli sample buffer for 7 min at 95°C. Eluted proteins were resolved on 10 % SDS-PAGE gels (home-made) and western blotted using standard procedure. The following primary antibodies were used: anti-AKAP2 (Bioscience) 1:500, anti-FLAG (Sigma) 1:1000 and anti-pCt (custom-made) 1:1000, anti-GFP (GeneTex) 1:4000. Chemiluminescent detection was performed, blots were visualized using Odyssey Fc Imaging System, LI-COR (Biosciences) and Image Studio Lite software.

6.2.2.4 Peptide spots

Peptides were spot-synthesized as 25 mers (see Table S4) on a Whatman 50 cellulose membrane using the AutoSpot-Robot ASS 222 (Intavis Bioanalytical Instruments) as described previously (Hundsrucker et al., 2010). Membranes were incubated with FLAG-IPed protein lysates and were detected using anti-FLAG (Sigma) 1:1000, as for western blotting. Chemiluminescent detection was performed, blots were visualized using Odyssey Fc Imaging System, LI-COR (Biosciences) and Image Studio Lite software.

6.2.2.5 Immunoblotting

H9c2 cell lysates were prepared using RIPA buffer (20 mM Tris-HCl, 150 mM NaCl, 0.1% Triton X-100, 0.1% SDS, 0.5% Sodium-deoxycholate, PhosSTOP, EDTA-free Protease Inhibitor Cocktail). Lysates were sonicated and centrifuged at 5000xg at 4°C for 5 minutes. Protein concentrations were quantified by Lowry's estimation method. After addition of Laemmli buffer (50 mM Tris-HCl, 0.1% SDS, 9% Glycerol, 1% β-mercaptoethanol, 0.02% Bromphenolblue, 25 mM DTT) lysate was cooked for 10 minutes and centrifuged again 5000xg and 4°C for 5 minutes. Total protein was separated on 4-15% SDS-polyacrylamide gel (Bio Rad), and transferred to a Nitrocellulose Blotting membrane (GE Healthcare). The following concentration of the primary antibodies were used: anti-AKAP2 (Bioscience) 1:1000, anti-β-actin (Sigma) 1:3000 and anti-pCt (custom-made) 1:1000. Chemiluminescent detection was performed using Pierce ECL Western Blotting Substrate (Thermo Fisher Scientific). All western blots were quantified with ImageJ Fiji.

6.2.2.6 qPCR

The total RNA was isolated from cultured H9c2 cells using the TRIzol reagent according to the manufacturer's instruction. The RNA was digested with DNase set

(Qiagen), cleaned with RNeasy Mini Kit (Qiagen) and reverse transcribed using First Strand cDNA Synthesis Kit. 50 ng of cDNA was used for real-time PCR analysis. The relative mRNA levels were quantified using gene-specific TaqMan assays (see Table S3) ViiA 7 Real-Time PCR System and Quant Studio 7. Results were analyzed using the comparative threshold cycle (2^-ΔΔCt) method (Livak & Schmittgen, 2001), normalized to housekeeping gene. The results are expressed as fold-increase of $\log_2$ (2^-ΔΔCt) over mock. Statistical significance was assessed using ΔCt.

6.2.2.7 RT-PCR

The total RNA was isolated from cultured H9c2 cells and from 54 hpf zebrafish embryos using the TRIzol reagent according to the manufacturer's instruction. The total RNA was reverse transcribed using First Strand cDNA Synthesis Kit and amplified using Phusion polymerase with primers for the interested genes (see Table S1). The PCR products were visualized using 3% agarose gel and Redsafe staining.

6.2.2.8 Drug treatment

H9c2 cells were plated for 48 hours prior to the experiment and incubated with the following drugs: 10 μM FSK, 10 μM PKI, 100 μM L314E for 1 hour or with 4 μM ISO for 3 minutes and with corresponding concentration of DMSO before harvesting or fixation.

6.2.2.9 Confocal microscopy

H9c2 cells were plated on poly-D-lysine coated coverslips 48 hours prior to the experiments and fixed after 24 hours transfection or after drug treatment in PBS supplemented with 4% PFA and 4% Sucrose for 20 minutes. Following primary antibodies were used: anti-II-III-loop (Millipore) 1:100; anti-F-actin (Thermo Fisher Scientific) 1:4; anti-pCt (Abnova) 1:500; anti-nucleolin (Abcam) 1:500. Confocal images were obtained on Leica TCS SP8 using LAS-FX software. For the localization studies, intensity was measured using ImageJ Fiji and maximal Z-projection.

6.2.3 Data and statistical analysis

All the graphs were generated and analyzed using GraphPad Prism 6. Data represent the mean ± SD of independent experiments indicated in figure legends. Statistical significance was assessed with Welch's test, Wilcoxon test or Mann-Whitney test. P

value of less than 0.05 was considered to be statistically significant. The levels of statistical significance were indicated as follows: *$P < 0.05$; **$P < 0.01$; ***$P < 0.001$; ****$P < 0.0001$.

7 Supplements

7.1 Supplementary figures

Supplementary Figure 1

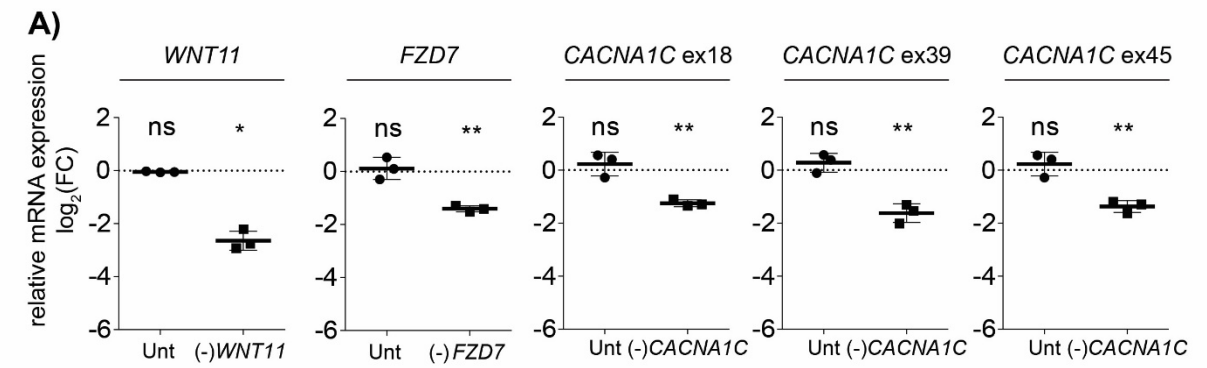

Supplementary Figure 1: Efficient knock down of the indicated gene using siRNA. (A) Relative mRNA expression of *WNT11*, *FZD7* and *CACNA1C* genes were measured in Untransfected (Unt), Scramble, *WNT11* ((-)*WNT11*), *FZD7* ((-)*FZD7*) or *CACNA1C* ((-)*CACNA1C*) siRNA transfected H9c2 cell via quantitative RT-PCR and normalized to the relative mRNA expression of *GAPDH* in Scramble siRNA transfected cells. Data represent the fold change $\log_2$ (2^-ΔΔCt) of the interested genes. (Mean ± SD of N = 3 experiments; ns *P*(*WNT11* in Unt)=0,0625; **P*(*WNT11* in (-)*WNT11*)=0.0156; ns *P*(*FZD7* in Unt)=0.6406; ***P*(*FZD7* in (-)*FZD7*)=0.0039; ns *P*(*CACNA1C* exon 18 in Unt)=0.0547; ***P*(*CACNA1C* exon 18 in (-)*CACNA1C*)=0.0039; ns *P* (*CACNA1C* exon 39 in Unt)=0.0547; ***P*(*CACNA1C* exon 39 in (-)*CACNA1C*)=0.0039; ns *P*(*CACNA1C* exon 45 in Unt)=0.0977; ***P*(*CACNA1C* exon 45 in (-)*CACNA1C*)=0.0039; Wilcoxon test).

Supplementary Figure 2

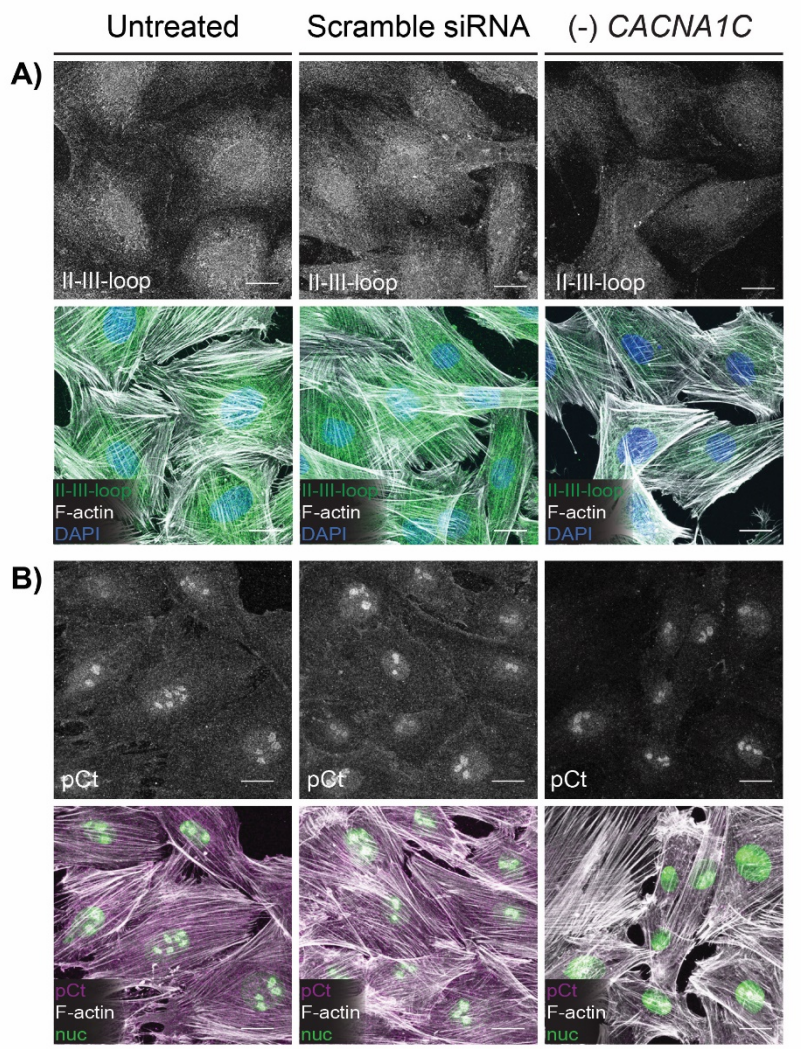

Supplementary Figure 2: Verification of the anti-II-III-loop and anti-pCt antibodies. Maximum intensity projection of confocal images of untreated, Scramble and *CACNA1C* siRNA transfected H9c2 cells. Following primary antibodies were used for the immunostaining: (A) anti-II-III-loop (Millipore) in dilution of 1:100 (gray/ green), anti-F-actin 1:4 (gray) or (B) anti-pCt (Abnova) 1:500 (gray/ magenta), anti-F-actin 1:4 (gray) and anti-Nuc 1:500 (green). DAPI (blue) staines nucleus. (N ≥ 3 experiments; n ≥ 79). The scale bar represents 20 μm.

Supplementary Figure 3

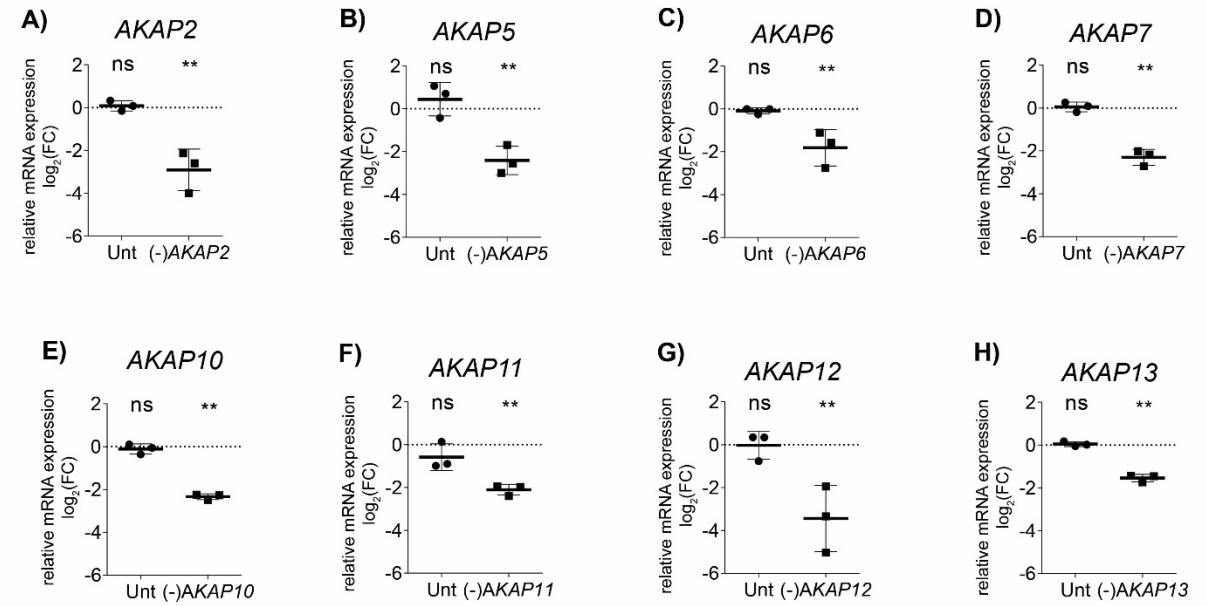

Supplementary Figure 3: Efficient downregulation of the preselected *AKAP*s in H9c2 cell. (A-H) Relative mRNA expression of the interested *AKAP* gene was measured in untreated, Scramble and corresponding *AKAP* siRNA transfected H9c2 cell via quantitative RT-PCR and normalized to the relative mRNA expression of *GAPDH* in Scramble siRNA transfected cells. Data represent the fold change $\log_2$ (2^-ΔΔCt) of the indicated gene. (Mean ± SD; N = 3 experiments; (A) ns *P*(Unt)=0.4258; ***P*((-)*AKAP2*)=0.0039; (B) ns *P*(Unt)=0.0742; ***P*((-)*AKAP5*)=0.0039; (C) ns *P*(Unt)=0,3594; ***P*((-)*AKAP6*)=0,0039; (D) ns *P*(Unt)=0,3008; ***P*((-)*AKAP7*)=0.0039. (E) ns*P*(Unt)=0.19510; ***P*((-)*AKAP6*)=0.0039; (F) ns *P*(Unt)=0.2188; ***P*((-)*AKAP11*)=0.0039; (G) ns *P*(Unt)=0.9453; ***P*((-)*AKAP12*)=0.0078; (H) ns *P* (Unt)=0.4258; ***P*((-)*AKAP13*)=0.0039; Wilcoxon test).

Supplementary Figure 4

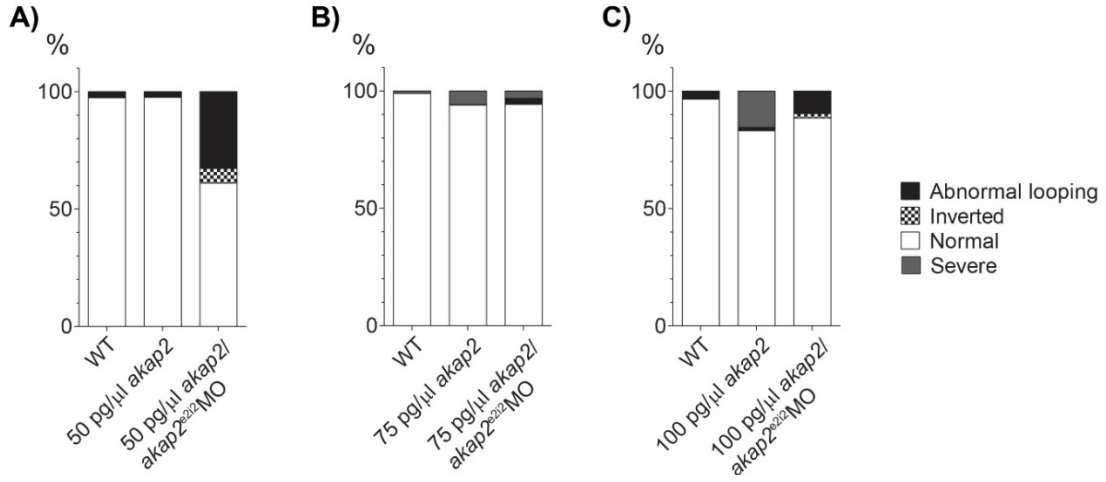

Supplementary Figure 4: Phenotype analysis of *akap2* mRNA injected embryos. Phenotype analysis of (A) 50 pg/µl, (B) 75 pg/µl or (C) 100 pg/µl *akap2* mRNA injected embryos considering the heart phenotype. (N ≥ 3 experiments; n ≥ 300).

Supplementary Figure 5

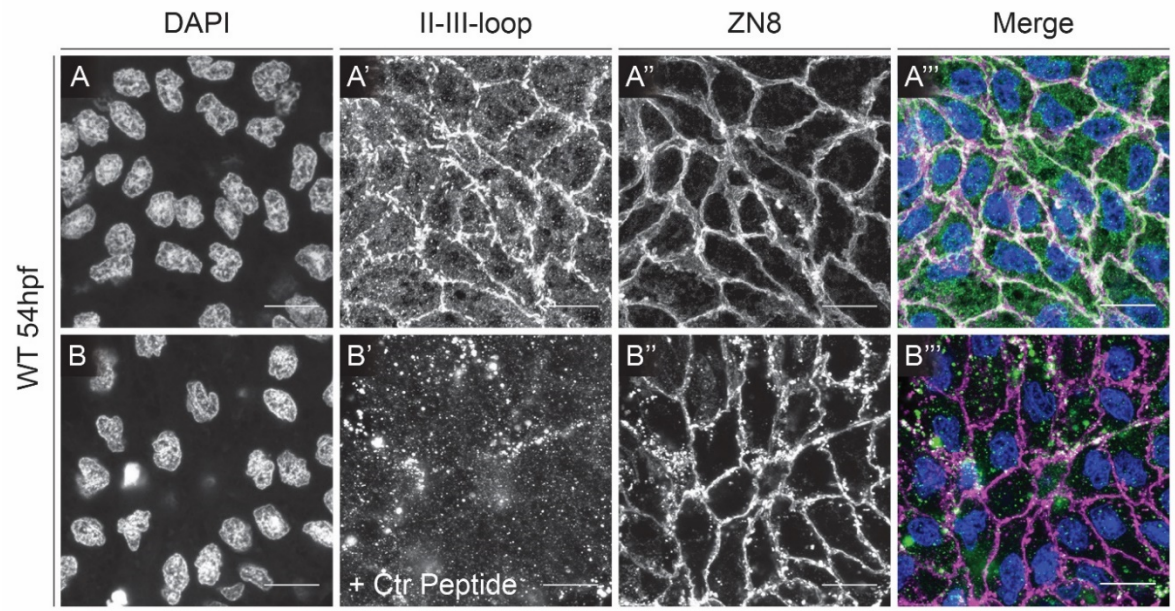

Supplementary Figure 5: Verification of the anti-II-III-loop. Maximum intensity projection of 7μm confocal section of WT zebrafish hearts at 54hpf. (A-B) DAPI (gray/blue) staines nucleus. Following primary antibodies were used for the immunostaining: (A') anti-II-III-loop antibody (Millipore) in dilution of 1:50 (gray/green), (B') anti-II-III-loop antibody (Millipore) was pre-incubated with its peptide (gray/green), (A'' and B'') anti-ZN8 (Hybridoma Bank) in dilution of 1:50 (gray/magenta). (N=3 experiments). The scale bar represents 10 μm.

Supplementary Figure 6

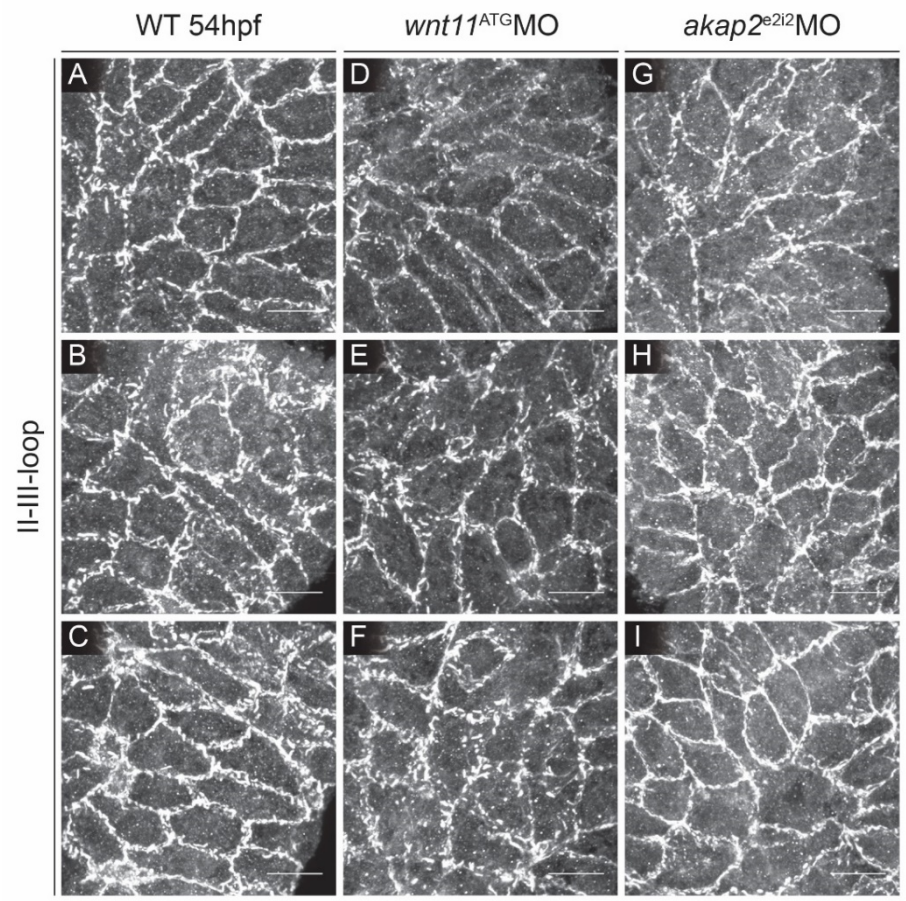

Supplementary Figure 6: Localization and abundance of the α1C subunit. (A-I) Maximum intensity projection of 7μm confocal section of WT (A-C), *wnt11*^{ATG}MO (D-F) and *akap2*^{e2i2}MO (G-I) zebrafish hearts at 54hpf. Following primary antibodies were used for the immunostaining: anti-II-III-loop antibody (Millipore) in dilution of 1:50 (gray). (N=3 experiments). The scale bar represents 10 μm.

7.2 Supplementary Tables

Supplementary Table 1

Primer name	Used for	Seq (5'->3')
H9c2 Cacna1c Fw	RT-PCR Figure 5A	ACG GCA CC TCT TAC CTT TT
H9c2 Cacna1c Rv	RT-PCR Figure 5A	CCG ACA GCA GTG AAT GAA GA
H9c2 Myogenin Fw	RT-PCR Figure 5A	TCG AGG CTC TGA AGA GAA GC
H9c2 Myogenin Rv	RT-PCR Figure 5A	CAC GAT GGA CGT AAG GGA GT
H9c2 Troponin T t2 Fw	RT-PCR Figure 5A	CAG AGA GGA GGA AGG TGC TG
H9c2 Troponin T t2 Rv	RT-PCR Figure 5A	CCT GGC AAG ACC TAG AGC TG
H9c2 Wnt11 Fw	RT-PCR Figure 5A	TCT GCG AGG CTC TTC TCT TC
H9c2 Wnt11 Rv	RT-PCR Figure 5A	ACC TCT CTC CAG GTC AAG CA
H9c2 Fzd7 Fw	RT-PCR Figure 5A	CAT GTT CCT CGG CTT CAT TT
H9c2 Fzd7 Rv	RT-PCR Figure 5A	CTG CGT TCA TGC TGA TGA CT
H9c2 Dvl2 Fw	RT-PCR Figure 5A	CCT TGG CCT GGT AAG TTT CA
H9c2 Dvl2 Rv	RT-PCR Figure 5A	AAC AAC TGG AGG TGG TGG TC
H9c2 β-catenin Fw	RT-PCR Figure 5A	GCC AGT GGA TTC CGT ACT GT
H9c2 β-catenin Rv	RT-PCR Figure 5A	TCA GCA CTC TGC TTG TGG TC
H9c2 GAPDH Fw	RT-PCR Figure 5A	GGT GAT GCT GGT GCT GAG TA
H9c2 GAPDH Rv	RT-PCR Figure 5A	ACT GTG GTC ATG AGC CCT TC
H9c2 Connexin 43 Fw	RT-PCR Figure 5A	GCT CCA CTC TCG CCT ATG TC
H9c2 Connexin 43 Rv	RT-PCR Figure 5A	GAG TTC ATG TCC AGC AGC AA
H9c2 Dvl1 Fw	RT-PCR Figure 5A	CTC TCT TGG GCT CTG TCA CC
H9c2 Dvl1 Rv	RT-PCR Figure 5A	AGG CCT CTC TCC TGT CTT CC
H9c2 Dvl3 Fw	RT-PCR Figure 5A	GCC TCA CGC CTA ATG AGA AG
H9c2 Dvl3 Rv	RT-PCR Figure 5A	TCT CCC GAA GCA CTC TGA CT
H9c2 akap2 attB1	FLAG-tagged *AKAP2*	GGGGACAAGTTTGTACAAAAAAGCAGGC TGGATGGAAATTGGGGTGTCCGTG
H9c2 akap2 attB2	FLAG-tagged *AKAP2*	GGGGACCACTTTGTACAAGAAAGCTGGG TGTTATTCATTGTCCTCCTCCTC
Danio rerio akap2 infusion Fw	*akap2* mRNA synthesis	CGGTATCGATAAGCTTCGGGACACTCAG GACTTCTAGC
Danio rerio akap2 infusion Rv	*akap2* mRNA synthesis	TAGAACTAGTGGATCCTTACTCTTCTTCT TCCTCTTCC
Danio rerio akap2 cDNA Fw	*akap2* MO verification	CGG GAC ACT CAG GAC TTC TAG C
Danio rerio *akap2* cDNA Rv	*akap2* MO verification	ACT GTT GTC CTC GGC TTT CTC CC

Supplementary Table 2

siRNA name	Source	Identifier
ON-TARGETplus Rat Non-targeting Control siRNA	Dharmacon	Cat# D-001810-01-20
ON-TARGETplus Rat Wnt11 (140584) siRNA - SMARTpool	Dharmacon	Cat# L-101650-02-0010
ON-TARGETplus Rat Cacna1c (24239) siRNA - SMARTpool	Dharmacon	Cat# L-080130-02-0010
ON-TARGETplus Rat Cdk15 (301440) siRNA - SMARTpool	Dharmacon	Cat# L-084243-02-0005
ON-TARGETplus Rat Akap2 (298024) siRNA - SMARTpool	Dharmacon	Cat# L-096895-02-0005

ON-TARGETplus Rat Akap5 (171026) siRNA - SMARTpool	Dharmacon	Cat# L-092699-02-0005
ON-TARGETplus Rat Akap6 (64553) siRNA - SMARTpool	Dharmacon	Cat# L-091596-02-0005
ON-TARGETplus Rat Akap7 (361458) siRNA - SMARTpool	Dharmacon	Cat# L-102358-02-0005
ON-TARGETplus Rat Akap10 (360540) siRNA - SMARTpool	Dharmacon	Cat# L-083671-02-0005
ON-TARGETplus Rat Akap11 (498549) siRNA - SMARTpool	Dharmacon	Cat# L-104261-02-0005
ON-TARGETplus Rat Akap12 (83425) siRNA - SMARTpool	Dharmacon	Cat# L-088741-02-0005
ON-TARGETplus Rat Akap13 (293024) siRNA - SMARTpool	Dharmacon	Cat# L-083007-02-0005

Supplementary Table 3

TaqMan probe name	Source	Identifier
TaqMan™Gene Expression Assay (FAM), Rat Gapdh	Thermo Fisher Scientific	Cat#4331182; ID:Rn01775763_g1
TaqMan™Gene Expression Assay (FAM), Rat Wnt11	Thermo Fisher Scientific	Cat#4331182; ID:Rn01510238_m1
TaqMan™Gene Expression Assay (FAM), Rat Fzd7	Thermo Fisher Scientific	Cat#4331182; ID:Rn01441541_m1
TaqMan™Gene Expression Assay (FAM), Rat Cacna1c exon 17/18	Thermo Fisher Scientific	Cat#4351372; ID:Rn01492559_m1
TaqMan™Gene Expression Assay (FAM), Rat Cacna1c exon 38/39	Thermo Fisher Scientific	Cat#4351372; ID:Rn00709314_m1
TaqMan™Gene Expression Assay (FAM), Rat Cacna1c exon 44/45	Thermo Fisher Scientific	Cat#4351372; ID:Rn01492578_m1
TaqMan™Gene Expression Assay (FAM), Rat Akap2	Thermo Fisher Scientific	Cat#4331182; ID:Rn01422768_m1
TaqMan™Gene Expression Assay (FAM), Rat Akap5	Thermo Fisher Scientific	Cat#4331182; ID:Rn01786021_m1
TaqMan™Gene Expression Assay (FAM), Rat Akap6	Thermo Fisher Scientific	Cat#4331182; ID:Rn00575148_m1
TaqMan™Gene Expression Assay (FAM), Rat Akap7	Thermo Fisher Scientific	Cat#4331182; ID:Rn01756034_m1
TaqMan™Gene Expression Assay (FAM), Rat Akap10	Thermo Fisher Scientific	Cat#4351372; ID:Rn01496138_m1
TaqMan™Gene Expression Assay (FAM), Rat Akap11	Thermo Fisher Scientific	Cat#4351372; ID:Rn01468361_m1
TaqMan™Gene Expression Assay (FAM), Rat Akap12	Thermo Fisher Scientific	Cat#4331182; ID:Rn01643001_m1
TaqMan™Gene Expression Assay (FAM), Rat Akap13	Thermo Fisher Scientific	Cat#4351372; ID:Rn01478249_m1
TaqMan™Gene Expression Assay (FAM), Zebrafish cacna1c exon 18	Thermo Fisher Scientific	Cat#4351372; ID: Dr03093529_m1
TaqMan™Gene Expression Assay (FAM), Zebrafish cacna1c exon 40	Thermo Fisher Scientific	Cat#4351372; ID: Dr03093552_g1
TaqMan™Gene Expression Assay (FAM), Zebrafish cacna1c exon 45	Thermo Fisher Scientific	Cat#4351372; ID: Dr03093556_g1
TaqMan™ Gene Expression Assay, VIC primer-limited, Zebrafish eef1a1l1	Thermo Fisher Scientific	Cat#4448484; ID:Dr03432748_m1
Custom TaqMan™ Gene Expression Assay (FAM), Zebrafish Akap2	Thermo Fisher Scientific	N/A CACCAGGTAAAATTG
Custom TaqMan™ Gene Expression Assay (FAM), Zebrafish Akap6	Thermo Fisher Scientific	N/A TCGACCCAGAAACAAGATCCCTA

Custom TaqMan™ Gene Expression Assay (FAM), Zebrafish Akap7	Thermo Fisher Scientific	N/A CCGCACGGACAAGTGTTAA
Custom TaqMan™ Gene Expression Assay (FAM), Zebrafish Akap10	Thermo Fisher Scientific	N/A CGTCAATGATGTCATGCAGCAGGGA
Custom TaqMan™ Gene Expression Assay (FAM), Zebrafish Akap11	Thermo Fisher Scientific	N/A AAAGTTGAGGACTGTGCAGACTTTT
Custom TaqMan™ Gene Expression Assay (FAM), Zebrafish Akap12b	Thermo Fisher Scientific	N/A TAATGGGAAAACGGATGATCAGACA
Custom TaqMan™ Gene Expression Assay (FAM), Zebrafish Akap13	Thermo Fisher Scientific	N/A TCAGGCTGTGTGTCCAGCTCATAAC

Supplementary Table 4

Peptide spots	Position	Amino acid sequence
PKA-RI	A5	MESGS TAASE EARSL RECEL YVQKH
	A4	TAASE EARSL RECEL YVQKH NIQAL
	A3	EARSL RECEL YVQKH NIQAL LKDSI
	A2	RECEL YVQKH NIQAL LKDSI VQLCT
	A1	YVQKH NIQAL LKDSI VQLCT ARPE
PKA-RIIa	B10	MSHIQ IPPGL TELLQ GYTVE VLRQQ
	B9	IPPGL TELLQ GYTVE VLRQQ PPDLV
	B8	TELLQ GYTVE VLRQQ PPDLV EFAVE
	B7	GYTVE VLRQQ PPDLV EFAVE YFTRL
	B6	VLRQQ PPDLV EFAVE YFTRL REAR
PKA-RIb	C10	MASPP ACPSE EDESL KGCEL YVQLH
	C9	ACPSE EDESL KGCEL YVQLH GIQQV
	C8	EDESL KGCEL YVQLH GIQQV LKDCI
	C7	KGCEL YVQLH GIQQV LKDCI VHLCI
	C6	YVQLH GIQQV LKDCI VHLCI SKPER
PKA-RIIb	C5	MSIEI PAGLT ELLQG FTVEV LRHQP
	C4	PAGLT ELLQG FTVEV LRHQP ADLLE
	C3	ELLQG FTVEV LRHQP ADLLE FALQH
	C2	FTVEV LRHQP ADLLE FALQH FTRLQ
	C1	LRHQP ADLLE FALQH FTRLQ QENEA
Control	A9	AAAAA AAAAA AAAAA AAAAA AAAAA
	A8	AAAAA AAAAA AAAAA AAAAA AAAAA
	A7	AAAAA AAAAA AAAAA AAAAA AAAAA
	A6	AAAAA AAAAA AAAAA AAAAA AAAAA

8 References

Abi-Gerges, N., Hove-madsen, L., Fischmeister, R., & Mery, P.-F. (1997). A comparative study of the effects of three guanylyl cyclase inhibitors on the L-type Ca2+ and muscarinic K+ currents in frog cardiac myocytes. *British Journal of Parmacology*, *121*, 1369–1377.

Abramson, S., Martin, M., Hughes, A., Harden, T. K., Neve, K. I. M. A., Barretti, D. A., & Molinoff, P. B. (1988). Interaction of beta-adrenergic receptors with the inhibitory guanine nucleotide-binding protein of adenylate cyclase in membranes prepared from cyc- S49 lymphoma cells. *Biochem Pharmacol*, *37*(22), 4289–4297.

Ai, Z., Fischer, A., Spray, D. C., Brown, A. M. C., & Fishman, G. I. (2000). Wnt-1 regulation of connexin43 in cardiac myocytes. *Journal of Clinical Investigation*, *105*(2), 161–171. https://doi.org/10.1172/JCI7798

Aye, T. T., Mohammed, S., van den Toorn, H. W. P., van Veen, T. A. B., van der Heyden, M. A. G., Scholten, A., & Heck, A. J. R. (2009). Selectivity in Enrichment of cAMP-dependent Protein Kinase Regulatory Subunits Type I and Type II and Their Interactors Using Modified cAMP Affinity Resins. *Molecular & Cellular Proteomics*, *8*(5), 1016–1028. https://doi.org/10.1074/mcp.M800226-MCP200

Aye, T. T., Soni, S., van Veen, T. A. B., van der Heyden, M. A. G., Cappadona, S., Varro, A., … Scholten, A. (2012). Reorganized PKA-AKAP associations in the failing human heart. *Journal of Molecular and Cellular Cardiology*, *52*(2), 511–518. https://doi.org/10.1016/j.yjmcc.2011.06.003

Bers, D. M. (2002). Cardiac excitation–contraction coupling. *Nature*, *415*(January), 198–205.

Bers, D. M., & Ziolo, M. T. (2001). When Is cAMP Not cAMP? *Circulation Research*, *89*, 373–375.

Brette, F., & Orchard, C. (2003). T-tubule function in mammalian cardiac myocytes. *Circulation Research*, *92*(11), 1182–1192. https://doi.org/10.1161/01.RES.0000074908.17214.FD

Brundel, B. J. J. M., Van Gelder, I. C., Henning, R. H., Tieleman, R. G., Tuinenburg, A. E., Wietses, M., … Crijns, H. J. G. M. (2001). Ion channel remodeling is related to intraoperative atrial effective refractory periods in patients with paroxysmal and persistent atrial fibrillation. *Circulation*, *103*(5), 684–690. https://doi.org/10.1161/01.CIR.103.5.684

Burkhard, S., & Bakkers, J. (2018). Spatially resolved RNA-sequencing of the embryonic heart identifies a role for Wnt/β -catenin signaling in autonomic control of heart rate. *eLIFE*, *7*, e31515. https://doi.org/10.7554/eLife.31515

Canton, D. A., Keene, C. D., Swinney, K., Langeberg, L. K., Nguyen, V., Pelletier, L., … Scott, J. D. (2012). Gravin Is a Transitory Effector of Polo-like Kinase 1 during Cell Division. *Molecular Cell*, *48*(4), 547–559. https://doi.org/10.1016/j.molcel.2012.09.002

Capdevila, J., Vogan, K. J., Tabin, C. J., & Izpisúa Belmonte, J. C. (2000). Mechanisms of Left–Right Determination in Vertebrates. *Cell*, *101*(1), 9–21. https://doi.org/10.1016/S0092-8674(00)80619-4

Carafoli, E., Santella, L., Branca, D., & Brini, M. (2001). Generation, control, and processing of cellular calcium signals. *Critical Reviews in Biochemistry and Molecular Biology*, *36*(2), 107–260. https://doi.org/10.1080/20014091074183

Carnegie, G. K., Smith, F. D., McConnachie, G., Langeberg, L. K., & Scott, J. D. (2004). AKAP-Lbc nucleates a protein kinase D activation scaffold. *Molecular Cell*, *15*(6), 889–899. https://doi.org/10.1016/j.molcel.2004.09.015

Carnegie, G. K., Soughayer, J., Smith, F. D., Pedroja, B. S., Zhang, F., Diviani, D., … Scott, J. D. (2008). AKAP-Lbc Mobilizes a Cardiac Hypertrophy Signaling Pathway. *Molecular Cell*, *32*(2), 169–179. https://doi.org/10.1016/j.molcel.2008.08.030

Catterall, W. A. (2000). Structure and regulation of voltage-gated Ca2+ channels. *Annual Reviews of Cell and Developmental Biology*, *16*(521), 555.

Chen-izu, Y., Xiao, R., Izu, L. T., Cheng, H., Kuschel, M., Spurgeon, H., & Lakatta, E. G. (2000). G(i)-dependent localization of beta(2)-adrenergic receptor signaling to L-type Ca(2+) channels. *Biophysical Journal*, *79*(November), 2547–2556.

Chen, X., Piacentino, V., Furukawa, S., Goldman, B., Margulies, K. B., & Houser, S. R. (2002). L-type Ca2+ channel density and regulation are altered in failing human ventricular myocytes and recover after support with mechanical assist devices. *Circulation Research*, *91*(6), 517–524. https://doi.org/10.1161/01.RES.0000033988.13062.7C

Chen, Y., Zhang, P., Tang, P., Lv, P., Li, X., Wang, Y., … Liu, Y. (2018). Wnt4 overexpression promotes thymoma developmentthrough a JNK-mediated planar cell polarity-like pathway. *Oncology Letters*, *15*(1), 83–90. https://doi.org/10.3892/ol.2017.7266

Cheng, E. P., Yuan, C., Navedo, M. F., Dixon, R. E., Nieves-Cintrón, M., Scott, J. D., & Santana, L. F. (2011). Restoration of normal L-type Ca2+ channel function during timothy syndrome by ablation of an anchoring protein. *Circulation Research*, *109*(3), 255–261. https://doi.org/10.1161/CIRCRESAHA.111.248252

Chi, N. C., Shaw, R. M., Jungblut, B., Huisken, J., Ferrer, T., Arnaout, R., … Stainier, D. Y. R. (2008). Genetic and physiologic dissection of the vertebrate cardiac conduction system. *PLoS Biology*, *6*(5), 1006–1019. https://doi.org/10.1371/journal.pbio.0060109

Chien, A. J., Zhao, X., Shirokov, R. E., Puri, T. S., Chang, C. F., Sun, D., … Hosey, M. M. (1995). Roles of a membrane-localized β subunit in the formation and targeting of functional L-type Ca2+channels. *Journal of Biological Chemistry*, *270*(50), 30036–30044. https://doi.org/10.1074/jbc.270.50.30036

Choudhry, P., & Trede, N. S. (2013). DiGeorge Syndrome Gene tbx1 Functions through wnt11r to Regulate Heart Looping and Differentiation. *PLoS ONE*, *8*(3).

https://doi.org/10.1371/journal.pone.0058145

Clapham, D. E. (1995). Calcium signaling. *Cell*, *80*(2), 259–268. https://doi.org/10.1016/0092-8674(95)90408-5

Cohen, E. D., Miller, M. F., Wang, Z., Moon, R. T., & Morrisey, E. E. (2012). Wnt5a and Wnt11 are essential for second heart field progenitor development. *Development*, *139*(11), 1931–1940. https://doi.org/10.1242/dev.069377

Daaka, Y., Luttrell, L. M., & Lefkowitz, R. J. (1997). Switching of the coupling of the beta2-adrenergic receptor to different G proteins by protein kinase A. *Nature*, *390*(NOVEMBER), 88–91. https://doi.org/10.1038/36362

Davare, M. A. (2001). A beta 2 Adrenergic Receptor Signaling Complex Assembled with the Ca2+ Channel Cav1.2. *Science*, *293*(5527), 98–101. https://doi.org/10.1126/science.293.5527.98

Davare, M. A., Horne, M. C., & Hell, J. W. (2000). Protein phosphatase 2A is associated with class C L-type calcium channels (Cav1.2) and antagonizes channel phosphorylation by cAMP-dependent protein kinase * cruited to this channel by an protein kinase A anchor. *Journal of Biological Chemistry*, *275*(50), 39710–39717. https://doi.org/10.1074/jbc.M005462200

Dawson, K., Aflaki, M., & Nattel, S. (2013). Role of the Wnt-Frizzled system in cardiac pathophysiology: A rapidly developing, poorly understood area with enormous potential. *Journal of Physiology*, *591*(6), 1409–1432. https://doi.org/10.1113/jphysiol.2012.235382

De Jongh, K. S., Murphy, B. J., Colvin, a a, Hell, J. W., Takahashi, M., & Catterall, W. A. (1996). Specific phosphorylation of a site in the full-length form of the alpha 1 subunit of the cardiac L-type calcium channel by adenosine 3',5'-cyclic monophosphate-dependent protein kinase. *Biochemistry*, *35*(32), 10392–402. https://doi.org/10.1021/bi953023c

Dirksen, R. T., & Beam, K. G. (1999). Role of calcium permeation in dihydropyridine receptor function. Insights into channel gating and excitation-contraction coupling. *The Journal of General Physiology*, *114*(3), 393–403. Retrieved from http://www.pubmedcentral.nih.gov/articlerender.fcgi?artid=2229453&tool=pmcentrez&rendertype=abstract

Diviani, D., Dodge-Kafka, K. L., Li, J., & Kapiloff, M. S. (2011). A-kinase anchoring proteins: scaffolding proteins in the heart. *American Journal of Physiology-Heart and Circulatory Physiology*, *301*(5), H1742–H1753. https://doi.org/10.1152/ajpheart.00569.2011

Diviani, D., Reggi, E., Arambasic, M., Caso, S., & Maric, D. (2016). Emerging roles of A-kinase anchoring proteins in cardiovascular pathophysiology. *Biochimica et Biophysica Acta - Molecular Cell Research*, *1863*(7), 1926–1936. https://doi.org/10.1016/j.bbamcr.2015.11.024

Diviani, D., Soderling, J., & Scott, J. D. (2001). AKAP-Lbc Anchors Protein Kinase A and Nucleates Gα 12-selective Rho-mediated Stress Fiber Formation. *Journal of*

Biological Chemistry, *276*(47), 44247–44257. https://doi.org/10.1074/jbc.M106629200

Dixon, R. E., Cheng, E. P., Mercado, J. L., & Santana, L. F. (2012). L-type Ca2+ channel function during Timothy Syndrome. *Trends in Cardiovascular Medicine*, *22*(3), 72–76. https://doi.org/10.1016/j.tcm.2012.06.015.L-type

Djiane, A., Riou, J.-F., Umbhauer, M., Boucaut, J.-C., & Shi, D.-L. (2000). Role of frizzled 7 in the regulation of convergent extension movements during gastrulation in Xenopus laevis. *Development*, *127*(14), 3091–100. https://doi.org/10.1242/dev.00435

Dodge-Kafka, K. L., Soughayer, J., Pare, G. C., Carlisle Michel, J. J., Landenberg, L. K., Kapiloff, M. S., & Scott, J. D. (2005). The protein kinase A anchoring protein mAKAP co-ordinates two integrated cAMP effector pathways. *Journal of MAgnetic Resonance*, *236*(7058), 574–578. https://doi.org/10.1016/j.jmr.2013.08.006

Dolmetsch, R. E., Pajvani, U., Fife, K., Spotts, J. M., & Greenberg, M. E. (2001). Signaling to the nucleus by an L-type calcium channel- calmodulin complex through the MAP kinase pathway. *Science*, *294*(5541), 333–339. https://doi.org/10.1126/science.1063395

Dong, F., Feldmesser, M., Casadevall, A., & Rubin, C. S. (1998). Molecular characterization of a cDNA that encodes six isoforms of a novel murine a kinase anchor protein. *Journal of Biological Chemistry*, *273*(11), 6533–6541. https://doi.org/10.1074/jbc.273.11.6533

Dorn, G. W., & Brown, J. H. (1999). Gq signaling in cardiac adaptation and maladaptation. *Trends in Cardiovascular Medicine*, *9*(1–2), 26–34. https://doi.org/10.1016/S1050-1738(99)00004-3

Edwards, H. V., Scott, J. D., & Baillie, G. S. (2012). The A-kinase-anchoring protein AKAP-Lbc facilitates cardioprotective PKA phosphorylation of Hsp20 on Ser ^{16}. *Biochemical Journal*, *446*(3), 437–443. https://doi.org/10.1042/BJ20120570

Eggers, C. T., Schafer, J. C., Goldenring, J. R., & Taylor, S. T. (2009). D-AKAP2 interacts with Rab4 and Rab11 throughi its RGS domains and regulates transferrin receptor recycling. *Journal of Biological Chemistry*, *284*(47), 32869–32880. https://doi.org/10.1074/jbc.M109.022582

Eisenberg, C. A., & Eisenberg, L. M. (1999). WNT11 promotes cardiac tissue formation of early mesoderm. *Developmental Dynamics*, *216*(1), 45–58. https://doi.org/10.1002/(SICI)1097-0177(199909)216:1<45::AID-DVDY7>3.0.CO;2-L

Ellis, S., Williams, M., Ways, N., Brenner, R., Sharp, A., Leung, A., … Harpold, M. M. (1988). Sequence and expression of mRNAs encoding the alpha 1 and alpha 2 subunits of a DHP-sensitive calcium channel. *Science*, *241*(4873), 1661–1664. https://doi.org/10.1126/science.2458626

Fabiato, A. (1985). Simulated calcium current can both cause calcium loading in and trigger calcium release from the sarcoplasmic reticulum of a skinned canine

cardiac Purkinje cell. *The Journal of General Physiology*, *85*(2), 291–320. https://doi.org/10.1085/JGP.85.2.291

Fan, G. F., Shumay, E., Wang, H. Y., & Malbon, C. C. (2001). The Scaffold Protein Gravin (cAMP-dependent Protein Kinase-anchoring Protein 250) Binds the β2-Adrenergic Receptor via the Receptor Cytoplasmic Arg-329 to Leu-413 Domain and Provides a Mobile Scaffold during Desensitization. *Journal of Biological Chemistry*, *276*(26), 24005–24014. https://doi.org/10.1074/jbc.M011199200

Foord, S. M., Bonner, T. O. M. I., Neubig, R. R., Rosser, E. M., Pin, J., Davenport, A. P., … Harmar, A. J. (2005). International Union of Pharmacology. XLVI. G Protein-Coupled Receptor List. *Pharmacological Reviews*, *57*(2), 279–288. https://doi.org/10.1124/pr.57.2.5.2

Fu, Y., Westenbroek, R. E., Scheuer, T., & Catterall, W. A. (2014). Basal and β-adrenergic regulation of the cardiac calcium channel CaV1.2 requires phosphorylation of serine 1700. *Proceedings of the National Academy of Sciences*, *111*(46), 16598–16603. https://doi.org/10.1073/pnas.1419129111

Fu, Y., Westenbroek, R. E., Yu, F. H., Clark, J. P., Marshall, M. R., Scheuer, T., & Catterall, W. A. (2011). Deletion of the distal C terminus of CaV1.2 channels leads to loss of beta-adrenergic regulation and heart failure in vivo. *The Journal of Biological Chemistry*, *286*(14), 12617–26. https://doi.org/10.1074/jbc.M110.175307

Fuller, M. D., Emrick, M. A., Sadilek, M., Scheuer, T., & Catterall, W. A. (2010). Molecular mechanism of calcium channel regulation in the fight-or-flight response. *Science Signaling*, *3*(141). https://doi.org/10.1126/scisignal.2001152

Fuller, M. D., Fu, Y., Scheuer, T., & Catterall, W. a. (2014). Differential regulation of CaV1.2 channels by cAMP-dependent protein kinase bound to A-kinase anchoring proteins 15 and 79/150. *The Journal of General Physiology*, *143*, 315–24. https://doi.org/10.1085/jgp.201311075

Ganesan, A. N., Maack, C., Johns, D. C., Sidor, A., & O'Rourke, B. (2006). Beta-Adrenergic stimulation of L-type Ca2+ channels in cardiac myocytes requires the distal carboxyl terminus of alpha 1C but not serine 1928. *Circulation Research*, *98*(2). https://doi.org/10.1161/01.RES.0000202692.23001.e2

Gao, T., Cuadra, A. E., Ma, H., Bünemann, M., Gerhardstein, B. L., Cheng, T., … Hosey, M. M. (2001). C-terminal fragments of the alpha 1C (CaV1.2) subunit associate with and regulate L-type calcium channels containing C-terminal-truncated alpha 1C subunits. *J Biol Chem*, *276*(24), 21089–21097. https://doi.org/10.1074/jbc.M008000200

Gao, T., Yatani, A., Dell'Acqua, M. L., Sako, H., Green, S. A., Dascal, N., … Hosey, M. M. (1997). cAMP-dependent regulation of cardiac L-type Ca2+ channels requires membrane targeting of PKA and phosphorylation of channel subunits. *Neuron*, *19*(1), 185–196. https://doi.org/10.1016/S0896-6273(00)80358-X

Gardner, L. A., Naren, A. P., & Bahouth, S. W. (2007). Assembly of an SAP97-AKAP79-cAMP-dependent protein kinase scaffold at the type 1 PSD-95/DLG/ZO1

motif of the human beta1-adrenergic receptor generates a receptosome involved in receptor recycling and networking. *Journal of Biological Chemistry*, *282*(7), 5085–5099. https://doi.org/10.1074/jbc.M608871200

Gardner, L. A., Tavalin, S. J., Goehring, A. S., Scott, J. D., & Bahouth, S. W. (2006). AKAP79-mediated targeting of the cyclic AMP-dependent protein kinase to the β1-adrenergic receptor promotes recycling and functional resensitization of the receptor. *Journal of Biological Chemistry*, *281*(44), 33537–33553. https://doi.org/10.1074/jbc.M601809200

Gilman, A. G. (1987). G Proteins: Transducers of Receptor-Generated Signals. *Annu. Rev. Biochem.*, *56*(1), 615–649. https://doi.org/10.1146/annurev.bi.56.070187.003151

Gold, M. G., Lygren, B., Dokurno, P., Hoshi, N., McConnachie, G., Taskén, K., … Barford, D. (2006). Molecular basis of AKAP specificity for PKA regulatory subunits. *Molecular Cell*, *24*(3), 383–395. https://doi.org/10.1016/j.molcel.2006.09.006

Gold, M. G., Reichow, S. L., O'Neill, S. E., Weisbrod, C. R., Langeberg, L. K., Bruce, J. E., … Scott, J. D. (2012). AKAP2 anchors PKA with aquaporin-0 to support ocular lens transparency. *EMBO Molecular Medicine*, *4*(1), 15–26. https://doi.org/10.1002/emmm.201100184

Gomez-Ospina, N., Panagiotakos, G., Portmann, T., Pasca, S. P., Rabah, D., Budzillo, A., … Dolmetsch, R. E. (2013). A promoter in the coding region of the calcium channel gene CACNA1C generates the transcription factor CCAT. *PloS One*, *8*(4), e60526. https://doi.org/10.1371/journal.pone.0060526

Gomez-Ospina, N., Tsuruta, F., Barreto-Chang, O., Hu, L., & Dolmetsch, R. (2006). The C terminus of the L-type voltage-gated calcium channel Ca(V)1.2 encodes a transcription factor. *Cell*, *127*(3), 591–606. https://doi.org/10.1016/j.cell.2006.10.017

Gordon, M. D., & Nusse, R. (2006). Wnt signaling: Multiple pathways, multiple receptors, and multiple transcription factors. *Journal of Biological Chemistry*, *281*(32), 22429–22433. https://doi.org/10.1074/jbc.R600015200

Gray, P. C., Johnson, B. D., Westenbroek, R. E., Hays, L. G., Yates, J. R., Scheuer, T., … Murphy, B. J. (1998). Primary structure and function of an A kinase anchoring protein associated with calcium channels. *Neuron*, *20*(5), 1017–1026. https://doi.org/10.1016/S0896-6273(00)80482-1

Grimm, M., & Brown, J. H. (2010). Beta-adrenergic receptor signaling in the heart: Role of CaMKII. *Journal of Molecular and Cellular Cardiology*, *48*(2), 322–330. https://doi.org/10.1016/j.yjmcc.2009.10.016

Hall, D. D., Feekes, J. A., Don, A. S. A., Shi, M., Hamid, J., Chen, L., … Hell, J. W. (2006). Binding of protein phosphatase 2A to the L-type calcium channel CaV1.2 next to Ser1928, its main PKA site, is critical for Ser1928 dephosphorylation. *Biochemistry*, *45*, 3448–3459.

Hansra, G., Bornancin, F., Whelan, R., Hemmings, B. A., & Parker, P. J. (1996). 12-O-Tetradecanoylphorbol-13-acetate-induced dephosphorylation of protein kinase Calpha correlates with the presence of a membrane-associated protein phosphatase 2A heterotrimer. *Biochemistry*, *271*(51), 32785–32788.

He, X., Semenov, M., Tamai, K., & Zeng, X. (2004). LDL receptor-related proteins 5 and 6 in Wnt/beta-catenin signaling: arrows point the way. *Development*, *131*(8), 1663–1677. https://doi.org/10.1242/dev.01117

Heisenberg, C.-P., Tada, M., Rauch, G.-J., Saúde, L., Concha, M. L., Geisler, R., … Wilson, S. W. (2000). Silberblick/Wnt11 mediates convergent extension movements during zebrafish gastrulation. *Nature*, *405*(6782), 76–81. https://doi.org/10.1038/35011068

Hendrickx, M., & Leyns, L. (2008). Non-conventional Frizzled ligands and Wnt receptors. *Development Growth and Differentiation*, *50*(4), 229–243. https://doi.org/10.1111/j.1440-169X.2008.01016.x

Hescheler, J., Meyer, R., Plant, S., Krautwurst, D., Rosenthal, W., & Schultz, G. (1991). Morphological, biochemical, and electrophysiological characterization of a clonal cell (H9c2) line from rat heart. *Circulation Research*, *69*(6), 1476–1486. https://doi.org/10.1161/01.RES.69.6.1476

Huang, C. J., Tu, C. T., Hsiao, C. D., Hsieh, F. J., & Tsai, H. J. (2003). Germ-line transmission of a myocardium-specific GFP transgene reveals critical regulatory elements in the cardiac myosin light chain 2 promoter of zebrafish. *Developmental Dynamics*, *228*(1), 30–40. https://doi.org/10.1002/dvdy.10356

Hulme, J. T., Konoki, K., Lin, T. W.-C., Gritsenko, M. A., Camp, D. G., Bigelow, D. J., & Catterall, W. A. (2005). Sites of proteolytic processing and noncovalent association of the distal C-terminal domain of CaV1.1 channels in skeletal muscle. *Proceedings of the National Academy of Sciences of the United States of America*, *102*(14), 5274–9. https://doi.org/10.1073/pnas.0409885102

Hulme, J. T., Lin, T. W.-C., Westenbroek, R. E., Scheuer, T., & Catterall, W. A. (2003). Beta-adrenergic regulation requires direct anchoring of PKA to cardiac CaV1.2 channels via a leucine zipper interaction with A kinase-anchoring protein 15. *Proceedings of the National Academy of Sciences of the United States of America*, *100*(22), 13093–8. https://doi.org/10.1073/pnas.2135335100

Hulme, J. T., Westenbroek, R. E., Scheuer, T., & Catterall, W. A. (2006). Phosphorylation of serine 1928 in the distal C-terminal domain of cardiac CaV1.2 channels during beta1-adrenergic regulation. *Proceedings of the National Academy of Sciences of the United States of America*, *103*(44), 16574–9. https://doi.org/10.1073/pnas.0607294103

Hulme, J. T., Yarov-Yarovoy, V., Lin, T. W. C., Scheuer, T., & Catterall, W. A. (2006). Autoinhibitory control of the CaV1.2 channel by its proteolytically processed distal C-terminal domain. *Journal of Physiology*, *576*(1), 87–102. https://doi.org/10.1113/jphysiol.2006.111799

Hundsrucker, C., Krause, G., Beyermann, M., Prinz, A., Zimmermann, B., Diekmann,

O., … Klussmann, E. (2006). High-affinity AKAP7delta-protein kinase A interaction yields novel protein kinase A-anchoring disruptor peptides. *The Biochemical Journal*, *396*(2), 297–306. https://doi.org/10.1042/BJ20051970

Hundsrucker, C., Skroblin, P., Christian, F., Zenn, H.-M., Popara, V., Joshi, M., … Klussmann, E. (2010). Glycogen synthase kinase 3beta interaction protein functions as an A-kinase anchoring protein. *Journal of Biological Chemistry*, *285*(8), 5507–5521. https://doi.org/10.1074/jbc.M109.047944

Iorga, B., Neacsu, C. D., Neiss, W. F., Wagener, R., Paulsson, M., Stehle, R., & Pfitzer, G. (2011). Micromechanical function of myofibrils isolated from skeletal and cardiac muscles of the zebrafish. *The Journal of General Physiology*, *137*(3), 255–270. https://doi.org/10.1085/jgp.201010568

Jarnæss, E., Ruppelt, A., Stokka, A. J., Lygren, B., Scott, J. D., & Taskén, K. (2008). Dual specificity A-kinase anchoring proteins (AKAPs) contain an additional binding region that enhances targeting of protein kinase A type I. *Journal of Biological Chemistry*, *283*(48), 33708–33718. https://doi.org/10.1074/jbc.M804807200

Jiang, Z., Pan, L., Chen, X., Chen, Z., & Xu, D. (2017). Wnt6 influences the viability of mouse embryonic palatal mesenchymal cells via the β-catenin pathway. *Experimental and Therapeutic Medicine*, *14*(6), 5339–5344. https://doi.org/10.3892/etm.2017.5240

Jones, B. W., Brunet, S., Gilbert, M. L., Nichols, C. B., Su, T., Westenbroek, R. E., … McKnight, G. S. (2012). Cardiomyocytes from AKAP7 knockout mice respond normally to adrenergic stimulation. *Proceedings of the National Academy of Sciences*, *109*(42), 17099–17104. https://doi.org/10.1073/pnas.1215219109

Jurevicius, J., & Fischmeister, R. (1996). cAMP compartmentation is responsible for a local activation of cardiac Ca2+ channels by beta-adrenergic agonists. *Proceedings of the National Academy of Sciences of the United States of America*, *93*(1), 295–299. https://doi.org/10.1073/pnas.93.1.295

Kammerer, S., Burns-Hamuro, L. L., Ma, Y., Hamon, S. C., Canaves, J. M., Shi, M. M., … Braun, A. (2003). Amino acid variant in the kinase binding domain of dual-specific A kinase-anchoring protein 2: a disease susceptibility polymorphism. *Proceedings of the National Academy of Sciences of the United States of America*, *100*(7), 4066–4071. https://doi.org/10.1073/pnas.2628028100

Katanaev, V. L., Ponzielli, R., Street, W., York, N., York, N., Luminy, C. De, & Cedex, M. (2005). Trimeric G protein-dependent Frizzled signaling in Drosophila. *Cell*, *120*, 111–122. https://doi.org/10.1016/j.cell.2004.11.014

Katchman, A., Yang, L., Zakharov, S. I., Kushner, J., Abrams, J., Chen, B.-X., … Marx, S. O. (2017). Proteolytic cleavage and PKA phosphorylation of α1C subunit are not required for adrenergic regulation of CaV1.2 in the heart. *Proceedings of the National Academy of Sciences*, *114*(34), 9194–9199. https://doi.org/10.1073/pnas.1706054114

Katoh, M. (2002). WNT3-WNT14B and WNT3A-WNT14 gene clusters (Review). *International Journal of Molecular Medicine*, *9*(6), 579–584.

Kim, G., Her, J., & Han, J. (2008). Ryk cooperates with Frizzled 7 to promote Wnt11-mediated endocytosis and is essential for Xenopus laevis convergent extension movements. *Journal of Cell Biology*, *182*(6), 1073–1082. https://doi.org/10.1083/jcb.200710188

Klauck, T. M., Faux, M. C., Labudda, K., Landenberg, L. K., Jaken, S., & Scott, J. D. (1996). Coordination of three signaling enzymes by AKAP79, a mammalian scaffold protein. *Science*, *271*, 6–9.

Kühl, M., Sheldahl, L. C., Craig, C., Moon, R. T., & Malbon, C. C. (2000). Ca2+/Calmodulin-dependent Protein Kinase II Is Stimulated by Wnt and Frizzled Homologs and Promotes Ventral Cell Fates in Xenopus. *Journal of Biological Chemistry*, *275*(17), 12701–12711. https://doi.org/10.1074/jbc.275.17.12701

Lacerda, A. E., Rampe, D., & Brown, A. M. (1988). Effects of protein kinase C activators on cardiac Ca2+ channels. *Nature*, *335*, 249–251. https://doi.org/10.1038/335249a0

Lai, L. P., Su, M. J., Lin, J. L., Lin, F. Y., Tsai, C. H., Chen, Y. S., … Lien, W. P. (1999). Down-regulation of L-type calcium channel and sarcoplasmic reticular Ca2+-ATPase mRNA in human atrial fibrillation without significant change in the mRNA of ryanodine receptor, calsequestrin and phospholamban: An insight into the mechanism of atrial elect. *Journal of the American College of Cardiology*, *33*(5), 1231–1237. https://doi.org/10.1016/S0735-1097(99)00008-X

Lee, S. W., Won, J. Y., Yang, J., Lee, J., Kim, S. Y., Lee, E. J., & Kim, H. S. (2015). AKAP6 inhibition impairs myoblast differentiation and muscle regeneration: Positive loop between AKAP6 and myogenin. *Scientific Reports*, *5*(October), 1–14. https://doi.org/10.1038/srep16523

Lemke, T., Welling, A., Christel, C. J., Blaich, A., Bernhard, D., Lenhardt, P., … Moosmang, S. (2008). Unchanged beta-adrenergic stimulation of cardiac L-type calcium channels in Cav1.2 phosphorylation site S1928A mutant mice *. *Journal of Biological Chemistry*, *283*(50), 34738–34744. https://doi.org/10.1074/jbc.M804981200

Li, J., Negro, A., Lopez, J., Bauman, A. L., Henson, E., Kafka-Dodge, K., & Kapiloff, M. S. (2010). The mAKAPβ Scaffold Regulates Cardiac Myocyte Hypertrophy via Recruitment of Activated Calcineurin. *J Mol Cell Cardiol*, *31*(9), 1713–1723. https://doi.org/10.1109/TMI.2012.2196707.Separate

Li, L., Yuan, H., Xie, W., Mao, J., Caruso, A. M., McMahon, A., … Wu, D. (1999). Dishevelled proteins lead to two signaling pathways. Regulation of LEF-1 and c-Jun N-terminal kinase in mammalian cells. *The Journal of Biological Chemistry*, *274*(1), 129–34. https://doi.org/10.1074/JBC.274.1.129

Li, X., Nooh, M. M., & Bahouth, S. W. (2013). Role of AKAP79/150 protein in β1-adrenergic receptor trafficking and signaling in mammalian cells. *Journal of Biological Chemistry*, *288*(47), 33797–33812. https://doi.org/10.1074/jbc.M113.470559

Lin, F., Wang, H. Y., & Malbon, C. C. (2000). Gravin-mediated formation of signaling

complexes in beta2 -adrenergic receptor desensitization and resensitization*. *Biochemistry*, *275*(25), 19025–19034. https://doi.org/10.1074/jbc.275.25.19025

Livak, K. J., & Schmittgen, T. D. (2001). Analysis of relative gene expression data using real-time quantitative PCR and the 2-ΔΔCT method. *Methods*, *25*(4), 402–408. https://doi.org/10.1006/meth.2001.1262

Lygren, B., Carlson, C. R., Santamaria, K., Lissandron, V., McSorley, T., Litzenberg, J., … Klussmann, E. (2007). AKAP complex regulates Ca2+ re-uptake into heart sarcoplasmic reticulum. *EMBO Reports*, *8*(11), 1061–1067. https://doi.org/10.1038/sj.embor.7401081

Männer, J. (2009). The anatomy of cardiac looping: A step towards the understanding of the morphogenesis of several forms of congenital cardiac malformations. *Clinical Anatomy*, *22*(1), 21–35. https://doi.org/10.1002/ca.20652

Manni, S., Mauban, J. H., Ward, C. W., & Bond, M. (2008). Phosphorylation of the cAMP-dependent protein kinase (PKA) regulatory subunit modulates PKA-AKAP interaction, substrate phosphorylation, and calcium signaling in cardiac cells. *Journal of Biological Chemistry*, *283*(35), 24145–24154. https://doi.org/10.1074/jbc.M802278200

Marks, M. L., Whisler, S. L., Clericuzio, C., & Keating, M. (1995). A new form of long QT syndrome associated with syndactyly. *Journal of the American College of Cardiology*, *25*(1), 59–64. https://doi.org/10.1016/0735-1097(94)00318-K

Marx, S. O., Kurokawa, J., Reiken, S., Motoike, H., D'Armiento, J., Marks, A. R., & Kass, R. S. (2002). Requirement of a Macromolecular Signaling Complex for beta Adrenergic Receptor Modulation of the KCNQ1-KCNE1 Potassium Channel. *Science*, *295*(5554), 496–499. https://doi.org/10.1126/science.1066843

Marx, S. O., Reiken, S., Hisamatsu, Y., Jayaraman, T., Burkhoff, D., Rosemblit, N., & Marks, A. R. (2000). PKA phosphorylation dissociates FKBP12.6 from the calcium release channel (ryanodine receptor): defective regulation in failing hearts. *Cell*, *101*(4), 365–376. https://doi.org/10.1016/S0092-8674(00)80847-8

McHugh, D., Sharp, E. M., Scheuer, T., & Catterall, W. a. (2000). Inhibition of cardiac L-type calcium channels by protein kinase C phosphorylation of two sites in the N-terminal domain. *Proceedings of the National Academy of Sciences of the United States of America*, *97*(22), 12334–8. https://doi.org/10.1073/pnas.210384297

Minobe, E., Maeda, S., Xu, J., Hao, L., Kameyama, A., & Kameyama, M. (2014). A new phosphorylation site in cardiac L-type Ca2+ channels (CaV1.2) responsible for its cAMP-mediated modulation. *AJP: Cell Physiology*, *307*(11), C999–C1009. https://doi.org/10.1152/ajpcell.00267.2014

Molkentin, J. D., Lu, J. R., Antos, C. L., Markham, B., Richardson, J., Robbins, J., … Olson, E. N. (1998). A calcineurin-dependent transcriptional pathway for cardiac hypertrophy. *Cell*, *93*(2), 215–228. https://doi.org/10.1016/S0092-8674(00)81573-1

Murphy, J. G., Sanderson, J. L., Gorski, J. A., Scott, J. D., Catterall, W. A., Sather, W.

A., & Dell'Acqua, M. L. (2014). AKAP-anchored PKA maintains neuronal L-type calcium channel activity and NFAT transcriptional signaling. *Cell Reports*, *7*(5), 1577–1588. https://doi.org/10.1016/j.celrep.2014.04.027

Nalesso, G., Thomas, B. L., Sherwood, J. C., Yu, J., Addimanda, O., Eldridge, S. E., … Dell'Accio, F. (2017). WNT16 antagonises excessive canonical WNT activation and protects cartilage in osteoarthritis. *Annals of the Rheumatic Diseases*, *76*(1), 218–226. https://doi.org/10.1136/annrheumdis-2015-208577

Nichols, A. S., Floyd, D. H., Bruinsma, S. P., Narzinski, K., & Baranski, T. J. (2013). Frizzled receptors signal through G proteins. *Cell Signaling*, *25*(6), 1468–1475. https://doi.org/10.1016/j.cellsig.2013.03.009.Frizzled

Nichols, C. B., Rossow, C. F., Navedo, M. F., Westenbroek, R. E., Catterall, W. A., Santana, L. F., & McKnight, G. S. (2010). Sympathetic stimulation of adult cardiomyocytes requires association of AKAP5 with a subpopulation of L-Type calcium channels. *Circulation Research*, *107*(6), 747–756. https://doi.org/10.1161/CIRCRESAHA.109.216127

Nystoriak, M. A., Nieves-cintrón, M., Patriarchi, T., Olivia, R., Prada, M. P., Morotti, S., … Navedo, M. F. (2017). Ser1928 phosphorylation by PKA stimulates the L-type Ca2+ channel CaV 1.2 and vasoconstriction during acute hyperglycemia and diabetes. *Science Signaling*, *10*(463). https://doi.org/10.1126/scisignal.aaf9647.Ser

Oliveria, S. F., Dell'Acqua, M. L., & Sather, W. A. (2007). AKAP79/150 Anchoring of Calcineurin Controls Neuronal L-Type Ca2+ Channel Activity and Nuclear Signaling. *Neuron*, *55*(2), 261–275. https://doi.org/10.1016/j.neuron.2007.06.032

Ono, B. Y. K., & Fozzard, H. A. (1992). Phosphorylation restores activity of L-type calcium channels after rundown in inside-out patches from rabbit cardiac cells. *J Physiol (Lond)*, *454*, 673–688.

Ono, B. Y. K., & Fozzard, H. A. (1993). Two phosphatase sites on the Ca2+ channel affecting different kinetic functions. *J Physiol*, *470*, 73–84.

Panáková, D., Werdich, A. A, & Macrae, C. a. (2010). Wnt11 patterns a myocardial electrical gradient through regulation of the L-type Ca(2+) channel. *Nature*, *466*(7308), 874–8. https://doi.org/10.1038/nature09249

Pandur, P., Lasche, M., Eisenberg, L. M., & Kühl, M. (2002). Wnt-11 activation of a non-canonical Wnt signalling pathway is required for cardiogenesis. *Nature*, *418*(August), 636–639. https://doi.org/10.1038/nature00909.1.

Pandur, P., Maurus, D., & Kühl, M. (2002). Increasingly complex: New players enter the Wnt signaling network. *BioEssays*, *24*(10), 881–884. https://doi.org/10.1002/bies.10164

Pare, G. C., Easlick, J. L., Mislow, J. M., McNally, E. M., & Kapiloff, M. S. (2005). Nesprin-1α contributes to the targeting of mAKAP to the cardiac myocyte nuclear envelope. *Experimental Cell Research*, *303*(2), 388–399. https://doi.org/10.1016/j.yexcr.2004.10.009

Patel, K., Fonarow, G. C., Ahmed, M., Morgan, C., Kilgore, M., Love, T. E., … Ahmed, A. (2014). Calcium channel blockers and outcomes in older patients with heart failure and preserved ejection fraction. *Circulation: Heart Failure*, *7*(6), 945–952. https://doi.org/10.1161/CIRCHEARTFAILURE.114.001301

Pederson, T. (1998). The plurifunctional nucleolus. *Nucleic Acids Research*, *26*(17), 3871–3876. https://doi.org/10.1093/nar/26.17.3871

Perrino, C., Feliciello, A., Schiattarella, G. G., Esposito, G., Guerriero, R., Zaccaro, L., … Chiariello, M. (2010). AKAP121 downregulation impairs protective cAMP signals, promotes mitochondrial dysfunction, and increases oxidative stress. *Cardiovascular Research*, *88*(1), 101–110. https://doi.org/10.1093/cvr/cvq155

Pierce, K. L., Premont, R. T., & Lefkowitz, R. J. (2002). Seven-transmembrane receptors. *Nature Reviews Molecular Cell Biology*, *3*(9), 639–650. https://doi.org/10.1038/nrm908

Posokhova, E., Shukla, A., Seaman, S., Volate, S., Hilton, M. B., Wu, B., … St.Croix, B. (2015). GPR124 functions as a WNT7-specific coactivator of canonical β-catenin signaling. *Cell Reports*, *10*(2), 123–130. https://doi.org/10.1016/j.celrep.2014.12.020

Raška, I., Shaw, P. J., & Cmarko, D. (2006). New Insights into Nucleolar Architecture and Activity. *International Review of Cytology*, *255*(6), 177–235. https://doi.org/10.1016/S0074-7696(06)55004-1

Redden, J. M., Le, A. V., Singh, A., Federkiewicz, K., Smith, S., & Dodge-Kafka, K. L. (2012). Spatiotemporal regulation of PKC via interactions with AKAP7 isoforms. *Biochemical Journal*, *446*(2), 301–309. https://doi.org/10.1042/BJ20120366

Reuter, H. (1983). Calcium channel modulation by neurotransmitters, enzymes and drugs. *Nature*, *301*(5901), 569–574. https://doi.org/10.1038/301569a0

Reuter, H., Stevens, C., Tsien, R., & Yellen, G. (1982). Properties of single calcium channels in cardiac cell culture. *Nature*, *297*, 501–504. Retrieved from http://www.nature.com/nature/journal/v297/n5866/abs/297501a0.html

Rohr, S. (2004). Role of gap junctions in the propagation of the cardiac action potential. *Cardiovascular Research*, *62*(2), 309–322. https://doi.org/10.1016/j.cardiores.2003.11.035

Rosado, M., Barber, C. F., Berciu, C., Feldman, S., Birren, S. J., Nicastro, D., & Goode, B. L. (2014). Critical roles for multiple formins during cardiac myofibril development and repair. *Molecular Biology of the Cell*, *25*(6), 811–827. https://doi.org/10.1091/mbc.E13-08-0443

Rubbi, C. P., & Milner, J. (2003). Disruption of the nucleolus mediates stabilization of p53 in response to DNA damage and other stresses. *EMBO Journal*, *22*(22), 6068–6077. https://doi.org/10.1093/emboj/cdg579

Saneyoshi, T., Kume, S., Amsaki, Y., & Mikoshiba, K. (2002). The wnt/calcium pathway activates nf-at and promotes ventral cell fate in xenopus embryos. *Nature*,

417(6886), 295–299. https://doi.org/10.1038/417295a

Satoh, H. (1995). Depression of the Spontaneous Embryonic Activity Chick by Phorbol Esters in Young Cardiomyocytes. *Jpn J Pharmacol*, *67*, 297–304.

Schotten, U., Haase, H., Frechen, D., Greiser, M., Stellbrink, C., Jimezen-Vazquez, J. F., … Hanrath, P. (2003). The L-type Ca2+-channel subunits α1C and β2 are not downregulated in atrial myocardium of patients with chronic atrial fibrillation. *Journal of Molecular and Cellular Cardiology*, *35*(5), 437–443. https://doi.org/10.1016/S0022-2828(03)00012-9

Schroder, E., Byse, M., & Satin, J. (2009). L-type calcium channel C terminus autoregulates transcription. *Circulation Research*, *104*(12), 1373–1381. https://doi.org/10.1161/CIRCRESAHA.108.191387

Schröder, F., Handrock, R., Beuckelmann, D. J., Hirt, S., Hullin, R., Priebe, L., … Herzig, S. (1998). Increased availability and open probability of single L-type calcium channels from failing compared with nonfailing human ventricle. *Circulation*, *98*(10), 969–976. https://doi.org/10.1161/01.CIR.98.10.969

Schulte, G. (2010). International Union of Basic and Clinical. *Pharmacological Reviews*, *62*(4), 632–667. https://doi.org/10.1124/pr.110.002931.632

Schulte, G. (2015). Frizzleds and WNT/β-catenin signaling - The black box of ligand-receptor selectivity, complex stoichiometry and activation kinetics. *European Journal of Pharmacology*, *763*, 191–195. https://doi.org/10.1016/j.ejphar.2015.05.031

Schulte, G., & Bryja, V. (2007). The Frizzled family of unconventional G-protein-coupled receptors. *Trends in Pharmacological Sciences*, *28*(10), 518–25. https://doi.org/10.1016/j.tips.2007.09.001

Sculptoreanu, A., Rotman, E., Takahashi, M., Scheuer, T., & Catterall, W. A. (1993). Voltage-dependent potentiation of the activity of cardiac L-type calcium channel alpha 1 subunits due to phosphorylation by cAMP-dependent protein kinase. *Proceedings of the National Academy of Sciences of the United States of America*, *90*(21), 10135–9. https://doi.org/10.1073/pnas.90.21.10135

Semsarian, C., Ahmad, I., Giewat, M., Georgakopoulos, D., Schmitt, J. P., McConnell, B. K., … Seidman, J. G. (2002). The L-type calcium channel inhibitor diltiazem prevents cardiomyopathy in a mouse model. *Journal of Clinical Investigation*, *109*(8), 1013–1020. https://doi.org/10.1172/JCI200214677

Sheldahl, L. C., Park, M., Malbon, C. C., & Moon, R. T. (1999). Protein kinase C is differentially stimulated by Wnt and Frizzled homologs in a G-protein-dependent manner. *Current Biology*, *9*, 695–699.

Shi, J., Gu, P., Zhu, Z., Liu, J., Chen, Z., Sun, X., … Zhang, Z. (2012). Protein phosphatase 2A effectively modulates basal L-type Ca2+current by dephosphorylating Cav1.2 at serine 1866 in mouse cardiac myocytes. *Biochemical and Biophysical Research Communications*, *418*(4), 792–798. https://doi.org/10.1016/j.bbrc.2012.01.105

Slusarski, D. C., Corces, V. G., & Moon, R. T. (1997). Interaction of Wnt and a Frizzled homologue triggers G-protein-linked phosphatidylinositol signalling. *Nature*, *390*(6658), 410–413. https://doi.org/10.1038/37138

Song, A., Zhang, Y., Han, L., Yegutkin, G. G., Liu, H., Sun, K., … Xia, Y. (2017). Erythrocytes retain hypoxic adenosine response for faster acclimatization upon re-ascent. *Nature Communications*, *8*. https://doi.org/10.1038/ncomms14108

Splawski, I., Timothy, K. W., Decher, N., Kumar, P., Sachse, F. B., Beggs, A. H., … Keating, M. T. (2005). Severe arrhythmia disorder caused by cardiac L-type calcium channel mutations. *Proceedings of the National Academy of Sciences*, *102*(23), 8089–8096. https://doi.org/10.1073/pnas.0502506102

Splawski, I., Timothy, K. W., Sharpe, L. M., Decher, N., Kumar, P., Bloise, R., … Keating, M. T. (2004). CaV1.2 calcium channel dysfunction causes a multisystem disorder including arrhythmia and autism. *Cell*, *119*(1), 19–31. https://doi.org/10.1016/j.cell.2004.09.011

Stainier, D. Y. R., Lee, R. K., & Fishman, M. C. (1993). Cardiovascular development in the zebrafish. I. Myocardial fate map and heart tube formation. *Development*, *119*(1), 31–40.

Takahashi, M., Seagar, M. J., Jones, J. F., Reber, B. F., & Catterall, W. A. (1987). Subunit structure of dihydropyridine-sensitive calcium channels from skeletal muscle. *Proceedings of the National Academy of Sciences of the United States of America*, *84*(15), 5478–82. https://doi.org/10.1073/pnas.84.15.5478

Tandan, S., Wang, Y., Wang, T. T., Jiang, N., Hall, D. D., Hell, J. W., … Hill, J. A. (2009). Physical and Functional Interaction Between Calcineurin and the Cardiac L-Type Ca2+ Channel. *Circulation Research*, *105*, 51–60. https://doi.org/10.1161/CIRCRESAHA.109.199828

Tanji, C., Yamamoto, H., Yorioka, N., Kohno, N., Kikuchi, K., & Kikuchi, A. (2002). A-Kinase Anchoring Protein AKAP220 Binds to Glycogen Synthase Kinase-3β (GSK-3β) and Mediates Protein Kinase A-dependent Inhibition of GSK-3β. *Journal of Biological Chemistry*, *277*(40), 36955–36961. https://doi.org/10.1074/jbc.M206210200

Terrenoire, C., Houslay, M. D., Baillie, G. S., & Kass, R. S. (2009). The cardiac IKs potassium channel macromolecular complex includes the phosphodiesterase PDE4D3. *Journal of Biological Chemistry*, *284*(14), 9140–9146. https://doi.org/10.1074/jbc.M805366200

Thakkar, A., Aljameeli, A., Thomas, S., & Shah, G. V. (2016). A-kinase anchoring protein 2 is required for calcitonin-mediated invasion of cancer cells. *Endocrine-Related Cancer*, *23*(1), 1–14. https://doi.org/10.1530/ERC-15-0425

Thomsen, A. R. B., Plouffe, B., Cahill, T. J., Shukla, A. K., Tarrasch, J. T., Dosey, A. M., … Lefkowitz, R. J. (2016). GPCR-G Protein-β-Arrestin Super-Complex Mediates Sustained G Protein Signaling. *Cell*, *166*(4), 907–919. https://doi.org/10.1016/j.cell.2016.07.004

Trotter, K. W., Fraser, I. D. C., Scott, G. K., Stutts, M. J., Scott, J. D., & Milgram, S. L. (1999). Anchoring Protein 18 Isoforms. *Journal of Cell Biology*, *147*(7), 1481–1492.

Tseng, G.-N., & Boyden, P. A. (1991). Different effects of intracellular Ca and protein kinase C on cardiac T and L Ca currents. *American Journal of Physiology*, *261*, 364–379.

van der Heyden, M. a G., Wijnhoven, T. J. M., & Opthof, T. (2005). Molecular aspects of adrenergic modulation of cardiac L-type Ca2+ channels. *Cardiovascular Research*, *65*(1), 28–39. https://doi.org/10.1016/j.cardiores.2004.09.028

van der Heyden, M. a, Rook, M. B., Hermans, M. M., Rijksen, G., Boonstra, J., Defize, L. H., & Destrée, O. H. (1998). Identification of connexin43 as a functional target for Wnt signalling. *Journal of Cell Science*, *111 (Pt 1*, 1741–9. Retrieved from http://www.ncbi.nlm.nih.gov/pubmed/9601103

Vargas, M. A. X., Tirnauer, J. S., Glidden, N., Kapiloff, M. S., & Dodge-Kafka, K. L. (2012). Myocyte enhancer factor 2 (MEF2) tethering to muscle selective A-kinase anchoring protein (mAKAP) is necessary for myogenic differentiation. *Cellular Signalling*, *24*(8), 1496–1503. https://doi.org/10.1016/j.cellsig.2012.03.017

Veeman, M. T., Axelrod, J. D., & Moon, R. T. (2003). A Second Canon : Functions and Mechanisms of Beta-Catenin-Independent Wnt Signaling. *Developmental Cell*, *5*(2002), 367–377.

Vega, R. B., Harrison, B. C., Meadows, E., Charles, R., Papst, P. J., Olson, E. N., … Mckinsey, T. a. (2004). Protein Kinases C and D Mediate Agonist-Dependent Cardiac Hypertrophy through Nuclear Export of Histone Deacetylase 5 Protein Kinases C and D Mediate Agonist-Dependent Cardiac Hypertrophy through Nuclear Export of Histone Deacetylase 5. *Molecular and Cellular Biology*, *24*(19), 8374–8385. https://doi.org/10.1128/MCB.24.19.8374

Verde, I., Vandecasteele, G., Lezoualc, F., & Fischmeister, R. (1999). Characterization of the cyclic nucleotide phosphodiesterase subtypes involved in the regulation of the L-type Ca 2 + current in rat ventricular myocytes. *British Journal of Parmacology*, (127), 65–74.

Vila Petroff, M. G., Egan, J. M., Wang, X., & Sollott, S. J. (2001). Glucagon-like peptide-1 increases cAMP but fails to augment contraction in adult rat cardiac myocytes. *Circulation Research*, *89*(5), 445–452. https://doi.org/10.1161/hh1701.095716

von Maltzahn, J., Bentzinger, F. C., & Rudnicki, M. A. (2012). Wnt7a/Fzd7 Signalling Directly Activates the Akt/mTOR Anabolic Growth Pathway in Skeletal Muscle. *Nature Cell Biology*, *14*(2), 186–191. https://doi.org/10.1038/ncb2404.Wnt7a/Fzd7

Watkins, S. J., Borthwick, G. M., & Arthur, H. M. (2011). The H9C2 cell line and primary neonatal cardiomyocyte cells show similar hypertrophic responses in vitro. *In Vitro Cellular and Developmental Biology - Animal*, *47*(2), 125–131. https://doi.org/10.1007/s11626-010-9368-1

Wei, X., Neely, A., Lacerda, A. E., Olcese, R., Stefani, E., Perez-Reyes, E., & Birnbaumer, L. (1994). Modification of Ca2+ channel activity by deletions at the carboxyl terminus of the cardiac alpha 1 subunit. *The Journal of Biological Chemistry*, *269*(3), 1635–40. Retrieved from http://www.ncbi.nlm.nih.gov/pubmed/7507480

William, H., & Rogers, T. B. (2004). Protein phosphatase 1 and an opposing protein kinase regulate steady-state L-type Ca 2 + current in mouse cardiac myocytes. *J Physiol*, *556*, 79–93. https://doi.org/10.1113/jphysiol.2003.059329

Witzel, S., Zimyanin, V., Carreira-Barbosa, F., Tada, M., & Heisenberg, C. P. (2006). Wnt11 controls cell contact persistence by local accumulation of Frizzled 7 at the plasma membrane. *Journal of Cell Biology*, *175*(5), 791–802. https://doi.org/10.1083/jcb.200606017

Wong, W., & Scott, J. D. (2004). AKAP signalling complexes: Focal points in space and time. *Nature Reviews Molecular Cell Biology*, *5*(12), 959–970. https://doi.org/10.1038/nrm1527

Yang, L., Dai, D., Yuan, C., Westenbroek, R. E., Yu, H., West, N., & De, H. O. (2016). Loss of β-adrenergic stimulated phosphorylation of CaV1.2 channels on Ser1700 leads to heart failure. *Proc Natl Acad Sci U S A*, *113*(49), E7976–E7985. https://doi.org/10.1073/pnas.1617116113

Yang, L., Katchman, A., Samad, T., Morrow, J. P., Weinberg, R. L., & Marx, S. O. (2013). Beta-Adrenergic regulation of the L-type Ca2+ channel does not require phosphorylation of alpha 1C Ser1700. *Circulation Research*, *113*(7), 871–880. https://doi.org/10.1161/CIRCRESAHA.113.301926

Yue, D. T., Herzig, S., & Marban, E. (1990). Beta-adrenergic stimulation of calcium channels occurs by potentiation of high-activity gating modes. *Proc Natl Acad Sci U S A*, *87*(2), 753–757. https://doi.org/10.1073/pnas.87.2.753

Zhang, Z.-H., Johnson, J. A., Chen, L., El-Sherif, N., Mochly-Rosen, D., & Boutjdir, M. (1997). C2 region-derived peptides of beta-protein kinase C regulate cardiac Ca2+ channels. *Circulation Research*, *80*(5), 720 LP-729. Retrieved from http://circres.ahajournals.org/content/80/5/720.abstract

Zühlke, R. D., & Reuter, H. (1998). Ca2+-sensitive inactivation of L-type Ca2+ channels depends on multiple cytoplasmic amino acid sequences of the alpha1C subunit. *Proc Natl Acad Sci U S A*, *95*(March), 3287–3294.

Zülke, R. D., Pitt, G. S., Deisseroth, K., Tsien, R. W., & Reuter, H. (1999). Calmodulin supports both inactivation and facilitation of L-type calcium channels. *Nature*, *42*(1995), 159–162.

9 Appendix

9.1 Abbreviations

APC	Adenomatosis Polyposis Coli
AC	Adenylyl Cyclase
AKAP	A-Kinase Anchoring Protein
ABD	A-Kinase Anchoring Protein Binding Domain
aa	amino acid(s)
AQP0	Aquaporin-0
AF	Atrial Fibrillation
β-AR	β-Adrenergic Pathway
bp	base pair(s)
β-Cat	β-Catenin
BSA	Bovine Serum Albumin
CCBs	Calcium Channel Blockers
CaMKII	Calcium/Calmodulin dependent serine/threonine Kinase II
CDI	Calcium-dependent inhibition
CaM	Calmodulin
CMs	Cardiomyocytes
CK1α	Casein Kinase 1α
JNK	c-Jun N-terminal Kinase
cDNA	complementary Deoxyribonucleic Acid
Cx43	Connexin 43
CT	C-terminal tail of the α1C subunit of the L-Type Calcium Channel
cAMP	cyclic Adenosine Monophosphate
cGMP	cyclic Guanosine Monophosphate
DNase	Deoxyribonuclease
DAG	Diacylglycerol
DCM	Dilated Cardiomyopathy
DMSO	Dimethyl Sulfoxide
DVL	Dishevelled
Daam1	Dishevelled associated activator of morphogenesis 1

dCT	distal C-terminal tail of the α1C subunit of the L-Type Calcium Channel
DMEM	Dulbecco's Modified Eagle Medium
F-HVM	Failing Human Ventricular Myocyte(s)
FBS	Fetal Bovine Serum
FACS	Fluorescence-Activated Cell Sorting
FSK	Forskolin
FZD	Frizzled
GSK3β	Glycogen Synthase Kinase 3β
GPCR	G Protein-Coupled Receptor
HDAC	Histone Deacetylase
h	hour(s)
hpf	hour(s) post fertilization
IP	Immunoprecipitation
IC	Inner Curvature
IP_3	Inositol-1,4,5-triphosphate
ISO	Isoproterenol
kDa	kilo-Dalton
KD	Knockdown
KO	Knockout
LZ	Leucine-Zipper
l	liter
LRP5/6	Low-density Lipoprotein Receptor related Protein 5/6
LTCC	L-Type Calcium Channel
mRNA	messenger Ribonucleic Acid
μg	microgram
μl	microliter
μm	micrometer
μM	micromolar
ml	milliliter
mM	millimolar
MYOG	Myogenin
NCX	Na^+/Ca^{2+} Exchanger
ng	nanogram
nl	nanoliter
NRVMs	Neonatal Rat Ventricular Myocytes

NST	Normal Tyrode's Solution
NFAT	Nuclear Factor of Activated T cells
OC	Outer Curvature
PFA	Paraformaldehyde
PBS	Phosphate Buffered Saline
PIP_2	Phosphatidylinositol-4,5-bisphosphate
PDE	Phosphodiesterase
PLN	Phospholamban
PLC	Phospholipase C
PCP	Planar Cell Polarity
PCR	Polymerase Chain Reaction
PKA	Protein Kinase A
PKC	Protein Kinase C
PKD	Protein Kinase D
PKI	Protein Kinase Inhibitor
PP1	Protein Phosphatase 1
PP2A	Protein Phosphatase 2A
PP2B	Protein Phosphatase 2B
pCT	proximal C-terminal tail of the α1C subunit of the L-Type Calcium Channel
ROCK	Rho-associated Kinase
GEF	Rho-Guanine nucleotide Exchange Factor
RNase	Ribonuclease
RNA	Ribonucleic acid
RT	Room Temperature
RyR	Ryanodine Receptor
SR	Sarcoplasmic Reticulum
SERCA	Sarcoplasmic Reticulum Ca^{2+}-ATPase
7TM	Seven Transmembrane
siRNA	small interfering Ribonucleic Acid
SD	Standard Deviation
TS	Timothy syndrome
TF	Transcription Factor
TPM	Troponin-T
WB	Western Blot
WT	Wild-Type

9.2 List of Figures

I herewith declare that I have produced this paper without the prohibited assistance of third parties and without making use of aids other than those specified; notions taken over directly or indirectly from other sources have been identified as such. This paper has not previously been presented in identical or similar form to any other German or foreign examination board.

Berlin, 29.03.2018 _____

Kitti Dóra Csályi